

12-1999

Mineral paragenesis and ore fluids at the Turquoise Ridge gold deposit, Nevada

Michiko Shigehiro
University of Nevada, Las Vegas

Follow this and additional works at: <https://digitalscholarship.unlv.edu/thesesdissertations>

 Part of the [Geochemistry Commons](#), and the [Geology Commons](#)

Repository Citation

Shigehiro, Michiko, "Mineral paragenesis and ore fluids at the Turquoise Ridge gold deposit, Nevada" (1999). *UNLV Theses, Dissertations, Professional Papers, and Capstones*. 1449.
<http://dx.doi.org/10.34917/3434815>

This Thesis is protected by copyright and/or related rights. It has been brought to you by Digital Scholarship@UNLV with permission from the rights-holder(s). You are free to use this Thesis in any way that is permitted by the copyright and related rights legislation that applies to your use. For other uses you need to obtain permission from the rights-holder(s) directly, unless additional rights are indicated by a Creative Commons license in the record and/or on the work itself.

This Thesis has been accepted for inclusion in UNLV Theses, Dissertations, Professional Papers, and Capstones by an authorized administrator of Digital Scholarship@UNLV. For more information, please contact digitalscholarship@unlv.edu.

MINERAL PARAGENESIS AND ORE FLUIDS
AT THE TURQUOISE RIDGE
GOLD DEPOSIT,
NEVADA

by

Michiko Shigehiro

Bachelor of Science
Temple University
1996

A thesis submitted in partial fulfillment
of the requirements for the

**Master of Science Degree
Department of Geoscience
College of Sciences**

**Graduate College
University of Nevada, Las Vegas
December 1999**

Copyright by Michiko Shigehiro 2000
All Rights Reserved

UNIVERSITY OF NEVADA LAS VEGAS

Thesis Approval
The Graduate College
University of Nevada, Las Vegas

October 13, 1999

The Thesis prepared by

Michiko Shigehiro


Entitled


Mineral Paragenesis and Ore Fluids at the Turquoise Ridge


Gold Deposit, Nevada


is approved in partial fulfillment of the requirements for the degree of


Master of Science in Geoscience


Examination Committee Chair


Dean of the Graduate College


Examination Committee Member


Examination Committee Member


Graduate College Faculty Representative

ABSTRACT

Mineral Paragenesis and Ore Fluids at the Turquoise Ridge Gold Deposit, Nevada

by

Michiko Shigehiro

Dr. Jean S. Cline, Examination Committee Chair
Associate Professor of Geoscience
University of Nevada, Las Vegas

In this study, mineral assemblages and related fluid inclusions at the Turquoise Ridge Carlin-type gold deposit were examined to answer the following questions: (1) What is the ore-stage mineral paragenesis? (2) At what pressures and temperatures did the deposits form? (3) What are the sources of ore fluids?

Pyrite with gold, jasperoid quartz, stibnite, orpiment, realgar, and calcite were successively deposited at Turquoise Ridge. Microthermometric data and isotopic ratios of inclusion fluids in ore-related minerals indicate entrapment of multiple generations of fluids in pre-ore, ore-, and late-ore stage minerals. Primary fluid inclusions in an ore-stage jasperoid quartz crystal have salinities of 12.6 to 19 wt. % NaCl equivalent, and most inclusions homogenized between 130 ° and 193 °C. Isotopic signatures of inclusion fluids in ore-stage jasperoid quartz, $\delta D = -33$ ‰ and $\delta^{18}O = +7.1$ to $+12.2$ ‰, and $\delta D = -46$ ‰ and $\delta^{18}O = +5.4$ to $+10.5$ ‰, are consistent with a magmatic or metamorphic source, or both, while inclusion fluids in late-ore stage calcite yielded $\delta^{18}O = 10$ to 14.5 ‰ and $\delta D = -110$ ‰, indicating trapping of an evolved meteoric fluid.

TABLE OF CONTENTS

ABSTRACT	iii
LIST OF FIGURES.....	vi
LIST OF TABLES	viii
LIST OF ABBREVIATION AND TERMS.....	ix
ACKNOWLEDGMENTS	x
CHAPTER 1 INTRODUCTION.....	1
CHAPTER 2 GENERAL GEOLOGY	5
Investigation of the Turquoise Ridge Deposit	5
Stratigraphy	5
Discussion of Stratigraphy	11
Structure	12
Discussion of Structure	13
Alteration	15
Previous Studies of Ore and Non-ore Mineral Assemblages	16
Pressures and Temperatures during Gold Mineralization	18
Origins of Ore Fluids Indicated by Oxygen and Hydrogen Isotopic Signatures	19
CHAPTER 3 METHODS OF STUDY	21
Sample Collection	21
X-ray Diffraction and Inductively Coupled Plasma Analyses	21
Petrography and Ore Microscopy	22
Electron Microprobe Analyses.....	23
Scanning Electron Microscope Analyses.....	23
Fluid Inclusion Studies.....	23
Freezing and Heating Studies.....	24
Oxygen and Hydrogen Isotope Analysis.....	25
CHAPTER 4 PETROGRAPHY AND ORE MICROSCOPY.....	26
Host Rocks	26
Discussion of Host Rocks	28
Mineral Paragenesis	29
Pre-Ore Stage Mineral Assemblage: Quartz - Pyrite - Marcasite.....	29
The Ore-Stage Mineral Assemblage: Pyrite - Marcasite - Gold - Jasperoid Quartz - K-spar (?).....	32
The Late-Ore Stage Mineral Assemblage: Pyrite/Marcasite - Jasperoid Quartz - Stibnite -Fluorite - Orpiment - Realgar - Calcite	34
Summary of Mineral Paragenesis.....	41
CHAPTER 5 FLUID INCLUSION STUDIES	43
Petrography and Microthermometry	43
Fluid Inclusions in Pre-Ore Stage Quartz.....	43
Pre-Ore Stage Vein Quartz.....	44
Pre-Ore Stage Quartz in Gouge.....	52

Pre-Ore Stage Quartz Crosscut by Ore-Stage Minerals	57
Discussion of Pre-Ore Stage Quartz Microthermometric Data	57
Fluid Inclusions in Ore-Stage Jasperoid Quartz.....	61
Ore-Stage Jasperoid Quartz.....	61
Ore-stage Jasperoid Quartz in Gouge.....	70
Discussion of Ore-Stage Jasperoid Quartz Microthermometric Data	74
Fluid Inclusions in Late Ore-Stage Minerals.....	76
CHAPTER 6 STABLE ISOTOPE ANALYSIS	78
Discussion of Stable Isotope Analysis	79
CHAPTER 7 SUMMARY AND DISCUSSION	83
CHAPTER 8 CONCLUSIONS	88
APPENDIX I LIST OF DRILL CORE SAMPLES FROM THE TURQUOISE RIDGE DEPOSIT	90
APPENDIX II LIST OF DOUBLY POLISHED THICK SECTIONS, POLISHED THIN SECTIONS, AND QUICK PLATES.....	117
List of Doubly Polished Thick Sections.....	118
List of Polished Thin Sections	118
List of Quick Plates.....	119
APPENDIX III RESULTS OF X-RAY DIFFRACTION ON TWO TYPES OF UNALTERED ORE HOST ROCKS	120
Results of X-ray Diffraction on TR 94-172 1637.5	121
Results of X-ray Diffraction on TR 94-172 1993	124
APPENDIX IV SUMMARY OF PETROGRAPHY AND ORE MICROSCOPY OF DOUBLY POLISHED THICK SECTIONS AND POLISHED THIN SECTIONS	126
Doubly Polished Thick Sections from a Drill Hole TR 94-172	127
Polished Thin Sections from a Drill Hole TR 94-172	131
Doubly Polished Thick Sections	132
APPENDIX V SUMMARY OF FLUID INCLUSION PETROGRAPHY	135
APPENDIX VI MICROTHERMOMETRIC DATA OF FLUID INCLUSIONS IN PRE-ORE STAGE QUARTZ AND ORE-STAGE JASPEROID QUARTZ.....	138
Microthermometric Data of Fluid Inclusions in Pre-Ore Stage Quartz.....	139
Microthermometric Data of Fluid Inclusions in Ore-Stage Jasperoid Quartz.....	144
REFERENCES CITED	149
VITA	152

LIST OF FIGURES

Figure 1	Location of the Turquoise Ridge deposit (after Bloomstein et al., 1991).....	3
Figure 2	Geologic map showing the location of the Turquoise Ridge deposit (Getchell Mine staff, 1998).	6
Figure 3	Cross-section A-A' along section 300 fence shown in Figure 4 (Culver, 1997; after Berentsen et al., 1996).	7
Figure 4	This Turquoise Ridge deposit map shows section 300 and drill holes from which samples were collected (after the Getchell Corp., 1996).	8
Figure 5	Three cross sections illustrating interpretations of structures at Turquoise Ridge.	14
Figure 6	Pre-ore stage, ore-stage, and late ore-stage mineral pragenesis at the Turquoise Ridge deposit.	30
Figure 7	Pyrite and marcasite are present in samples from the Turquoise Ridge deposit.	31
Figure 8	Photomicrographs of sample TR 95-122 1617.5 showing preferred location of ore-stage pyrite crystals.	35
Figure 9	Photomicrographs of sample TR 95-122 1617.5 showing the two types of quartz taken under crossed polarized transmitted light.	36
Figure 10	Electron microprobe analyses identified quartz (a) and (b), and SEM image (c) shows potassium feldspar inclusions in a sample TR 95-122 1619.5.	37
Figure 11	Photomicrograph of sample TR 94-172 1661.5 shows over-growth textures of ore-stage minerals under crossed polarized transmitted light.	39
Figure 12	Salinities (a) and homogenization temperatures (b) of primary fluid inclusions in pre-ore stage quartz.	45
Figure 13	Salinities (a) and homogenization temperatures (b) of unknown-primary (?) fluid inclusions in pre-ore stage quartz.	46
Figure 14	Salinities (a) and homogenization temperatures (b) of secondary fluid inclusions in pre-ore stage quartz.	47
Figure 15	Salinities (a) and homogenization temperatures (b) of unknown fluid inclusions in pre-ore stage quartz.	48
Figure 16	Salinities (a) and homogenization temperatures (b) of all fluid inclusions in pre-ore stage quartz.	49
Figure 17	Microthermometric data for fluid inclusions in pre-ore stage vein quartz.	50
Figure 18	Microthermometric data for fluid inclusions in pre-ore stage quartz in TR 95-95 1760.5.	51
Figure 19	Microthermometric data for fluid inclusions in pre-ore stage quartz in TR 94-172 1912.4.	53
Figure 20	Microthermometric data for fluid inclusions in pre-ore stage quartz in gouge.	54
Figure 21	Microthermometric data for fluid inclusions in pre-ore stage quartz in gouge in TR 94-172 1865.5.	55
Figure 22	Microthermometric data for fluid inclusions in pre-ore stage quartz in gouge in TR 94-172 1913.	56
Figure 23	Microthermometric data for fluid inclusions in pre-ore stage quartz that are cross-cut by ore-stage mineral assemblage in TR 95-122 1619.5.	58
Figure 24	Microthermometric data for all fluid inclusions in pre-ore stage quartz.	59
Figure 25	Salinities (a) and homogenization temperatures (b) of primary fluid inclusions in ore-stage jasperoid quartz.	62
Figure 26	Salinities (a) and homogenization temperatures (b) of unknown-primary (?) fluid inclusions in ore-stage jasperoid quartz.	63
Figure 27	Salinities (a) and homogenization temperatures (b) of secondary fluid inclusions in ore-stage jasperoid quartz.	64

Figure 28	Salinities (a) and homogenization temperatures (b) of unknown fluid inclusions in ore-stage jasperoid quartz.....	65
Figure 29	Salinities (a) and homogenization temperatures (b) of all fluid inclusions in ore-stage jasperoid quartz.	66
Figure 30	Salinities (a) and homogenization temperatures (b) of primary fluid inclusions in an euhedral ore-stage jasperoid quartz in sample TR 95-122 1617.5.....	68
Figure 31	Primary fluid inclusions in growth zones (a) and results of electron microprobe analyses of pyrite crystals in an euhedral ore-stage jasperoid quartz crystal in TR 95-122 1617.5.	69
Figure 32	Microthermometric data for fluid inclusions in ore-stage jasperoid quartz in TR 95-122 1617.5.	71
Figure 33	Microthermometric data for fluid inclusions in ore-stage jasperoid quartz in TR 95-122 1619.5.	72
Figure 34	Microthermometric data for fluid inclusions in ore-stage jasperoid quartz in gouge in TR 94-172 1913.	73
Figure 35	Microthermometric data for all fluid inclusions in ore-stage jasperoid quartz.....	75
Figure 36	Oxygen and hydrogen isotopic ratios of inclusion fluids in pre-ore, ore, and late-ore stage minerals from the Turquoise Ridge deposit.	81

LIST OF TABLES

Table 1	Results of inductively coupled plasma (ICP) analysis and loss of ignition (LOI) on TR 94-172 1637.5 (the Middle unit) and TR 94-172 1993 (the Lower unit).....	27
Table 2	Results of electron microprobe analyses weight %) on seven pyrite crystals in an euhedral ore-stage quartz crystal in TR 95-122 1617.5.	33
Table 3	Results of electron microprobe analyses on (a) and (b) from TR 95-122 1617.5.....	38
Table 4	Oxygen and hydrogen isotopic ratios of inclusion fluids in pre-ore stage quartz, ore-stage jasperoid quartz, and late-ore stage realgar and calcite..	80

LIST OF ABBREVIATION AND TERMS

$^{\circ}\text{C}$ = degrees in Centigrade.

cm = centimeters.

CO_2Th = temperature at which liquid and vapor CO_2 homogenize to the liquid phase.

CO_2Tmc = temperature at which solid CO_2 hydrate (clathrate) melts.

cps = counts per second

Deg. = degree

deg/min = degree per minute

F. I. = fluid inclusion.

FWHM = Full width half max.

homogenization temperature = temperature at which two phases homogenize to one phase.

km = kilometers.

Ma = million years ago

μm = micrometers.

mm = millimeters.

NaCl equivalent = fluid salinity assuming all salt present is NaCl.

oz/ton = ounce per ton.

ppm = parts per million

py = pyrite.

qtz = quartz.

rlg = realgar.

sec = seconds.

ST. DEV = standard deviation.

Th = homogenization temperature.

Tm = ice melting temperature.

wt. % NaCl equivalent = fluid salinity assuming all salt present is NaCl.

ACKNOWLEDGEMENTS

I would like to give my sincere thanks to thesis committee members Dr. Jean S. Cline, Dr. Margaret Rees and Dr. Wanda J. Taylor, and Graduate College representative Dr. Stephen Lepp.

The following individuals are acknowledged for their contribution to this thesis project. Dick Nanna and the staff of Getchell Gold gave me a permission to collect samples, access to assays and geologic data, and opportunities for discussion. Tracy Cail and Kelli Weaver provided me with electron microprobe data. Adam Merrill helped with sample preparation and provided XRD data. Sarah Lundberg and Nick Wilson assisted with scanning electron microscope studies. Dr. Clay Crow and the staff of Chemical Lime Co., Henderson, Nevada, arranged XRD analyses. Dr. Albert Hofstra at U.S.G.S. Denver, Colorado, conducted oxygen and hydrogen isotope analyses. My thanks also go to Dr. Clay Crow and Jason Smith for maintaining a laboratory and equipment in excellent condition, and providing me with an efficient environment for sample preparation along with their kind encouragement during a difficult time. This project was funded by the Society of Economic Geologists student research grant program, the Ralph J. Roberts Center for Research in Economic Geology at the University of Nevada, Reno, and the Department of Geoscience, University of Nevada, Las Vegas. The Nevada NSF EPSCoR Women in Science and Engineering Program awarded me research assistantships for two academic years and the opportunity to cultivate and demonstrate my academic potential.

I very much thank Tracy Cail, Joel Rotert, Kelli Weaver, and Nathan Williams for their peer reviews and generous friendship. I am especially thankful to Kelli Weaver for walking with me in the hardest rain and always standing by me. I am grateful to Dr. Edward Hasenohr, Julia Johnson, and the students, faculty, and staffs of the Department of Geology at Temple University and the Geoscience Department at University of Nevada, Las Vegas.

I would like to send my most sincere gratitude to my parents who have kept faith in me and supported me unconditionally. Without them, this thesis would not have been completed.

CHAPTER 1

INTRODUCTION

Nevada is currently the third leading gold producer in the world following South Africa and Australia (Nevada Bureau of Mines and Geology, 1997). Gold production in Nevada reached 8.86 million ounces in 1998, which was 76 % of the gold production in the United States and 11 % of the world's gold production (State of Nevada Commission on Mineral Resources, 1999).

Gold exploration in Nevada began in 1849. Placer gold was discovered in the Carson River near the town of Dayton in that year. Further exploration over many years eventually led to a discovery of disseminated gold in sedimentary host rocks in northern Nevada. In 1962, a large gold deposit containing invisible gold was discovered near a town named Carlin. This deposit, which contains gold disseminated in Paleozoic calcareous host rocks, was named the Carlin gold deposit. With the discovery of additional similar deposits, mining of disseminated gold in northern Nevada became a valuable sector of the mineral industry. Growth in the gold mining industry consequently brought local communities economic growth.

The economic impact of the mining industry in Nevada communities is significant. In 1996, the mining industry in Nevada provided 14,400 jobs with an average annual salary \$47,540 compared to the average salary of \$26,630 per employee in Nevada (State of Nevada Commission on Mineral Resources, 1999). In 1995, about \$141 million of tax revenues were paid by the mining industry to the state of Nevada (State of Nevada Commission on Mineral Resources, 1999). In addition to the economic resources, mining companies donate public services to local communities such as building schools and transportation.

While gold production in Nevada increases, the loss of gold reserves becomes an important issue. Decline in gold exploration and production will eventually lead to economic depression in mining towns and loss of revenue for the state of Nevada. The estimated geologic reserves of gold in Nevada were approximately 88 million ounces in 1998, which, at a gold price of \$300 per ounce, is worth \$26.4 billion (State of Nevada Commission on Mineral Resources, 1999). These geologic gold reserves could sustain the mining industry for another twenty to thirty years (State of Nevada Commission on Mineral Resources,

1999); however, mining operations must be profitable to continue. Gold prices fluctuate and recently were as low as \$270 per ounce; therefore, drilling and exploration expenses need to be minimized. Currently, the gold reserves are growing as mining from surface oxide pits is converted to underground operations. Limiting the number of exploration sites requires less expenditure, and also protects wild life and environments from destruction. To improve the effectiveness of exploration and reduce exploration expenditure, an improved understanding of the geology of Carlin-type gold deposits is necessary.

Despite the growth of Carlin-type gold production and its economic contribution, the source of gold, ore fluids, and geologic processes that concentrated gold mineralization are still unknown. A better understanding of these aspects of Carlin-type gold systems will help to economically mine current reserves and discover new ore bodies in Nevada as well as extend gold exploration into regions that have had geologic histories similar to those of Carlin-type gold deposits.

The Turquoise Ridge gold deposit, the subject of this study, is located 72 km northeast of Winnemucca, Nevada, and approximately 600 meters northeast of the Getchell gold deposit (Figure 1). Oxidized gold mineralization at the surface of the Turquoise Ridge deposit was discovered in 1993 as part of an extensive mapping program near the earlier discovered and better known Getchell deposit. Although the gold at the surface was economically insignificant, it led to the discovery of large deep ore bodies and current economic gold production from the Turquoise Ridge underground mine. Disseminated gold mineralization in Lower Paleozoic calcareous sedimentary host rocks at Turquoise Ridge is a characteristic of Carlin-type gold. However, the Turquoise Ridge ore body occurs at greater depth than many Carlin-type gold deposits. The Turquoise Ridge ore body is approximately 244 meters in width, 305 meters in length (Getchell Gold Corp., 1996), and extends from 420 meters to 840 meters below the current surface at Turquoise Ridge (Berentsen et al., 1999). The minable gold reserve at the Turquoise Ridge underground mine is 3.7 million tons averaging 0.338 ounces of gold per ton (Getchell Gold Corp., 1996).

In this study, mineral assemblages and related fluid inclusions at the Turquoise Ridge gold deposit were examined to answer the following questions: (1) What is the ore-stage mineral paragenesis? (2) At what pressures and temperatures did the deposits form? (3) What are the sources of ore fluids? Mineral assemblages were studied to determine which minerals precipitated with gold. Fluid inclusions in these ore-stage minerals were evaluated to determine fluid salinities and minimum trapping pressures and

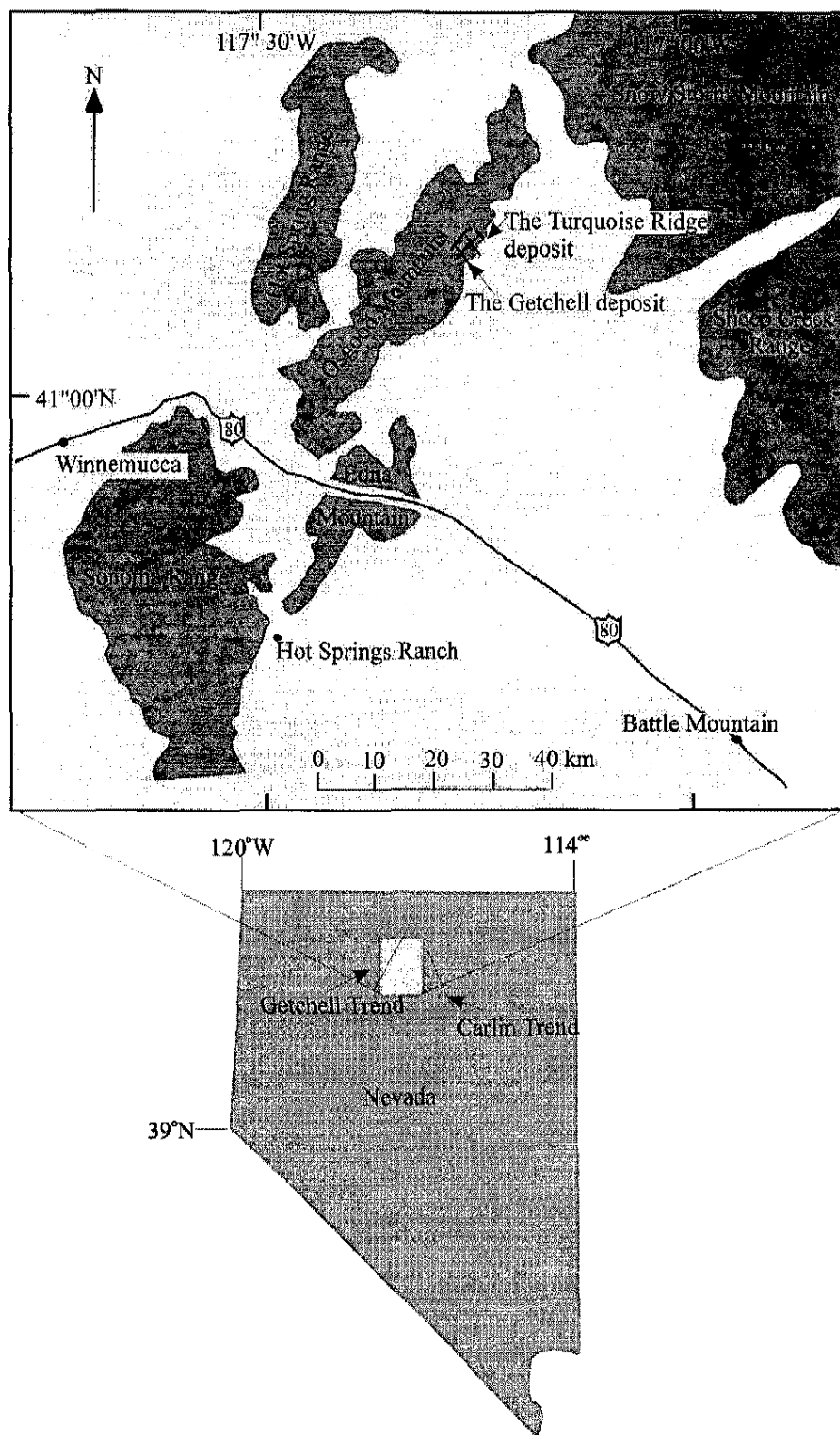


Figure 1. Location of the Turquoise Ridge deposit (after Bloomstein et al., 1991).

temperatures. Oxygen and hydrogen isotopic ratios of inclusion fluids were determined to identify fluid sources.

The genetic relationship between the Turquoise Ridge and the Getchell deposits was also examined. Although the two deposits are only 600 meters apart, previous studies at the Turquoise Ridge and the Getchell deposits indicate differences in mineral paragenesis, ore deposition mechanisms, and sources of ore fluids. One difference is the number of gold mineralization events. Cline (1999) observed a single gold hydrothermal event at the Getchell deposit, but Groff's study (1996) suggested multiple stages of mineralization including two gold stages. The depth of the ore body at the Turquoise Ridge deposit may indicate that it is a deeper part of the same system as Getchell, or the two deposits may have formed separately. General geology and previous studies at the Turquoise Ridge deposit (Groff, 1996) and the Getchell deposit (Groff, 1996; Cline et al., 1997; Cline, 1999) are discussed in the next chapter. Data and interpretations from these previous studies will be evaluated in light of finds in this study. Additionally, studies of the Getchell deposit provide information that is not available at the relatively new and less understood Turquoise Ridge deposit.

CHAPTER 2

GENERAL GEOLOGY

Investigation of the Turquoise Ridge Deposit

In this chapter, important factors that control the location of Carlin-type gold ore bodies, ore-associated alteration and mineralization, conditions of gold deposition, and possible sources of ore fluids are discussed. Previous studies at the Turquoise Ridge deposit (Groff, 1996), the Getchell deposit (Groff, 1996; Cline, 1999), and other Carlin-type gold deposits are used to address and subsequently evaluate the similarities and differences among them and the finding of this Turquoise Ridge study. Gold mineralization at the Turquoise Ridge deposit is along a high angle normal fault and extends into contact zone between the Cambrian and Ordovician silt- or clay-rich dolomite and limestone units and that are folded and cross cut by the fault. The close proximity of gold mineralization to the high-angle Turquoise Ridge fault suggests that the fault served as a conduit for hydrothermal fluids to migrate upward and deposit gold.

Stratigraphy

In north-central Nevada, a regionally extensive succession of Cambrian and Ordovician silt- or clay-rich calcareous dolomite and limestone units include the Cambrian Preble, Upper Cambrian to Ordovician Comus, and Ordovician Valmy Formations (Figure 2, 3, and 4). The eastern facies of the Preble and Comus formations contain shallow marine carbonate and shale successions that grade westward into a deep marine siliceous and volcanic facies, the Valmy Formation. The western facies were thrust and emplaced over the eastern facies during the Late Devonian to Early Mississippian. Stratigraphic units have been obscured at the Turquoise Ridge deposit by overprinting of multiple periods of alteration and tectonic deformation. Consequently, Turquoise Ridge geologists assigned the names of Lower Sediments and mine. Middle Sediments to Paleozoic host rocks at the Turquoise Ridge deposit based on vertical position at the mine. Also, colors of rocks are used to identify Lower Sediments and Middle Sediments. The black Lower

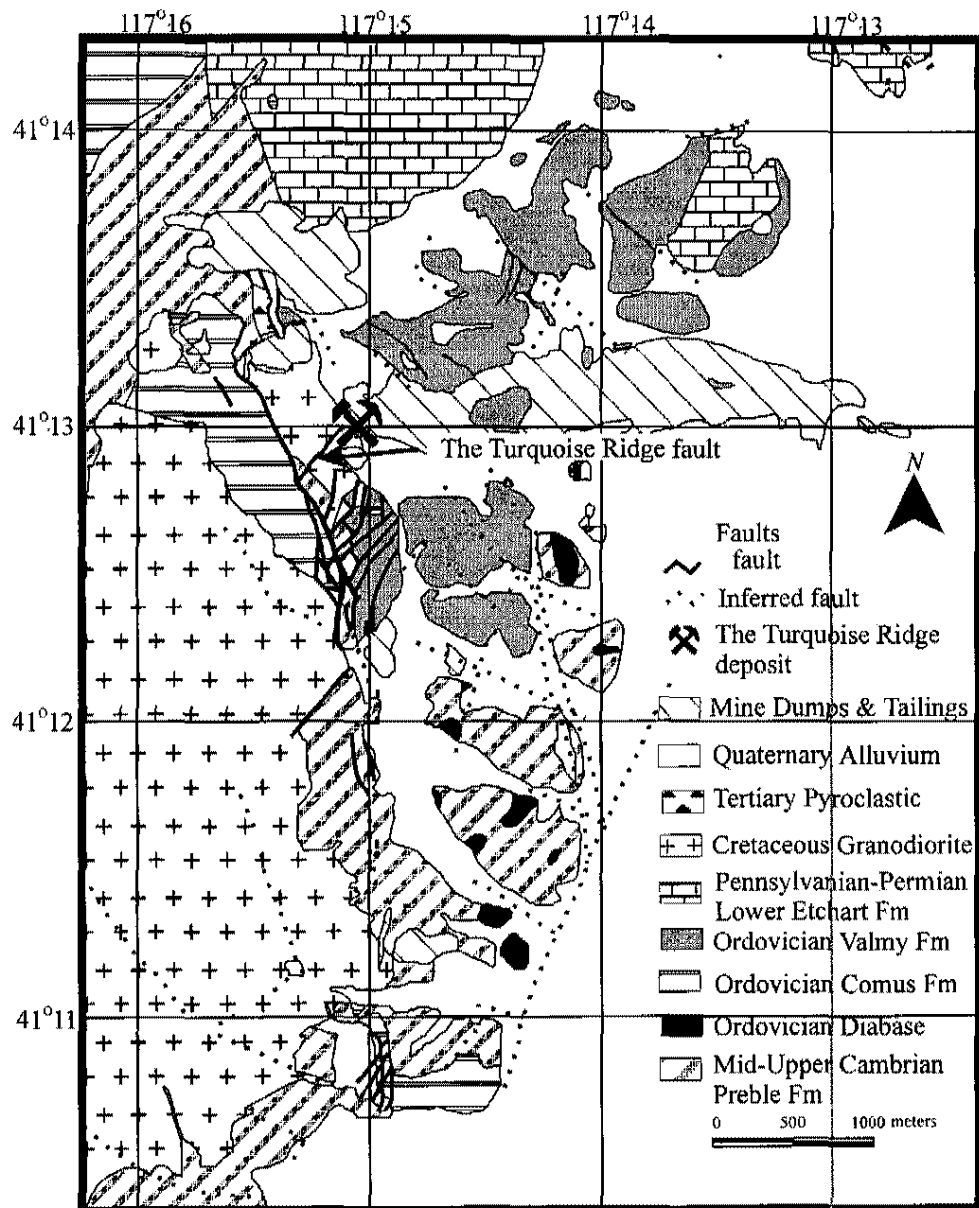


Figure 2. Geologic map showing the location of the Turquoise Ridge deposit (Getchell Mine staff, 1998).

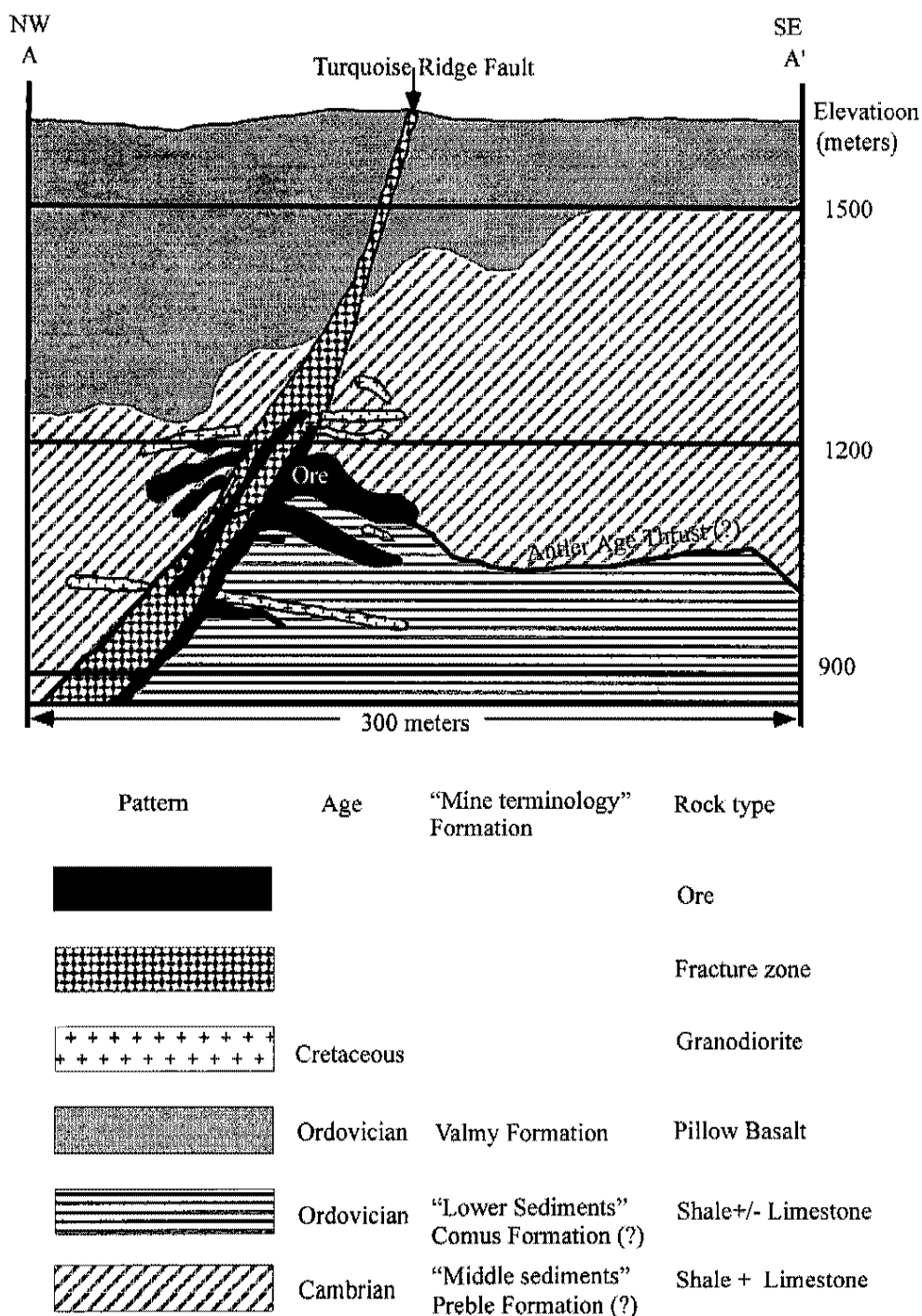


Figure 3. Cross-section A-A' along section 300 fence shown in Figure 4 (Culver, 1997; after Berentsen et al., 1996). Tailings are not shown on the cross section. Contact between Valmy and Middle Sediments may be fault rather than the depositional contact shown.

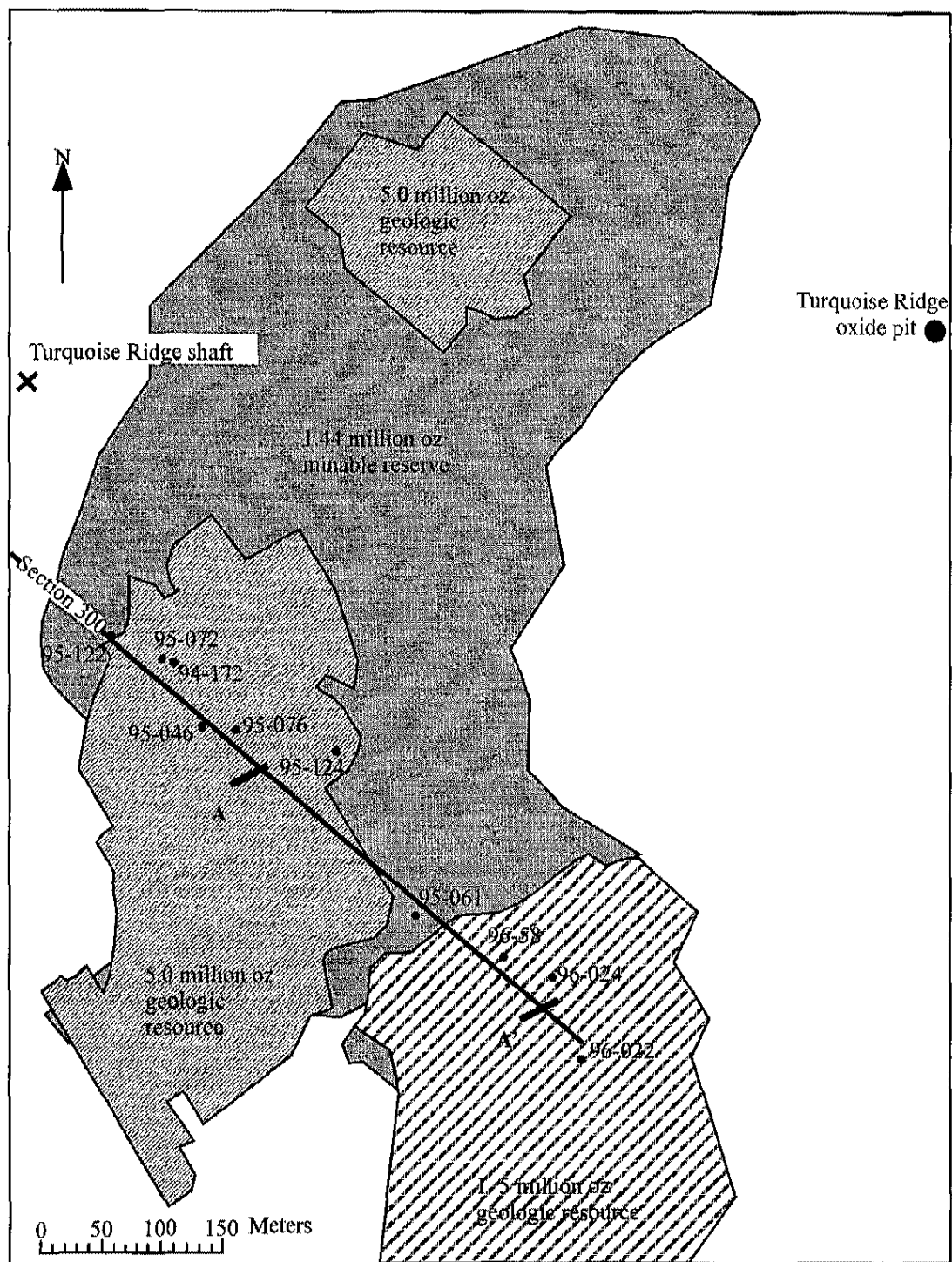


Figure 4. This Turquoise Ridge deposit map shows section 300 and drill holes from which samples were collected (after the Gatchell Corp., 1996).

Sediments and the brown Middle Sediments have been tentatively referred to the Ordovician Comus and the Cambrian Preble Formations, respectively, by Turquoise Ridge mine geologists (Culver, pers. comm., 1997; Figure 3).

Within north-central Nevada, deformed Cambrian phyllitic shale, sandstone, and limestone commonly comprise the Preble Formation (Hotz and Willden, 1964; Madden-McGuire, 1991; Rees and Rowell, 1980). The Preble Formation crops out on the southeastern flank of the Osgood Mountains, Edna Mountain, and the eastern flank of the Sonoma Range (Figure 1). The lower Preble Formation contains both clastic and carbonate sedimentary rocks but dominantly consists of phyllitic shale, and bioclastic and hemipelagic limestone (Rees and Rowell, 1980). The middle Preble is heterogeneous with successions of interbedded shale and quartz-rich sandstone, and interbedded phyllitic shale and limestone that were deposited by sediment gravity flows from the shelf. The upper Preble Formation consists of dominantly phyllitic shale and siltstone with rare shelf-derived limestone. This succession was deposited in a deep outer shelf environment with a carbonate platform to the east and an ocean basin to the west (Dickinson, 1992).

Black shale, tuffaceous shale, dolomite, limestone, and minor amounts of chert and siltstone comprise the Upper Cambrian to Ordovician Comus Formation in north-central Nevada (Hotz and Willden 1964; Hsu et al., 1995). The lower part consists of black to dark gray, thin-bedded shaly chert. Dolomitic limestone and dolomite are the primary components in the upper Comus Formation. The Comus Formation or the equivalent unit (the Lower Sediments) also contains basalt, pillow lava, flow breccia, tuff, and hyaloclastite (Smith and Ketner, 1964; Madden-McGuire and Marsh, 1991; Berentsen et al., 1996).

The Comus Formation indicates depositional environments that graded eastward from an anoxic low-energy ocean-floor to a shelf, and may have interfingered with the Upper Preble Formation. This relationship is consistent with faunal data indicating that the lower Comus Formation may be as old as late Cambrian (Hotz and Willden, 1964). Determination of the stratigraphic position of the Comus Formation is difficult because the unit is fault bounded at Turquoise Ridge. However, graptolites and trilobites suggest that the age of the Comus Formation is Early to Middle Ordovician, and maybe as old as Late Cambrian (Hotz and Willden, 1964). Graptolites and trilobites in the Valmy Formation are of Early Ordovician age (Hotz and Willden, 1964). The presence of pillow basalt indicates that the depositional environment of the Comus Formation also overlapped or interfingered with the Valmy Formation.

Previous studies suggested that the contact between the Preble and Comus Formations was a thrust in the Osgood Mountain quadrangle (Hotz and Willden, 1964; Madden-McGuire and Marsh, 1991). However, the contact was described as depositional at the Turquoise Ridge deposit (Berentsen et al., 1996). This controversy is discussed further in the following structure section.

The Ordovician Valmy Formation in north-central Nevada commonly consists of chert, quartzite, siliceous shale, siltstone, sandstone, minor limestone, and bedded barite (Roberts, 1964; Hotz and Willden, 1964). Altered volcanic rocks are also present, and pillow lava is metamorphosed to greenstone. The occurrence of interbedded siliciclastic rocks and pillow basalt with minor tuff and hyaloclastite in the Valmy Formation indicates submarine volcanic activity. The occurrence of interbedded siliciclastic sediments and alkaline basalt suggests the source of the basalt was a volcanic arc that developed along the continental margin (Poole et al., 1992).

At the Turquoise Ridge deposit, the Middle Sediments that may correlate with the Cambrian Preble Formation consist of alternating brown fissile biotized phyllitic shale and thick-bedded limestone. Shale and limestone locally were metamorphosed to hornfels and marble that host the ore (Madden-McGuire and Marsh, 1991).

The black Lower Sediments, which may correlate with the Ordovician Comus Formation, consists of siliceous and carbonaceous shale, and locally recrystallized silty limestone (Berentsen et al., 1996). These rocks were also locally metamorphosed to phyllite and marble. A diabase sill that is genetically and temporally related to the basalt flow in the lower Ordovician Valmy Formation (Berentsen et al., 1996) intruded the calcareous sedimentary rocks.

At the Turquoise Ridge deposit, the lower 152 to 305 meters of the Valmy Formation represent a submarine volcanic environment. Basalt flows, pillow lava, flow breccia and lithic tuff are present (Berentsen et al., 1996). Interbedded shale and chert of the Valmy Formation host uneconomic gold mineralization in oxide pits at the Turquoise Ridge deposit. The lower part of the succession mainly consists of submarine volcanic sedimentary rocks. Interbedded chert, siliceous black shale (hyaloclastites), quartzite, and minor lithic tuff comprise the upper part and overlie the basalt flows and pillows (Berentsen et al., 1996). These deep marine sediments were regionally metamorphosed to greenstone and hornfels.

In some locations within the deposit, the gold mineralization occurs along bedding, which suggests the importance of stratigraphic control in part of the ore body. Figure 3 from Berentsen et al. (1996) shows that the carbonate units host the ore bodies in preference to the Valmy Formation.

Discussion of Stratigraphy

Formal identification of the stratigraphic units at the Turquoise Ridge deposit is difficult because of overprinting of multiple periods of alteration and structural deformation. Although the Paleozoic host rocks have been referred to as the Cambrian Preble Formation and the Ordovician Comus Formation at the Turquoise Ridge deposit, identification of these formations has been questioned. Berentsen et al.'s (1996) study suggested that the Ordovician Comus Formation overlies the Cambrian Preble Formation. A recent study (Culver, pers. comm., 1997) suggests that the Preble Formation overlies the Comus Formation in an overturned antinclinal fold. Because of the controversy over the identification of stratigraphy, currently, Turquoise Ridge mine geologists use the terms Middle Sediments and Lower Sediments to refer to discrete identifiable stratigraphic units and do not use formal stratigraphic nomenclature (Berentsen, pers. comm., 1997).

In addition, the contacts between each of the stratigraphic units have been variably interpreted as both depositional and structural. The contact between the Lower Sediments (Comus?) and Middle Sediments (Preble?) was mapped as a thrust by Berentsen et al. (1996). A recent study (Culver, pers. comm., 1997) suggested that the contact was depositional and an overturned anticline placed the older Middle Sediments above the younger Lower Sediments. Hotz and Willden (1964) suggested that the contact between these two formations is a high-angle reverse fault.

The contact between the Middle Sediments and the overlying Valmy Formation has also been variably interpreted. It was mapped as depositional by Berentsen et al. (1996), but was suggested to be a thrust by Hotz and Willden (1964). The controversy regarding the contacts between units has yet to be resolved and is beyond the scope of this thesis. Throughout this study, the two units hosting the gold at Turquoise Ridge will be referred to as the Lower unit and Middle unit implying no stratigraphic or structural relationships, but mere vertical occurrence at the mine.

Structure

At least one major structure and possibly other structures control distribution of gold mineralization at the Turquoise Ridge deposit (Figure 3). These structures may have formed during any of four orogenic events: the Late Devonian to Early Mississippian Antler Orogeny, the Late Permian to Early Triassic Sonoma Orogeny, the Mid-late Jurassic to Mid-Cretaceous Sevier Orogeny, or Cenozoic extension that eventually formed the Basin and Range province (Miller et al., 1992; Dickinson, 1992).

Regionally, during the Late Devonian and Early Mississippian Antler Orogeny, deep marine siliceous and volcanic deposits were thrust eastward and placed over shallow marine carbonate sediments in which the ore bodies subsequently were deposited (Miller et al., 1992). Berentsen et al. (1996) suggested that compressional stress during the orogeny probably generated N30°E trending recumbent isoclinal folds and fracture zones, which strike N30°E and dip 45 to 60° NW at Turquoise, although there was no evidence presented to support this hypothesis.

Regional contraction of strata also resulted from the Late Permian to Early Triassic Sonoma Orogeny that emplaced the Golconda allochthon (Burchfiel et al., 1992), and resulted from the Mid-late Jurassic to Mid-Cretaceous Sevier Orogeny. This contraction may have brought Turquoise Ridge host rocks to the surface, and subjected strata to weathering (Berentsen et al., 1996). Overprinted structures suggest polyphase or multiple contractions: a N35°W trending fold created a dome by refolding an older fold, and a fault, called an Antler-age by Berentsen et al. (1996) was folded (Figure 3). The age of refolding was suggested to be Jurassic, however, no data were provided to support this age. The Turquoise Ridge deposit is proximal to both Sonoma and Sevier orogenic belts. Older structures, therefore, could have been refolded during either the Sonoma or Sevier orogenies.

A previous study at the Turquoise Ridge mine (Berentsen et al., 1996) suggests that in the Oligocene, E-W extension of the region resulted in motion along a high-angle normal fault (the Turquoise Ridge fault; Figure 3), along which the ore body developed. The normal fault cuts the Cretaceous intrusion and offsets gold mineralization indicating reactivation of the fault after the gold mineralization (Reid, pers. comm., 1995). This high-angle fault, which strikes N43°E and dips approximately 65°NW along the section 300 fence (Figure 4), intersects a fracture zone (Berentsen et al., 1996). The presence of gold mineralization in the Turquoise Ridge fault indicates that this high-angle normal fault served as a conduit for hydrothermal

fluids to migrate upward and deposit gold. The development of an ore body along the intersection of a normal fault and fracture zone is common in many Carlin-type gold deposits.

Discussion of Structure

Overprinting of faulting and folding, and the lack of detailed mapping in the region makes construction of cross sections and determination of ages of folds and faults difficult at the Turquoise Ridge deposit. Consequently, structural and stratigraphic relationships remain controversial. The published cross section by Berentsen et al. (1996) does not illustrate the fold described in the text. Additionally, the ages of faults and folds suggested by the study (Berentsen et al., 1996) lack sufficient evidence from which one can draw well-founded conclusions regarding timing of structural events. Three diagrammatic cross sections that may aid in illustrating the controversial interpretation of structures at the Turquoise Ridge deposit are presented here (Figure 5 a, b, and c). Although each cross sections exhibits part of the structural history at the Turquoise Ridge deposit, they are not entirely consistent with each other on either regional scale or in structural history because of the lack of datable minerals and lack of needed mappable relationships. However, they provide an abstract framework and depict the complexity of structures at the Turquoise Ridge deposit.

The location of the Roberts Mountains thrust at the Turquoise Ridge deposit is controversial. The Roberts Mountains thrust classically divides the mineralized eastern from non-mineralized western assemblages at many Carlin-type gold deposits. However, the Antler thrust contact was mapped within the eastern assemblage at the Turquoise Ridge deposit (Berentsen et al., 1996). This interpretation puts the Comus Formation above the Preble Formation. This contact was variably interpreted as depositional (Kreschmer, 1984), a low-angle reverse fault associated with the Basin and Range extension in late Eocene (Hotz and Willden, 1964; Thorman et al., 1991), and a detachment structure associated with intrusion of a Cretaceous granodiorite pluton (Reid, 1995). Alternatively, if the older Middle Sediments overlies the younger Lower Sediments as suggested by recent study (Culver, pers. comm., 1997), the contact between the two units may be structural. However, this disagrees with the interpretation that the Antler-age Roberts Mountains thrust that typically placed the western deep-water near-arc Valmy Formation over the eastern carbonate shelf and platform Comus Formation (Hotz and Willden, 1964) because at Turquoise Ridge the

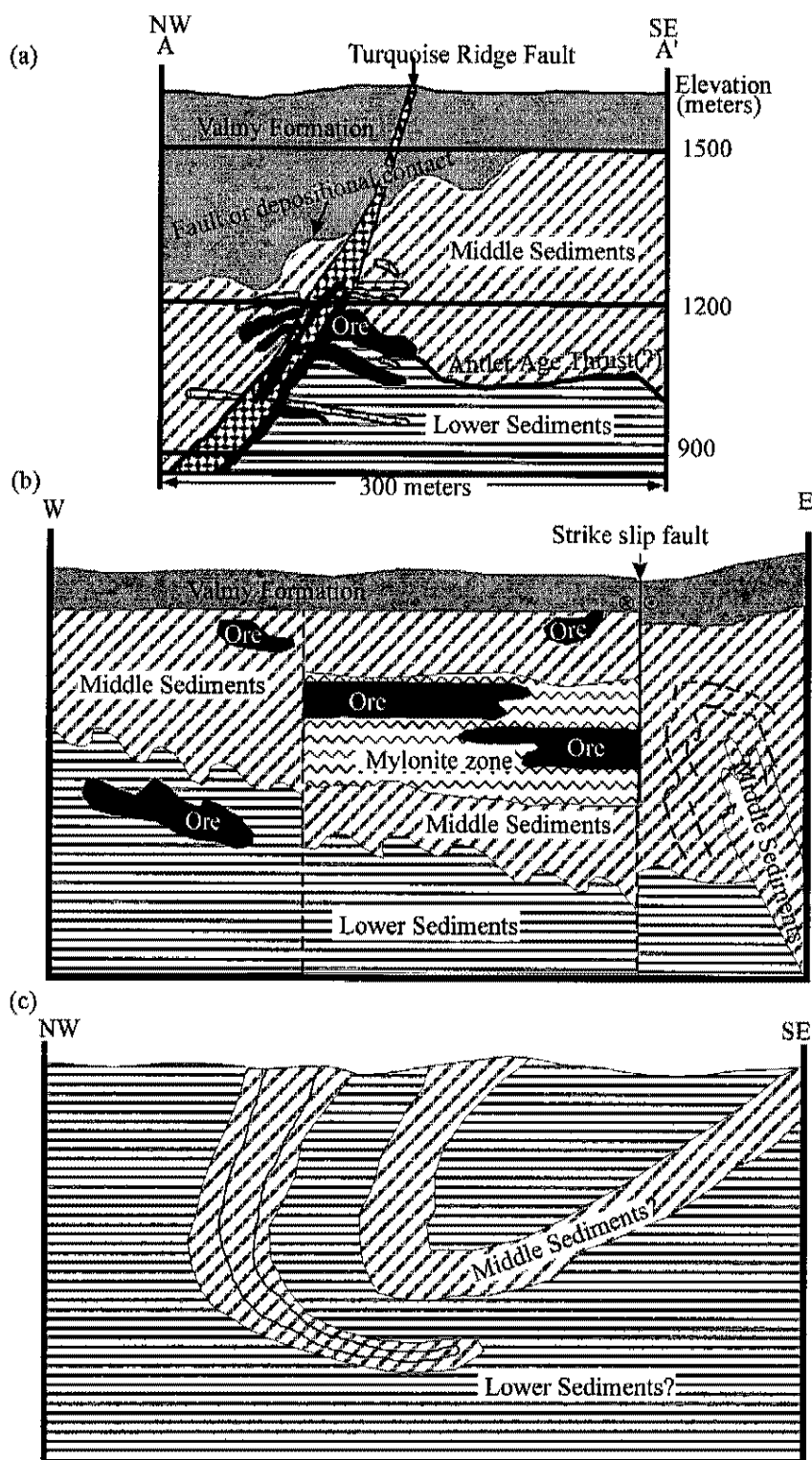


Figure 5. Three cross-sections illustrating interpretations of structures at Turquoise Ridge. Sketches (a) and (c) are not to scale. See Figures 2 or 3 for explanation of symbols.

(a) A cross-section along section 300 fence (after Berentsen et al., 1996; Culver, 1997)

(b) An isoclinal recumbent fold offset by a high-angle fault (Culver, 1997)

(c) Refolding of an older fault (Reid, 1995).

Preble Formation lies between the Comus and Valmy formations (Culver, pers. comm., 1997). It is, therefore, reasonable to conclude that the deep marine sediments of the Valmy Formation were thrust over the shallow shelf succession, and the contact between the Comus and Preble Formations would be a fault but not the Antler-age Roberts Mountains thrust.

If the contact between the Preble and Comus formations is a detachment fault associated with the Eocene extension or an Antler-age thrust, the age of gold mineralization, 42 Ma, suggested by Groff (1996) is permissive. Gold mineralization cannot predate the faulting event because the ore bodies occur along the contact between the two units that is crosscut by the Turquoise Ridge fault. In addition to the ore-related hydrothermal event in the late Eocene, Groff's study (1996) suggested that the first main gold mineralization occurred 80 to 83 million years ago. This event does not seem to temporally correspond to any structures at the Turquoise Ridge deposit. The contact between the Preble and Comus Formations, in any case, is older than gold mineralization but younger than the normal fault that cross cut the Preble and Comus contact.

The Turquoise Ridge fault is younger than Cretaceous because it cuts the Cretaceous granodiorite intrusion (Hotz and Willden, 1964). The ore bodies are confined in the fracture zone along the high-angle Turquoise Ridge fault, and the contact between the Preble and Comus formations. If the Turquoise Ridge fault served as a feeder zone for hydrothermal ore fluids, the fault is older than the ore hydrothermal event. Therefore, the age of the Turquoise Ridge fault is Eocene or older but younger than Cretaceous. Structural studies at the mine suggest that during the Oligocene the Turquoise Ridge fault was reactivated based on offset in the ore body.

Alteration

Decarbonatization, silicification, sulfidation, and argillization are important alteration assemblages associated with gold mineralization at the many Carlin-type gold deposits (Arehart, 1996). Although alteration has not been specifically studied at the Turquoise Ridge deposit, the Turquoise Ridge ore bodies occur in intensively silicified rocks and are associated with pyrite (Groff, 1996), which are general characteristics of the Carlin-type gold deposits.

Decarbonatization involves the removal of carbonate in calcareous sedimentary host rocks by reaction with an acidic fluid, and increased the porosity and permeability of wall rock. Volume decrease of wall rock due to decarbonatization may have resulted in brecciation in some cases (Hofstra et al., 1991). Decarbonatization provided space for fluids to migrate and react with the rocks, leading to precipitation of gold and associated minerals. The degree of decarbonatization depended on the lithology of wall rock. Originally permeable silty or sandy to calcareous carbonates are more strongly altered than mudstone and shale (Archart, 1996). Removal of carbonate from host rocks also exposed iron in host rocks to the ore fluids, initiating sulfidation (Hofstra et al., 1991).

A positive correlation between the degree of pyritization and gold indicates that sulfidation contributed to ore deposition (Hofstra et al., 1991). Ore fluids transporting bisulfide-complexed gold reacted with iron in host rocks, precipitating pyrite and gold. At the Getchell deposit, ore fluids with minor CO₂ were responsible for decarbonatizing calcareous host rocks, and transporting and precipitating gold (Cline, 1999).

Jasperoid quartz and gold mineralization are commonly spatially related at Carlin-type gold deposits. Solid calcite inclusions in quartz indicate silicification and replacement of carbonate by silica during ore-stage mineral deposition.

Argillization is recognized in Carlin-type deposits at the mine scale; however, it is difficult to distinguish ore-stage clay minerals from non-ore stage clay minerals (Archart, 1996). In the Carlin deposit, Kuehn and Rose (1992) observed replacement of sericite by kaolinite and dickite near ore fluid conduits. The presence of kaolinite and dickite indicates that fluids had a pH of 3-4 and temperature ranged from ~150° to 250°C (Thompson et al., 1996). Sericite and illite are present in some deposits; however, these minerals may have formed during non-ore related events.

Previous Studies of Ore and Non-Ore Mineral Assemblages

Study by Groff (1996) describes mineral assemblages at the Turquoise Ridge deposit, and Groff's (1996) and Cline's (1999) studies examine mineral assemblages at the adjacent Getchell deposits, respectively. Cline (1999) defined a pre-ore mineral assemblage that contains vein quartz and pyrite associated with intrusion of a granodiorite stock. Additionally, trace sphalerite, chalcopyrite, galena, and a

fine-grained mica, perhaps sericite in altered granodiorite, comprise the pre-ore mineral assemblage. This assemblage is fractured, and fractures are filled with gold ore-stage minerals. Assays indicated that gold is not present in pre-ore minerals, and ion microprobe analyses showed no or minor gold and arsenic in pre-ore stage pyrite (Cline, 1999).

Pyrite in the Getchell ore-stage assemblage is finely crystalline and framboidal, and contains 1.7 to 15 weight % arsenic (Cline et al., 1997). Ore-stage pyrite commonly has a pre-ore stage pyrite core with an ore-stage porous rim. Secondary ion mass spectrometry analyses identified as much as 600 ppm gold in the fine-crystalline rims and demonstrated a strong positive correlation between gold and arsenic. These fine, gold-bearing pyrite crystals were encompassed by jasperoid quartz and also occur along boundaries between jasperoid quartz crystals. Minor orpiment and fluorite additionally comprise the ore-stage mineral assemblage.

Realgar, calcite, and minor pyrite, marcasite, and stibnite comprise the late-ore assemblage at the Getchell deposit (Cline, 1999). Both realgar and calcite exhibit open-space-filling textures. Where realgar occurs in contact with ore-stage jasperoid quartz, the realgar contains gold-bearing pyrite. This pyrite is absent in massive realgar not associated with ore-stage jasperoid. The presence of rare fine gold-bearing pyrite in realgar indicates that the formation of gold-bearing pyrite continued to the beginning of late-ore stage deposition.

Groff (1996) suggested five stages of gold mineralization occurred at the Getchell and Turquoise Ridge deposits. Ages of economic gold mineralization were determined to be 83 and 42 Ma using $^{40}\text{Ar}/^{39}\text{Ar}$ methods on adularia and biotite, respectively. One primary biotite, one primary feldspar, and one hydrothermal biotite were collected from the Getchell deposit. One primary hornblende and one secondary K-feldspar were collected from the Getchell underground. The Turquoise Ridge deposit provided one primary biotite. Stage one mineralization according to Groff (1996) occurred at 95 Ma and consisted of igneous intrusion and formation of a pyrrhotite-rich skarn. Stage two occurred 3 million years after stage one, and consisted of base metal mineralization associated with gold. Stage three, at 83 Ma, was the major gold event at the Getchell deposit, and quartz, finely crystalline pyrite, arsenopyrite, potassium feldspar, sericite, and kaolinite were associated with gold mineralization. During stage four at 75 Ma, gold mineralization occurred in pyrite-rich quartz in the matrix of a localized hydrothermal breccia.

Groff's (1996) final stage of mineralization was economic and occurred at 42 Ma and contains realgar, quartz, pyrite, and stibnite followed by precipitation of orpiment, calcite, and potassium feldspar. The mineralization overprinted stage three, and mineralization exhibits primarily open-space-filling textures.

The distinction between stages three and five gold mineralizing events was made based on the ratio of gold to silver deposited during these two events and the presence of orpiment-realgar mineralization in stage five (Groff, 1996). Stage three exhibited 1:1 silver to gold ratio and lacked orpiment and realgar. Stage five mineralization showed low silver to high gold ratios of 1:100 and is associated with orpiment and realgar in the Getchell open pit.

Pressures and Temperatures during Gold Mineralization

Fluid inclusion studies at the Getchell open pit mine (Cline, 1999) show that ore fluids were trapped in ore-stage jasperoid quartz at minimum temperatures of 180 ° to 220 °C, and salinities of ore fluids ranged between 4 and 5 wt. % NaCl equivalent. Quadrupole mass spectrometer gas analyses detected CO₂ and H₂S in ore-stage inclusions. Secondary three-phase H₂O-CO₂ inclusions in fluorite indicate a minimum pressure of 330 bars sometime during or after deposition of gold (Cline, 1999). Assuming lithostatic pressure during trapping, the estimated minimum depth of the system during trapping of inclusions in fluorite was ~1.5 kilometers.

Groff's microthermometric data and results of gas analyses (1996) suggested periodic injection of boiling fluids from degassing of a deep igneous intrusion during the hydrothermal event. Groff (1996) studied samples from the Turquoise Ridge deposit, and obtained homogenization temperatures as high as 360 °C and salinities as high as 41 weight % NaCl equivalent from inclusions in stage three jasperoid quartz and stage five calcite. Fluid inclusions in quartz associated with barren realgar, pyrite and stibnite homogenized at 100 ° to 110 °C and did not indicate boiling. Boiling was indicated by fluid inclusions in stage five quartz and orpiment, which homogenized at 140 ° to 160 °C. Fluid inclusions in realgar and banded calcite indicated a change from boiling to non-boiling conditions during the deposition of these minerals. The non-boiling event was followed by another period of gold mineralization and fluid boiling. Fluid inclusions in later stage five barite and calcite indicated that the condition returned to non-boiling and gold mineralization ceased. Gas analyses (Groff, 1996) showed that ore fluids had high concentrations of

CH₄ and N₂. According to pressure calculations based on the microthermometric data and gas compositions, Groff et al. (1997) determined that gold mineralization occurred at a maximum depth of 5 km at 92 Ma, 2 km at 83 Ma, and < 1 km at 42 Ma.

Origins of Ore Fluids Indicated by Oxygen and Hydrogen Isotopic Signatures

Oxygen and hydrogen isotopic signatures of inclusion fluids in ore-stage minerals from the Getchell open-pit deposit indicate a deep fluid source (Cline et al., 1997). The oxygen values from Getchell are similar to oxygen signatures from deposits on the Carlin Trend; however, the hydrogen isotopic signatures of the Getchell inclusions in ore-stage quartz range from -50 to -97 ‰ (Cline et al., 1997). These signatures indicate a magmatic or metamorphic ore fluid source. Signatures of fluids in calcite, $\delta D_{H_2O} = -69$ to -125 ‰ and $\delta^{18}O_{H_2O} = 14$ to 2 ‰, are interpreted to result from mixing of ore fluids and evolved meteoric fluids (Cline et al., 1997). Inclusions in late-ore stage realgar have $\delta^{18}O_{H_2O}$ values and δD_{H_2O} close to meteoric fluid signatures. These inclusions are interpreted to have trapped post-hydrothermal fluids.

Groff's (1996) isotopic signatures of inclusion fluids from stage three and five minerals from Turquoise Ridge and Getchell exhibit a larger range of values than those determined for Getchell inclusions by Cline et al. (1997). Data indicate that barren fluids and ore-stage fluids have different isotopic signatures. δD_{H_2O} and $\delta^{18}O_{H_2O}$ isotopic signatures of stage three quartz range between -75.9 and -153 ‰ and between 5.2 and 11.8 ‰, respectively. $\delta^{18}O_{H_2O}$ from stage five quartz from Getchell range from -3.7 to 12.8 ‰. δD_{H_2O} values of stage five quartz inclusions were not determined. Stage five calcite inclusions range in δD_{H_2O} between -88 and -134 ‰, and $\delta^{18}O_{H_2O}$ range from -9 to 11.3 ‰. Gas analyses indicating high concentrations of CH₄ and N₂ suggested that the negative isotopic signatures resulted from fluid interaction with organic black shale. Groff (1996) concluded that the positive $\delta^{18}O_{H_2O}$ values and significantly negative δD_{H_2O} values reflected mixing of magmatic fluid and fluid that reacted with organic shale, and that microthermometric data, gas, and stable isotope analyses indicated a magmatic contribution to the gold mineralizing event.

δD_{H_2O} signatures of inclusion fluids from the Getchell and Turquoise Ridge deposits are higher than those determined for other Carlin-type gold deposits. δD_{H_2O} and $\delta^{18}O_{H_2O}$ signatures of inclusion fluids from other Carlin-type gold deposits are generally ~ -150 ‰, and -10 ‰ to $+5$ ‰, respectively (Arehart, 1996).

CHAPTER 3

METHODS OF STUDY

Sample Collection

To examine host rocks, mineral parageneses, fluid inclusions, and oxygen and hydrogen isotopes of inclusion fluids, approximately 600 core samples were collected from 17 drill holes along section 300 of the Turquoise Ridge gold deposit during June, 1997 (Figure 3). Section 300 (Berentsen et al., 1996; Figure 3) is a transect across the central ore zone of high-grade mineralization in the Turquoise Ridge deposit. Sample selection criteria were based on mineralogical description in previous studies at the Getchell deposit (Groff 1996; Cline, 1999) and the Turquoise Ridge deposit (Groff, 1996), and assay data of drill core intervals. Samples were collected from non-ore grade assemblages that typically contain quartz and pyrite in veins and recrystallized calcite. Proximal to mineralized zones, the sampling interval was shortened to examine zoning of hydrothermal alteration related to the ore-forming event. Decarbonization, silicification, and the presence of fine pyrite crystals were indicators of ore-grade mineralization. In particular, samples of coarse jasperoid quartz, orpiment, calcite, and realgar, that would provide paragenetic information and contain fluid inclusions, were selected. Samples numbers indicate the drill hole number (e.g. TR 94-172) followed by footage (e.g. 1609.5).

X-ray Diffraction and Inductively Coupled Plasma Analyses

To identify major minerals in unmineralized host rocks, x-ray diffraction (XRD) was conducted on drill core samples from TR 94-172 1637.5 and 1993. The samples were crushed and powdered using mortar and pestle prior to analyses. The analyses were conducted using Scintag X-ray diffractometer at Chemical Lime Co., Henderson, Nevada. The samples were analyzed from 2.00 to 70 degrees 2 theta at a rate of 6.00 degrees per minute.

Inductively coupled plasma (ICP) analyses were conducted to determine the major element composition of the two samples that were analyzed using XRD. ICP produces atomic-line emission spectra identifying elements in a sample. Samples were dissolved in an acid solution, nebulized, and transferred to a plasma torch, where excitation occurs. A grating spectrometer disperses the atomic-line emission spectra, and photomultiplier tubes record the intensities of the spectra. A comparison of sample intensity to the standard intensity gives the major element concentration. Loss on ignition (LOI) determined the loss of water and carbon dioxide from samples. Samples were heated to determine the amount of unbound and bound water, and carbon dioxide that were liberated at 600°C and 1000°C, respectively. Leeman ICP was used to analyze samples. Kevin Anderson at Chemical Lime Co., Fortworth, Texas, conducted ICP and LOI.

Petrography and Ore Microscopy

Minerals and textural relationships in assayed core samples were examined to identify minerals that precipitated prior to, during, and after gold mineralization. Nikon Opti Phot-Pol and Olympus BX 60 system microscopes were used for petrography and ore-microscopy.

Seventy samples that exhibited cross-cutting relationships, growth textures, and high- and low-grade mineral assemblages were selected for preparation of polished thin and doubly polished thick sections, and unpolished quick plates. Fifteen doubly polished thick sections and seven polished thin sections were prepared from drill core from a 100 meter interval in drill hole TR 94-172 (Figure 3). The seven polished thin sections provided details for non-ore assemblages; thick sections were used for petrography and fluid inclusion studies of ore-stage and late-ore stage minerals. Additionally, polished thick sections were made from two low-grade samples from TR 95-39 and TR 95-95, five high ore-grade samples from drill holes TR 95-46, TR 95-72, TR 95-76, TR 95-95, and TR 96-66, and five remarkably high-grade samples from TR 95-122. One thin section from TR 95-39 was made to study vein quartz and pyrite. Quick plates were prepared to refine the distribution of ore-stage jasperoid quartz and fluid inclusion petrography in the ore-stage minerals. Forty-three unpolished thick quick plates were made from samples from 15 different drill holes. The unpolished thick sections have not been used to collect microthermometric data due to their insufficient optical clarity.

Electron Microprobe Analyses

Fine pyrite crystals were selected for electron microprobe analyses to quantify arsenic and gold in iron sulfide minerals in ore-grade sample TR 95-122 1617.5. Electron microprobe analyses were conducted at the University of New Mexico using a JEOL JXA733 Superprobe. Beam current was set 30 nanoamps using 25 kilovolts. Reference profiles were collected on standards, and secondary standards with compositions similar to unknown minerals provided correction factors. Taylor pyrite was used as a standard for iron and sulfur. Pure element standards were used for cobalt, nickel, copper, silver, and gold. Synthetic gallium arsenide, TiCl_3 , and Sb_2Te_3 provided standards of arsenic, thallium, and antimony.

Electron microprobe analyses were also conducted on crystals in TR 95-122 1619 to identify crystals in the sample. The crystals were analyzed using JEOL JXA733 at University of New Mexico. Beam current was at 20 nanoamps using 15 kilovolts.

Scanning Electron Microscope Analyses

Scanning electron microscope (SEM) analyses were conducted on crystals in TR 95-122 1619.5 that could not be identified using petrographic microscope. The samples were analyzed using JEOL JSM-5600 with beam current at 20 kilovolts with spot size of 43 micrometers at the University of Nevada Las Vegas.

Fluid Inclusion Studies

A Linkam TH 600 heating and freezing stage mounted on an Olympus BX 60 microscope was used to collect microthermometric data. The combination of 10x oculars, an 80x objective, and a 1.25x or 1.6x magnifier provided optimum magnification for collection of ice melting temperatures. For measurement of homogenization temperatures, 10x oculars and an 80x objective provided adequate resolution and optical clarity as well as a large field of view. Ice melting temperatures and homogenization temperatures were collected using Linksys Temperature Programming software. The stage was calibrated using melting temperatures of liquid carbon dioxide and the critical temperature of water.

Five types of inclusions were delineated based on their origin: (1) primary, (2) unknown – primary (?), (3) secondary, (4) pseudosecondary, and (5) unknown (Roedder, 1984). Primary inclusions were recognized by their presence along growth zones, indicating that the inclusions formed during crystal

growth. It is important to note that the age of inclusions in one growth zone could differ from the age of inclusions in another growth zone in the same crystal by thousands of years. Inclusions in questionable growth zones are grouped as unknown-primary (?) inclusions. Secondary fluid inclusions were identified by their alignment along healed fracture planes. Pseudosecondary fluid inclusions occur along fractures that formed and sealed during crystal growth and are recognized by their occurrence within a healed fracture that terminates at a crystal boundary or growth zone. Inclusions that did not exhibit criteria diagnostic for primary, secondary, or pseudosecondary inclusions have an unknown origin.

Data were gathered only from fluid inclusions that could be grouped into fluid inclusion assemblages (FIA) according to criteria of Goldstein and Reynolds (1994). These inclusions are spatially related, exhibit similar phase ratios, are part of the same generation, and formed under the same conditions at the same time. Fluid inclusions along a growth zone or single healed fracture belong to a single FIA. Because inclusions within a single FIA formed under the same conditions, homogenization temperatures are expected to be consistent. Leaking of inclusions may be detected by higher homogenization temperatures than other fluid inclusions in the same FIA.

Freezing and Heating Studies

Doubly polished thick sections were cut into approximately 3 by 5 mm chips for microthermometry. Because of the vuggy nature of the samples and the thinness of sections (< 50 micrometers), most sample wafers were not removed from the glass slides. This method left the sample chips intact. However, melting of the epoxy during heating made it difficult to determine homogenization temperatures. Cycling of temperatures was conducted to determine salinities of inclusion fluids based on freezing point depression. During freezing, the stage was initially cooled to -196°C . As the stage was cooled, any change in inclusions was recorded. Following freezing, temperature was increased to -40°C at a heating rate of 25°C per minute; above -40°C the heating rate was gradually decreased to record phase changes in the inclusions. Generally, the stage was heated to -30°C at a heating rate of 20°C per minute and to -20°C at 15°C per minute. Finally, the heating rate was dropped to 10°C per minute to observe the phase change in the fluid inclusions that indicates the approximate ice-melting temperature. After the ice was completely melted, the section was again frozen, and heated in the same sequence up to several tenths of a degree below the

approximate observed ice melting temperature. The temperature was then cycled between cooling and heating. As long as ice was present, expansion and contraction of the vapor bubble were observed as ice melted or grew, respectively. During this cycling, the heating rate was dropped to 5 °C per minute, and the sample was incrementally heated until no ice or size change of the vapor bubble was observed. The upper temperature at which bubbles expanded and did not shrink during cooling was recorded as the ice melting temperature and converted to salinity in accordance with an equation by Bodnar and Vityk (1994). To determine minimum trapping temperatures of fluid inclusions, a single heating run was conducted on each chip, because overheating of homogenized inclusions may cause stretching or decrepitation of inclusions. A heating rate of 5 °C per minute was used when the vapor bubble decreased in size.

Oxygen and Hydrogen Isotope Analysis

The δD_{H_2O} and $\delta^{18}O_{H_2O}$ compositions of inclusion fluids were analyzed by Dr. Albert Hofstra at the U.S.G.S., Denver. Inclusion fluids were extracted from samples by thermal decrepitation. The δD_{H_2O} and $\delta^{18}O_{H_2O}$ was determined according to the method of Richardson et al. (1988). A total of six samples, including two samples pre-ore stage quartz, two samples of ore-stage jasperoid quartz, plus calcite and realgar were analyzed. Pre-ore stage vein quartz was collected from a non-ore sample. A second sample of pre-ore stage quartz and a realgar sample were collected from a high-grade sample. Two other high-grade samples provided jasperoid quartz for analyses. Calcite was collected from a low-grade sample. Samples were crushed using a mortar and pestle, and individual crystals were selected with tweezers under a binocular microscope. Crystals were washed with distilled water in an ultra-sonic bath.

CHAPTER 4

PETROGRAPHY AND ORE MICROSCOPY

Host Rocks

Two distinctive rock units, the Middle and Lower units, host gold mineralization at the Turquoise Ridge deposit. The relict bedding and recrystallized calcite in these host rocks suggest that they were originally calcareous shale and limestone. Assays demonstrate that the gold mineralization is associated with alteration. Drill cores were evaluated using petrography, X-ray diffraction (XRD), inductively coupled plasma (ICP), and loss of ignition (LOI) analyses to determine the mineralogy of unmineralized host rocks at Turquoise Ridge.

In drill core, the unmineralized Middle unit is brownish green, dark green, and reddish brown in color. Altered Middle unit exhibits alternating light gray to white layers interbedded with greenish-gray layers. The layers are generally a few millimeters in thickness, conform to relict bedding, and form highly permeable zones. Calcite veins cut approximately perpendicular to bedding planes. Recrystallized calcite lenses are also present along the bedding planes. Iron-sulfide minerals, primarily pyrite and pyrrhotite, are present as accessory minerals in the Middle unit. Some samples contain approximately 5 to 10 % clay. In thin section, calcite, dolomite, biotite, cordierite, pyrite, and pyrrhotite were identified. Local boudinaged and mylonitic textures indicate local ductile deformation.

ICP and LOI analyses show that silicate and carbonate minerals are the main constituents of the Middle unit (Table 1). LOI analyses of the sample 1637.5 from drill hole TR 94-172 suggest that the Middle unit contains significant carbon dioxide, consistent with the presence of calcite and dolomite indicated by XRD (Table 1). Additionally, ICP indicated that quartz is also a major constituent of the Middle unit.

The Lower unit is dark gray to black in drill core. Marcasite crystals occur along planes that conform to faint relict bedding suggesting that the marcasite was formed during shallow-burial diagenesis. A few millimeter-thick calcite veins cut each other, and pyrite crystals occur in the veins. The Lower unit lacks a

Table 1. Results of inductively coupled plasma (ICP) analysis and loss of ignition (LOI) on TR 94-172 1637.5 (the Middle unit) and TR 94-172 1993 (the Lower unit).

	TR 94-172 1637.5	TR 94-172 1993
	the Middle unit	the Lower unit
	weight %	weight %
CaO	27.7	4.5
MgO	8.02	2.41
SiO ₂	28.91	67.05
Al ₂ O ₃	7.27	14.02
Fe ₂ O ₃	5.95	3.85
Na ₂ O	0.41	0.85
K ₂ O	0.35	4.59
SrO	0.04	0.02
MnO	0.138	0.053
LOI @ 1000°C	21.03	2.33
LOI @ 600°C	2.66	1.08
Total	99.87	99.67

mylonitic texture and is fractured, suggesting that the Lower unit underwent brittle deformation. Samples contain less than approximately 5 % clay. In thin section, the Lower unit exhibits a dark microcrystalline texture, and constituent minerals cannot be identified. Fractures are filled with anhedral quartz crystals and subhedral to anhedral calcite crystals. The quartz and calcite veinlets are nearly perpendicular to relict bedding.

ICP and LOI analyses of sample TR 94-172 1993 show that the Lower unit consists primarily of quartz (Table 1). XRD analyses indicate that the Lower unit contains abundant quartz and minor microcline, illite, biotite, calcite, and dolomite. The black color is a result of the presence of carbon. The results of LOI indicate that only minor CO₂ is present and support the XRD data. The samples TR 94-172 16137.5 and 1913 contain 5 to 10 % clay, and the result of chemical analyses may slightly reflect the effect of alteration.

Discussion of Host Rocks

Petrographic, XRD, ICP, and LOI analyses suggest that the Middle and Lower units are metamorphosed sedimentary rocks. Relict bedding in both rocks indicates that they were originally sedimentary rocks. The Middle unit primarily contains silicate and carbonate minerals, and recrystallized calcite is locally present. The high silica content in the Middle and Lower units reflects either the silica content of original rock or the addition of silica to the rock during diagenesis and metamorphism. The microcrystalline texture and high silica content may indicate that the Lower unit was originally hemipelagic shale.

Variations in the carbonate and silicate contents of the two types of ore-host rocks do not appear to have effected gold mineralization, and ore bodies developed in both the Middle and Lower units. However, extremely high-grade samples for this study were collected only from the Middle unit. At the Twin Creeks mine, which is located approximately 8 km northeast of the Getchell mine, Atkin (1989) reported that highly decalcified host rocks controlled ore localization. Following this interpretation, the carbonate-rich Middle unit should be a preferable host rock than the siliceous Lower unit. Alternatively, grade may be related to depth or fracture porosity rather than rock type. Although Atkin (1989) and Arehart (1996) suggested strong lithologic control over localization of gold and observed strata-bound ore, strong

stratigraphic control was not indicated at the Turquoise Ridge deposit. Additionally, the ore-stage assemblage in both rock types consists of the same minerals and does not exhibit any variation.

Mineral Paragenesis

Secondary minerals that form overgrowths on, or exhibit cross-cutting relationships with, the host rocks have been identified in the Middle and Lower units. The textural relationships show that the ore-related minerals precipitated successively during a single gold hydrothermal event, and the multiple stages of gold mineralization described by Groff (1996) were not identified. Stages of mineral precipitation were divided into pre-ore stage, ore stage, and late-ore stage assemblages based on Cline's study (1999). Cross-cutting relationships and the precipitation of younger minerals on older crystals were used to determine relative ages of minerals. Electron microprobe analyses that identified gold, and assays of samples were used to distinguish between ore-stage and non-ore mineralization. Minerals are listed for each of the following assemblages according to the order in which they precipitated.

Pre-Ore Stage Mineral Assemblage: Quartz - Pyrite - Marcasite

Quartz, pyrite, and marcasite in veins that cut the Middle unit represent the pre-ore assemblage (Figure 6). Assays show that the pre-ore mineral assemblage contains less than 0.001 ounces per ton gold. Pre-ore stage minerals are present in some high-grade samples, but where present, they are fractured and are crosscut by ore-stage mineralization.

Quartz in veins is coarsely crystalline and exhibits euhedral to anhedral morphologies. Quartz crystals range in size from 25 micrometers to 2 millimeters. Although crystal size and shape vary, subhedral quartz crystals are dominant, average 200 micrometers in diameter, and exhibit an equigranular texture. Crystal terminations and open spaces between euhedral crystals document open-space precipitation of this mineral. Pyrite crystals in the pre-ore stage are anhedral to euhedral, but euhedral crystals are most common (Figure 7a). Cubic pyrite crystals range from 5 to 25 micrometers, and average 15 micrometers in diameter. Although pyrite crystals are locally strained or fractured, they generally polish well and exhibit high relief. The pyrite crystals contain few or no solid inclusions.

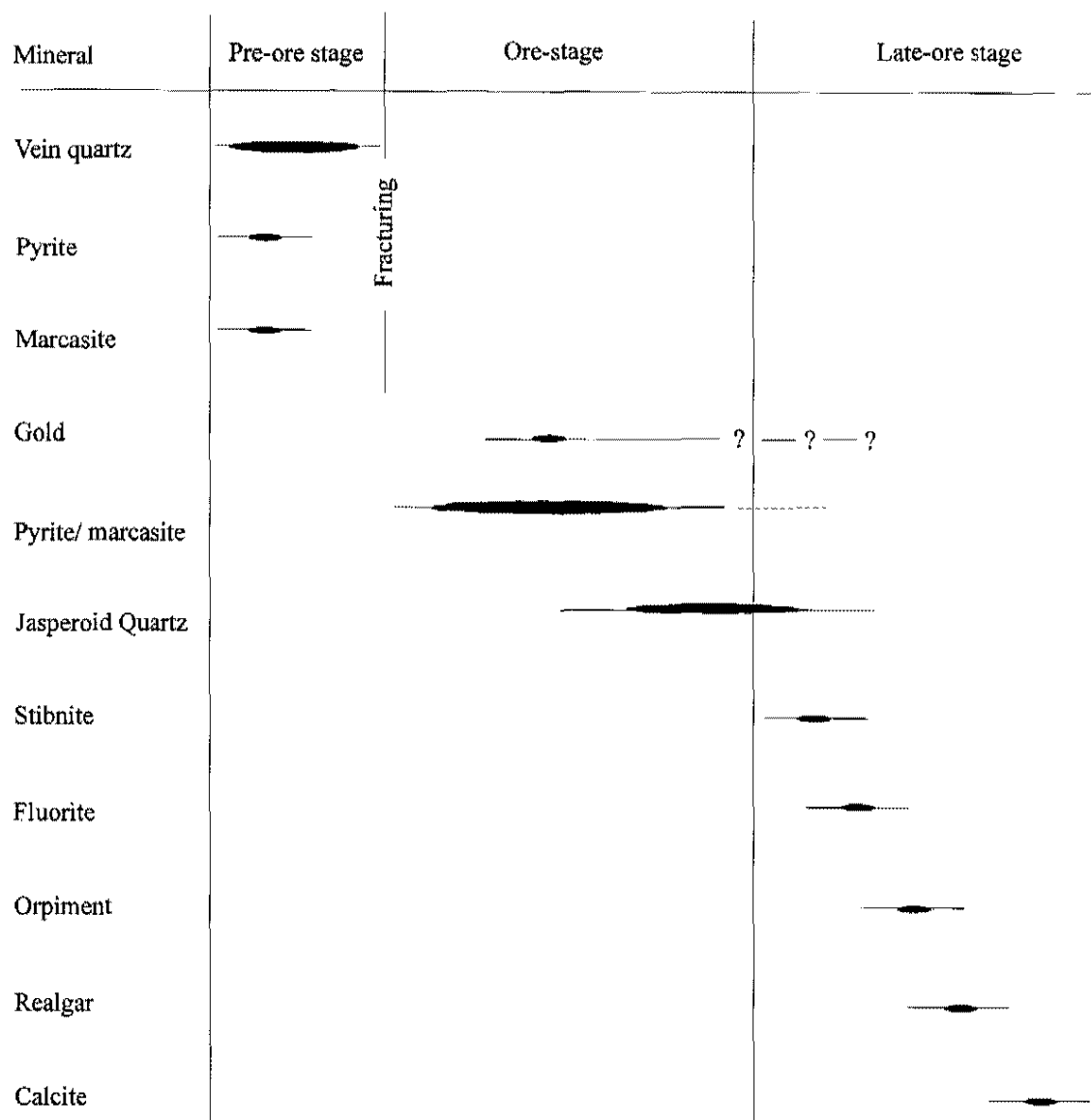


Figure 6. Pre-ore stage, ore-stage, and late ore-stage mineral pragenesis at the Turquoise Ridge deposit.

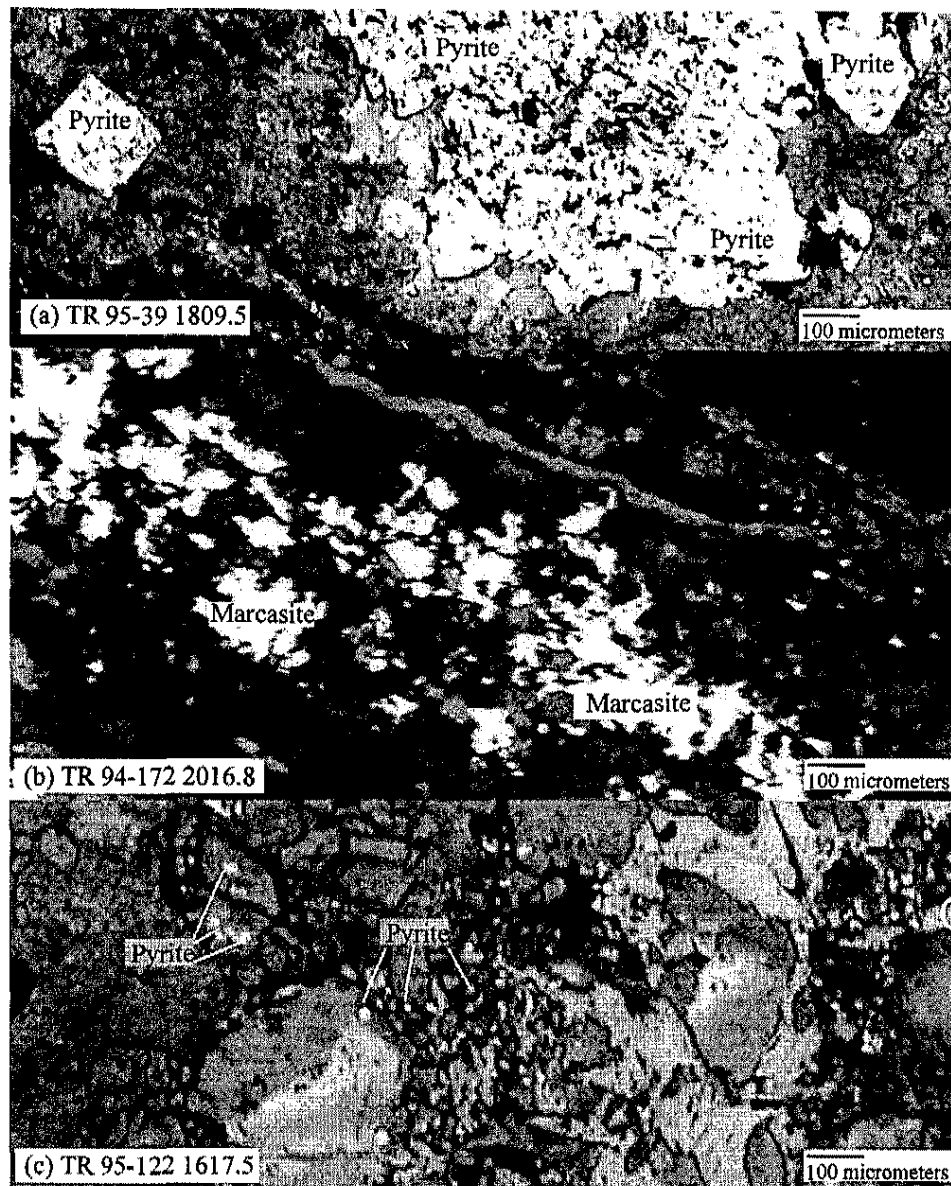


Figure 7. Pyrite and marcasite are present in samples from the Turquoise Ridge deposit. Photomicrographs (a), (b), and (c) were taken under plan polarized reflected light.

- (a) Pre-ore stage pyrite. Euhedral to subhedral pyrite crystals exhibit high relief.
- (b) Marcasite crystals conform to relict bedding indicating their formation during shallow burial diagenesis.
- (c) Ore-stage pyrite. Anhydrous pyrite crystals polish poorly.

Marcasite crystals in vein-filling quartz are porous, fractured, polish poorly, and exhibit euhedral to subhedral morphologies. Individual 5 to 10 micrometers marcasite crystals commonly form spherical aggregates, which range from one to a few millimeters in diameter and are coarse enough to be identified in hand specimen. Lath-shaped marcasite crystals also occur along bedding planes, particularly, in the Lower unit, and these marcasite crystals appear to be formed during shallow burial (Figure 7b) and genetically different from the marcasite in veins.

Textural relationships indicate that the timing of quartz, pyrite, and marcasite precipitation overlapped. Quartz encompassed pyrite and marcasite crystals, and pyrite and marcasite locally precipitated on quartz. The relative timing of pyrite and marcasite precipitation is not clear because of the lack of crosscutting relationships. Pre-ore stage minerals are crosscut by ore-stage minerals indicating that pre-ore stage minerals were fractured; ore-stage hydrothermal fluids moved through these fractures and precipitated ore stage minerals.

The Ore-Stage Mineral Assemblage: Pyrite - Marcasite - Gold - Jasperoid Quartz - K-spar (?)

Ore-stage pyrite crystals are typically spherical and finely crystalline, averaging 5 micrometers or less in diameter (Figure 7c). The crystals commonly form rims around euhedral to anhedral pre-ore stage pyrite crystals. The pyrite cores exhibit a good polish, but ore stage rims polish poorly. Electron microprobe analyses of fine pyrite crystals confirmed the presence of gold in seven pyrite crystals; gold ranged from 1100 to 3200 ppm (Table 2). Electron microprobe analyses show that ore-stage pyrite crystals are rich in trace elements, particularly arsenic.

Aggregates of marcasite laths in ore-grade samples resemble porous pyrite masses that particularly are associated with gold mineralization. Commonly, it is difficult to distinguish marcasite from finely crystalline pyrite because of the small crystal size and poor polish of these crystals. However, a few marcasite crystals exhibit anisotropism, distinguishing them from pyrite.

Jasperoid quartz is finely microcrystalline and exhibits the typical jigsaw puzzle, reticulated jasperoid texture. Remnants of calcite inclusions encompassed by quartz indicate that quartz replaced calcite. Subhedral to anhedral jasperoid quartz crystals exhibit a wide range of crystal sizes, from 100 micrometers to 200 micrometers, typical of jasperoid quartz. Ore-stage pyrite crystals are consistently present within

Table 2. Results of electron microprobe analyses (weight %) on seven pyrite crystals in an euhedral ore-stage quartz crystal in TR 95-122 1617.5.

	Pyrite #1	Pyrite #2	Pyrite #3	Pyrite #4
Element	weight % element	weight % element	weight % element	weight % element
S	45.473	45.463	44.209	45.451
Fe	29.978	29.575	31.442	33.561
Co	0.056	0.037	0.019	0.022
Ni	0.022	0.016	-	-
Cu	1.718	1.577	0.853	-
Zn	0.039	0.034	-	0.022
Ag	0.098	0.195	0.773	1.112
Au	0.123	0.110	0.317	0.110
Hg	2.380	2.367	1.257	1.411
Tl	3.761	3.311	2.300	2.524
As	15.328	14.126	14.388	12.983
Sb	0.873	0.972	0.351	0.988
Te	0.147	0.149	0.220	0.097
Total	99.999	97.632	96.130	98.292

	Pyrite #5	Pyrite #6	Pyrite #7
Element	weight % element	weight % element	weight % element
S	47.924	50.644	50.848
Fe	36.572	37.743	38.139
Co	0.037	0.055	0.026
Ni	-	-	-
Cu	0.524	1.161	0.233
Zn	-	-	-
Ag	-	-	-
Au	0.198	0.148	0.133
Hg	-	-	-
Tl	1.329	0.911	0.475
As	12.614	10.411	10.917
Sb	1.298	0.703	0.943
Te	-	-	-
Total	100.676	101.777	101.810

jasperoid quartz crystals and along jasperoid quartz crystals boundaries (Figure 8). The pyrite crystals also occur along fractures in pre-ore quartz, and along pre-ore and jasperoid quartz crystal boundaries (Figure 8). The consistent presence of gold-bearing pyrite within and adjacent to jasperoid quartz crystals suggests that gold and pyrite mineralization occurred immediately prior to, or with jasperoid quartz precipitation. However, jasperoid quartz crystals that do not contain pyrite are also present. The presence of pyrite-bearing and pyrite-free jasperoid quartz reflects either multiple generations of jasperoid quartz or a period of gold/pyrite deposition that is shorter than quartz precipitation. While pre-ore stage vein quartz crystals are intensively fractured, minerals in the ore assemblage generally lack fractures (Figure 9). This absence of fractures shows that ore-stage minerals precipitated after vein formation.

High-grade sample 1619.5 from drill hole TR 95-122 contains potassium feldspar inclusions. In the sample, quartz crystals occur as aggregates as coarse as 300 micrometers (Figure 10a and b). Fine pyrite crystals are present in rims in aggregates of quartz crystals. The crystal faces of quartz are subsequently encompassed by realgar. Although euhedral quartz crystals are locally present and exhibit crystal termination on the rim of the aggregates, the radial crystal habit is not typical of quartz (Figure 10 a and b). However, electron microprobe analyses on the sample indicated that individual crystals of aggregates are quartz. SEM images show inclusions in quartz, and EDS spectra indicate that the inclusions are potassium feldspar (Table 3). It is not clear if these potassium feldspar inclusions were precipitated during the gold hydrothermal event. However, if the association between precipitation of potassium feldspar and the gold mineralizing event is confirmed, the age of gold event may be constrained by dating these inclusions.

The Late-Ore Stage Mineral Assemblage: Pyrite/Marcasite - Jasperoid Quartz - Stibnite - Fluorite Orpiment - Realgar - Calcite

The late-ore stage mineral assemblage was determined based on presence of finely crystalline pyrite crystals, and assays that indicate the presence of no or little gold in the intervals of the samples. Late-ore stage minerals, in particular, exhibit coarse, open-space textures (Figure 11). Assays and overgrowth textures indicate that the late-ore stage minerals precipitated after the ore-stage mineral assemblage (Figure 6).

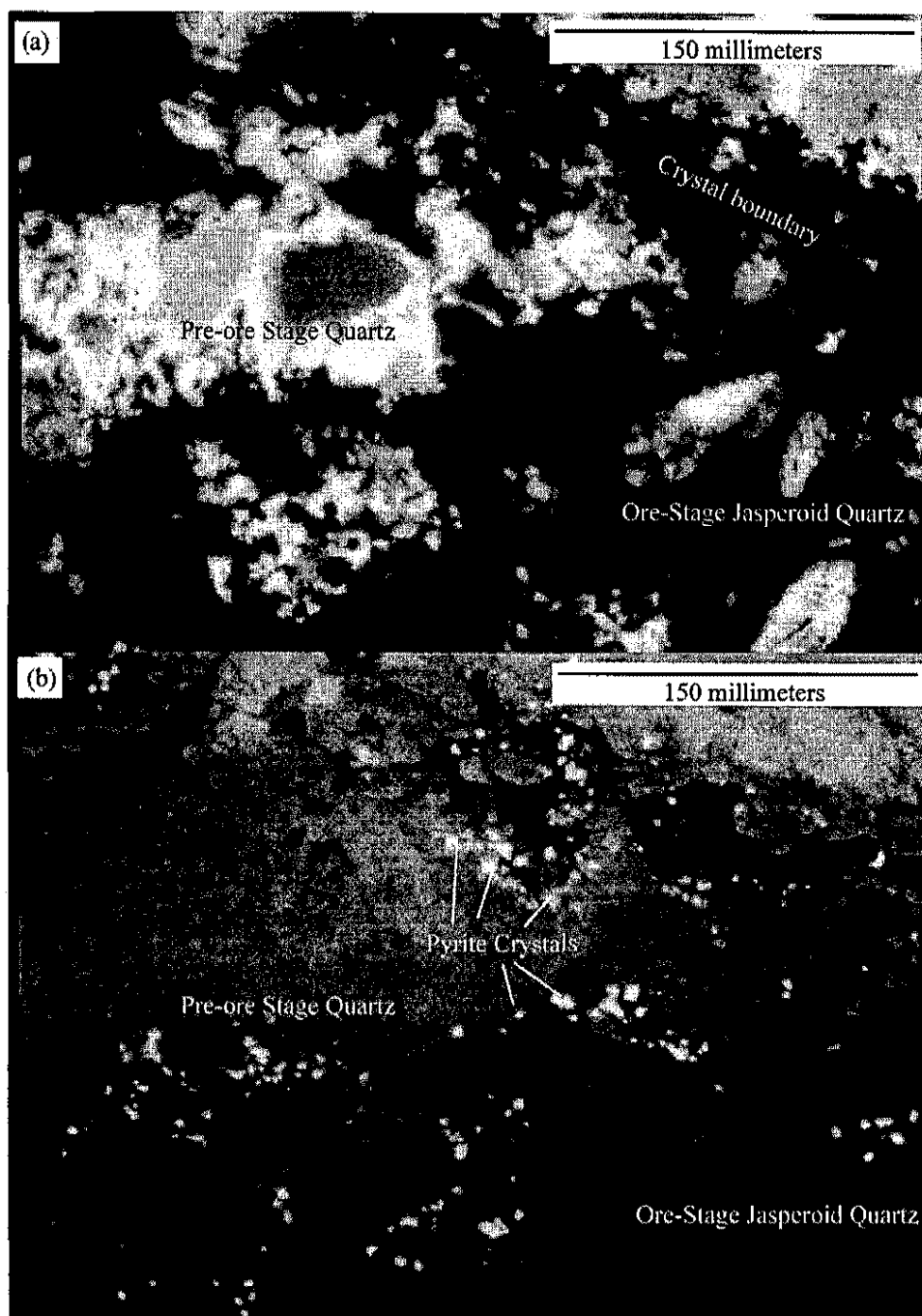


Figure 8. Photomicrographs of sample TR 95-122 1617.5 showing preferred location of ore-stage pyrite crystals. (a) and (b) were taken under crossed polarized transmitted light and reflected light, respectively.

- (a) Pre-ore stage quartz and ore-stage quartz. Pre-ore stage quartz is coarsely crystalline. Jasperoid quartz crystals show reticulated texture.
- (b) Ore-stage pyrite crystals are consistently present in ore-stage jasperoid quartz, between jasperoid quartz crystals, and along jasperoid quartz and pre-ore stage quartz crystal boundaries.

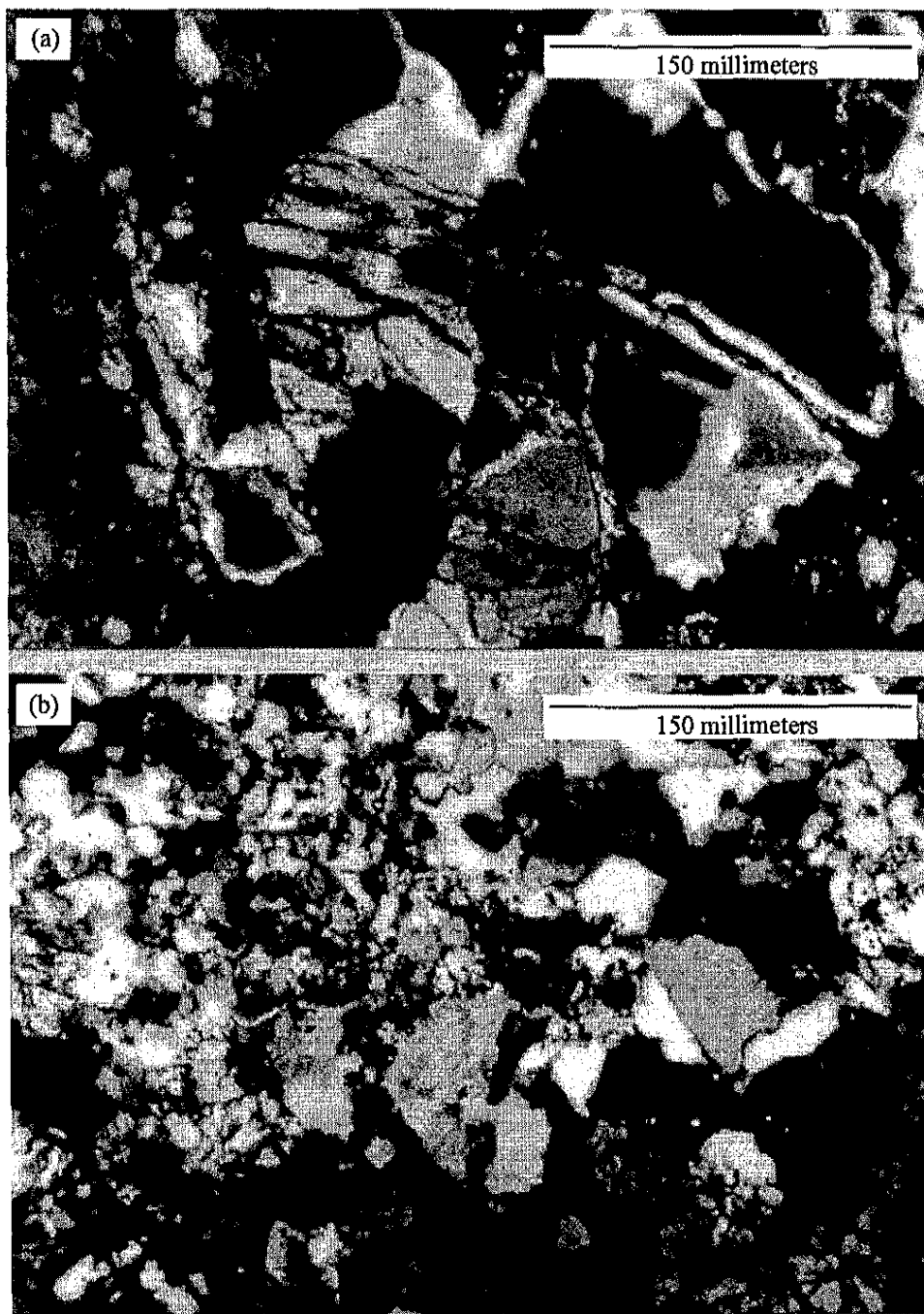


Figure 9. Photomicrographs of sample TR 95-122 1617.5 showing the two types of quartz taken under crossed polarized transmitted light. (a) vein quartz in ore-grade sample, and (b) ore-stage jasperoid quartz. Fractures are absent in ore-stage jasperoid quartz, indicating jasperoid quartz precipitation after vein quartz precipitation.



Figure 10. Electron microprobe analyses identified quartz (a) and (b), and SEM image (c) shows potassium feldspar inclusions in a sample TR 95-122 1619.5. Quartz crystals do not exhibit typical optical properties in this sample. Photomicrographs (a) and (b) were taken under crossed polarized transmitted light.

Table 3. Results of electron microprobe analyses on (a) and (b) from TR 95-122 1617.5. Refer Figure 10 for the samples (a) and (b).

Sample	(a)	(b)
Element	weight %	weight %
Si	45.885	45.981
Al	0.155	0.294
Mg	0.015	-
Na	0.016	0.019
K	0.32	0.013
O	54.432	52.58
Total	98.535	98.823

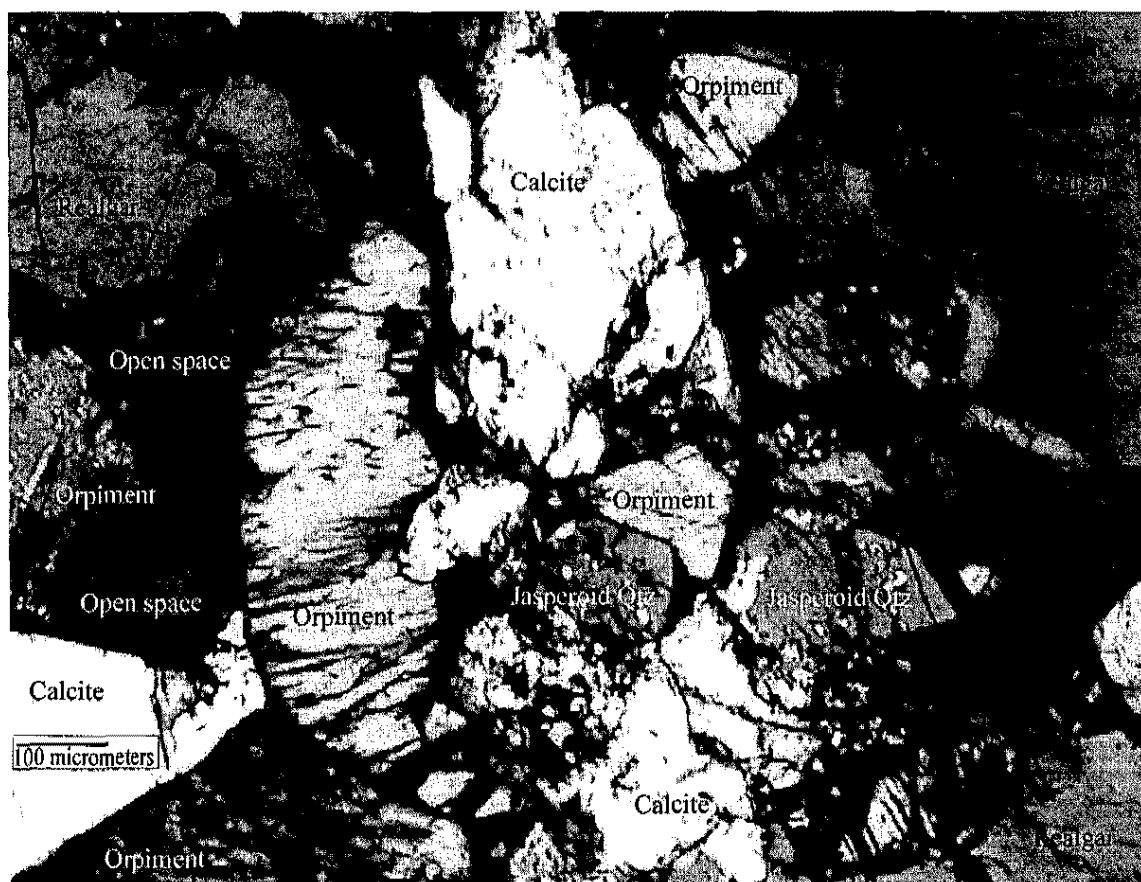


Figure 11. Photomicrograph of sample TR 94-172 1661.5 shows over-growth textures of ore-stage minerals under crossed polarized transmitted light. Subhedral jasperoid quartz crystals are encompassed by orpiment. Realgar precipitated on orpiment crystal faces, and calcite fills open spaces between these late-stage minerals.

Late-ore stage pyrite crystals are sparse and preferentially occur along jasperoid quartz crystal boundaries. The restricted presence of pyrite crystals may indicate that the pyrite crystals in quartz crystal boundaries may have formed later than ore-stage pyrite crystals within jasperoid quartz crystals, and cessation of pyrite precipitation. Cubic and spherical pyrite crystals are present. Cubic crystals exhibit a good polish and range from 5 to 10 micrometers in size. Spherical crystals are generally less than 4 micrometers in diameter, and have low relief and polish poorly. Both types of crystals are porous with fuzzy crystal boundaries.

Marcasite occurs as individual coarse laths and fine aggregates in the late-ore stage assemblage. Some aggregates of acicular crystals have the appearance of porous pyrite, but they are anisotropic. These late-ore stage marcasite crystals exhibit high relief, where ore-stage marcasite crystals take poor polish.

Jasperoid quartz in the late-ore stage assemblage contains very sparse finely crystalline calcite within the crystals. The presence of sparse calcite inclusions may indicate that replacement of calcite by quartz was nearly complete by this stage of gold hydrothermal event. Stibnite forms over jasperoid quartz crystals. Acicular stibnite crystals range from 50 to 100 micrometers.

Fluorite is an extremely sparse mineral at the Turquoise Ridge deposit. It was identified in only one sample, TR 94-172 1660.5. Fluorite forms cubic crystals ranging from 3 to 30 micrometers in diameter that are rimmed by finely crystalline pyrite crystals, and are encompassed by orpiment. The euhedral to subhedral fluorite crystals are not fractured.

Orpiment is associated with realgar, fluorite, and calcite in the late ore-stage assemblage, and is abundant in samples in which realgar is rare. Subhedral orpiment formed coarse crystals that precipitated in open space. Crystals range from approximately 300 to 900 micrometers in diameter. Orpiment contains and is rimmed by finely crystalline marcasite and pyrite crystals that are less than 4 micrometers in diameter.

Realgar precipitated in open space on ore-stage minerals and is encompassed by late-ore stage calcite. The open-space texture suggests that realgar formed after ore-stage minerals formed. Realgar primarily precipitated on jasperoid quartz and contains abundant subhedral stibnite crystals. In low-grade samples, realgar locally precipitated on orpiment and filled fractures in orpiment, indicating realgar precipitated after orpiment.

Coarse calcite mineralization filled open spaces as large as 7.5 millimeters. Subhedral to anhedral calcite precipitated on jasperoid quartz, orpiment, and realgar, and filled fractures in orpiment. Calcite locally contains fine iron-sulfide crystals, which may be either pyrite or marcasite. Cross-cutting relationships show that most calcite precipitated after realgar; however, realgar locally crosscuts calcite. These relationships indicate the close timing of realgar and calcite precipitation.

Summary of Mineral Paragenesis

Pre-ore stage euhedral to subhedral quartz crystals and euhedral to subhedral pyrite and marcasite in veins that cut the Lower unit indicate open-space precipitation of vein minerals. Quartz crystals are finely crystalline adjacent to the host rocks and become coarser toward the center of vein. The fine crystals indicate rapid crystallization, possibly from the loss of heat by the hydrothermal fluid along the wall rock (Guilbert and Park, 1986). Coarser crystals in the center of the vein suggest slower quartz precipitation from a cooler fluid during the later vein formation (Guilbert and Park, 1986). Pyrite and marcasite generally form over quartz, but quartz locally encompasses pyrite and marcasite. These textural relationships may indicate that a single fluid transported silica, iron, and sulfur, and precipitated quartz, pyrite, and marcasite in veins.

Fractures in the Lower unit that were filled with quartz, pyrite, and marcasite may have formed by thermal contraction due to cooling of the Cretaceous granodiorite intrusion. Alternatively, the Lower unit may have been fractured during extension associated with local or large-scale tectonic events. As quartz veins are only identified in the Lower unit, local extension or contraction is indicated rather than a larger scale event. The proximity between the quartz veins and the Cretaceous granodiorite suggests that fracturing is associated with the intrusion and the quartz veins may have a magmatic source.

The presence of small calcite inclusions in ore-stage jasperoid quartz crystals indicates that carbonate rock was originally present and was replaced by silica. This interpretation agrees with the significant carbonate content indicated by XRD, ICP, and LOI analyses of unaltered rocks. The loss of carbonate suggests that acidic fluids moved through calcareous rocks prior to, or at the beginning of the ore-stage hydrothermal event.

Petrographic studies indicate a sequential precipitation of (1) pyrite with gold, (2) jasperoid quartz, (3) stibnite, (4) fluorite, (5) orpiment, (6) realgar, and (7) calcite during a single hydrothermal event. This mineral paragenesis agrees with previous studies at the Getchell gold deposit (Cline, 1999). Although Groff 's (1996) study suggested multiple generations of orpiment and realgar, cross-cutting relationships observed during this study consistently exhibit orpiment precipitation followed by realgar precipitation in the late-ore stage.

CHAPTER 5

FLUID INCLUSION STUDIES

Petrography and Microthermometry

Fluid inclusions in pre-ore quartz, ore-stage jasperoid quartz, and late ore-stage fluorite, orpiment, realgar, and calcite were studied to identify their general distribution, size, shape, phase ratios, and origins, and to determine salinities and homogenization temperatures.

Microthermometric data were collected from fluid inclusions in pre-ore stage quartz, ore-stage jasperoid quartz, and an euhedral quartz crystal from a high-grade sample. Data collected from secondary and unknown fluid inclusions were compared to data from primary fluid inclusions to identify changes in the fluid with time. Few primary fluid inclusions were recognized in this study; secondary and unknown fluid inclusions in pre-ore stage quartz and ore-stage jasperoid quartz provided most of the microthermometric data.

Fluid Inclusions in Pre-Ore Stage Quartz

Pre-ore quartz contains primarily two-phase, liquid-rich, liquid-vapor inclusions; however, two-phase vapor-rich, vapor-only, and liquid-only inclusions are also present. Rare three-phase inclusions that contain liquid, vapor, and a solid phase are present. The dominant fluid inclusion population contains two phases and the vapor bubble occupies 5 volume % of the inclusion. The fluid inclusions range from 2.5 to 5 micrometers in diameter and average 3.5 micrometer in diameter. Some clear quartz crystals in veins in the Lower unit contain abundant primary inclusions in their cores. The primary inclusions average 5 micrometers in diameter and contain vapor bubbles that occupy 5 volume % of the inclusions. Pre-ore quartz crystals that are crosscut by ore-stage minerals primarily contain secondary inclusions along fracture planes. Some secondary inclusions occurring along fracture planes exhibit inconsistent phase ratios indicating that these inclusions likely formed by necking.

Microthermometric data were collected from pre-ore stage quartz in five samples: two samples in veins from TR 94-172 1912.4 and TR 95-95 1760.5, two samples from fault gouge from TR 94-172 1865.5 and 1913, and one sample from TR 95-122 1619.5. Two gouge samples and TR 95-122 1617.5 were crosscut by the ore-stage mineral assemblage.

Primary fluid inclusions in pre-ore stage quartz crystals have salinities between 4 and 7 weight % NaCl equivalent and 21 and 23 weight % NaCl equivalent (Figure 12a). These fluid inclusions homogenized between 150 ° and 180 °C (Figure 12b).

Unknown but possibly primary inclusions have salinities that cluster between 6 and 12 weight % NaCl equivalent and between 18 and 23 weight % NaCl equivalent (Figure 13a). These inclusions exhibited a wide range of homogenization temperatures, 140 ° to 260 °C with no mode (Figure 13b).

Secondary inclusions have a range of salinities from 1 to 22 weight % NaCl equivalent with slight modes between 6 and 8 weight % and between 12 and 13 weight % NaCl equivalent (Figure 14a). Homogenization temperatures are evenly spread between 150 ° and 250 °C (Figure 14b).

Salinities of unknown inclusions ranged from 0.8 to 23 weight % NaCl equivalent, and there is small mode between 6 and 11 weight % NaCl equivalent (Figure 15a). Unknown inclusions homogenized over a wide temperature range from 140 ° to 300 °C (Figure 15b).

The wide range of salinities and homogenization temperatures of inclusions in pre-ore quartz may reflect variations between quartz in vein, in fault gouge, and in a sample that is crosscut by ore-stage minerals (Figure 16a and b). The following discussion examines salinities and homogenization temperatures of each of the pre-ore stage quartz samples.

Pre-Ore Stage Vein Quartz

Inclusions in pre-ore stage vein quartz have consistent salinities but show a wide range of homogenization temperatures (Figure 17a, b, and c). Primary fluid inclusions in vein quartz crystals from TR 95-95 1760.5 have salinities between 4 and 7 weight % NaCl equivalent (Figure 18a and b), and inclusions homogenized between 150 ° and 180 °C (Figure 18a and c).

Unknown-primary (?) inclusions were identified in vein quartz sample, TR 94-172 1912.4. These inclusions have salinities between 6 and 12 weight % NaCl equivalent with a small mode at 7 to 9 weight

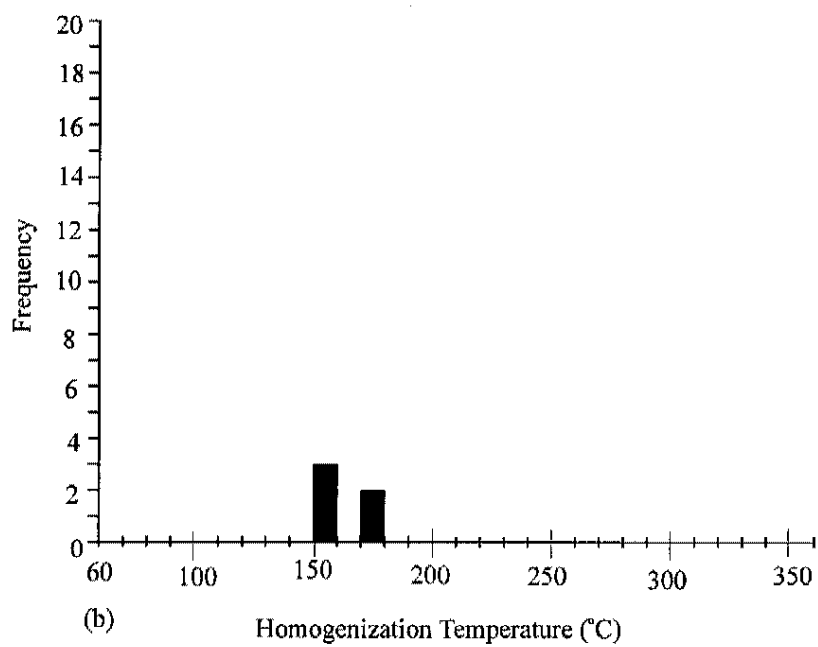
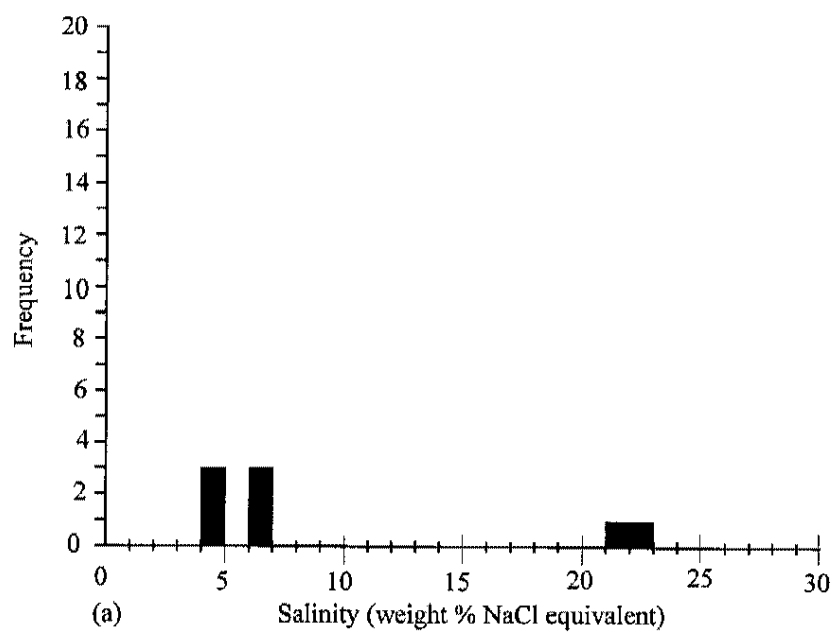


Figure 12. Salinities (a) and homogenization temperatures (b) of primary fluid inclusions in pre-ore stage quartz.

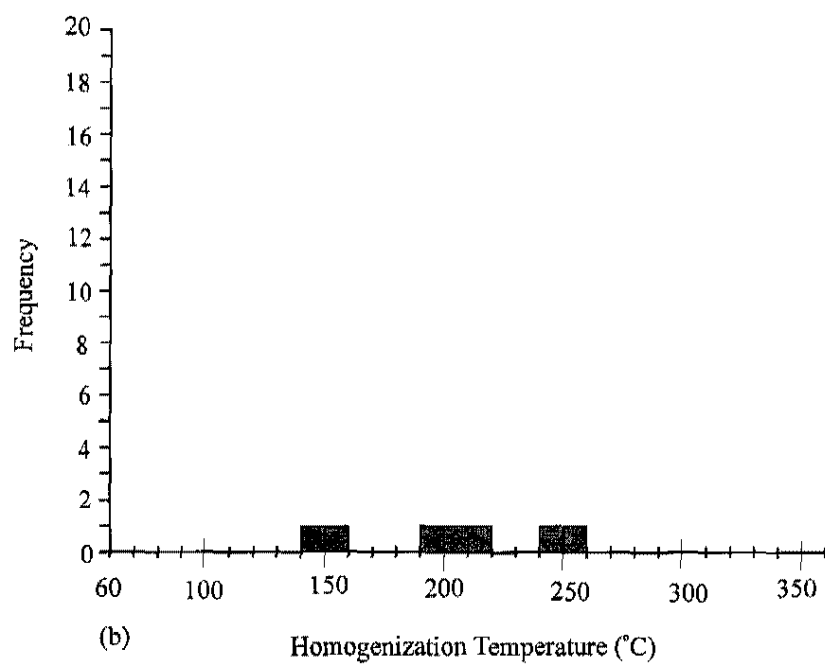
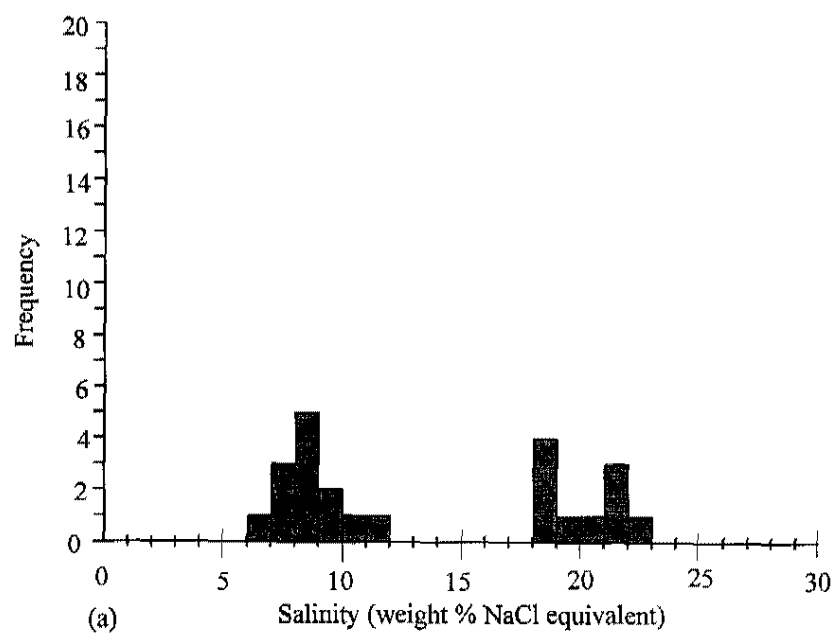


Figure 13. Salinities (a) and homogenization temperatures (b) of unknown-primary (?) fluid inclusions in pre-ore stage quartz.

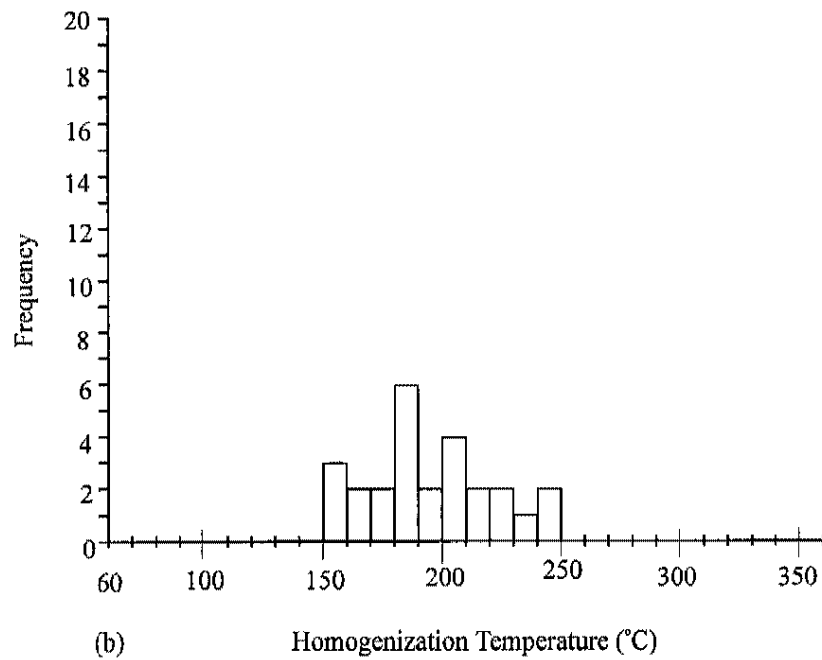
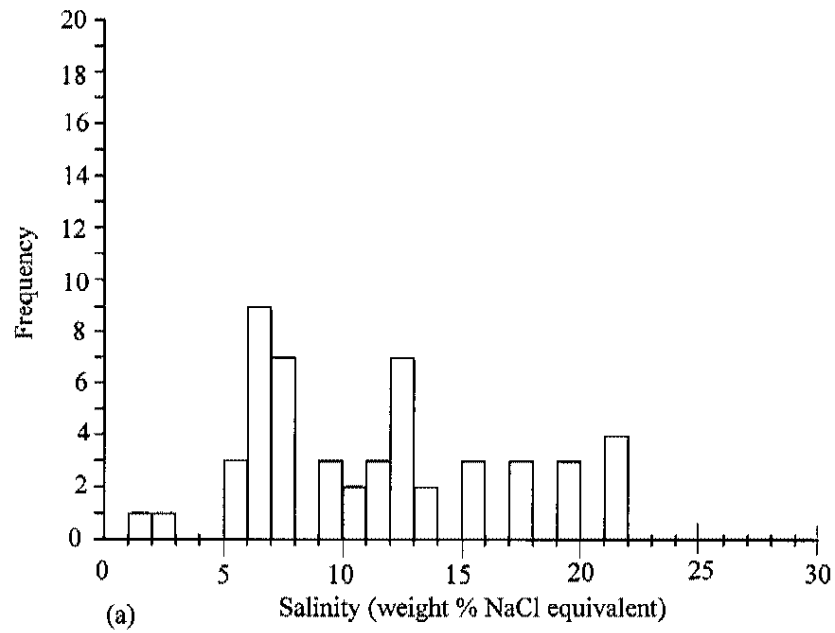


Figure 14. Salinities (a) and homogenization temperatures (b) of secondary fluid inclusions in pre-ore stage quartz.

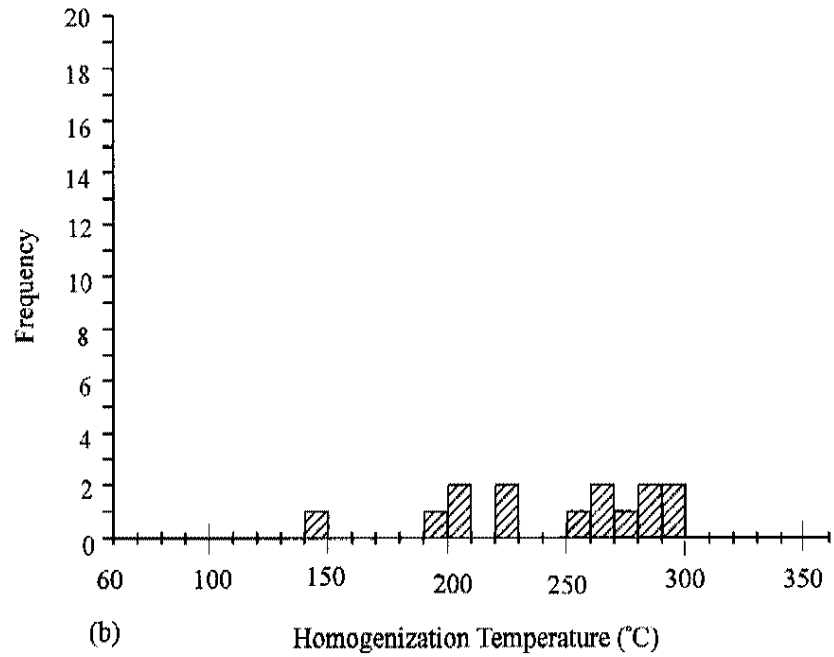
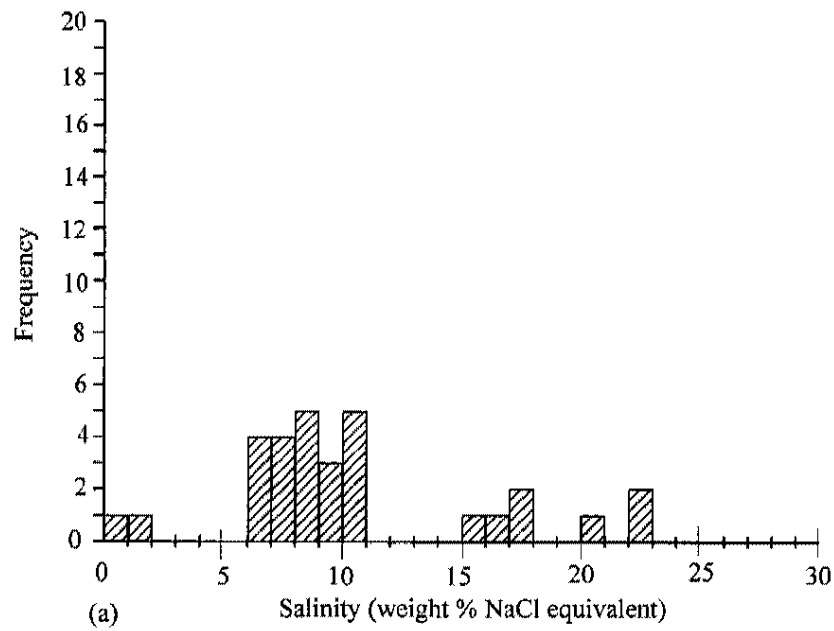


Figure 15. Salinities (a) and homogenization temperatures (b) of unknown fluid inclusions in pre-ore stage quartz.

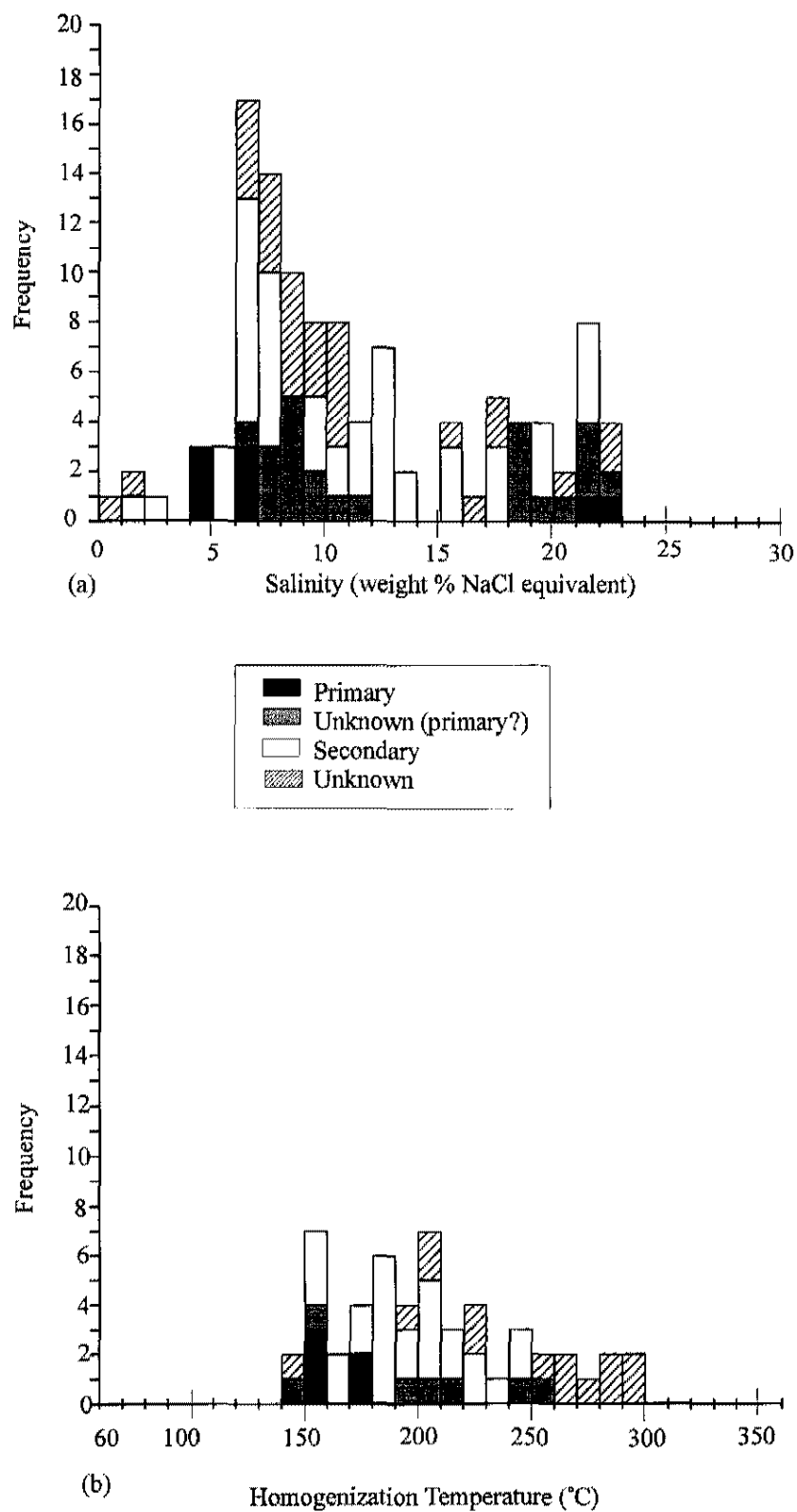


Figure 16. Salinities (a) and homogenization temperatures (b) of all fluid inclusions in pre-ore stage quartz.

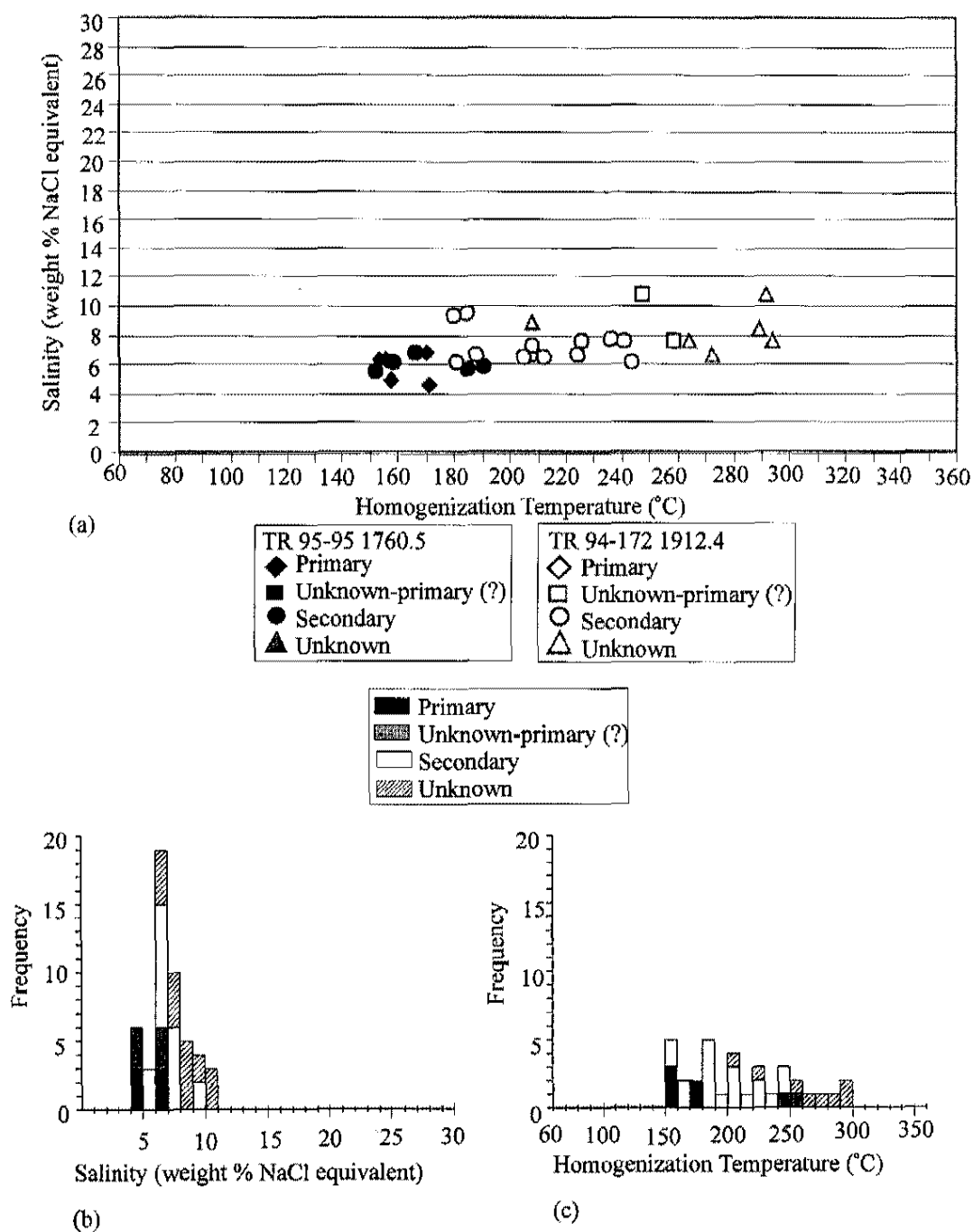


Figure 17. Microthermometric data for fluid inclusions in pre-ore stage vein quartz.

- (a) Plot of homogenization temperatures versus salinities. Data that do not have both homogenization temperatures and salinities are not shown on this chart.
- (b) Histogram of salinities of fluid inclusions.
- (c) Histograms of homogenization temperatures of fluid inclusions.

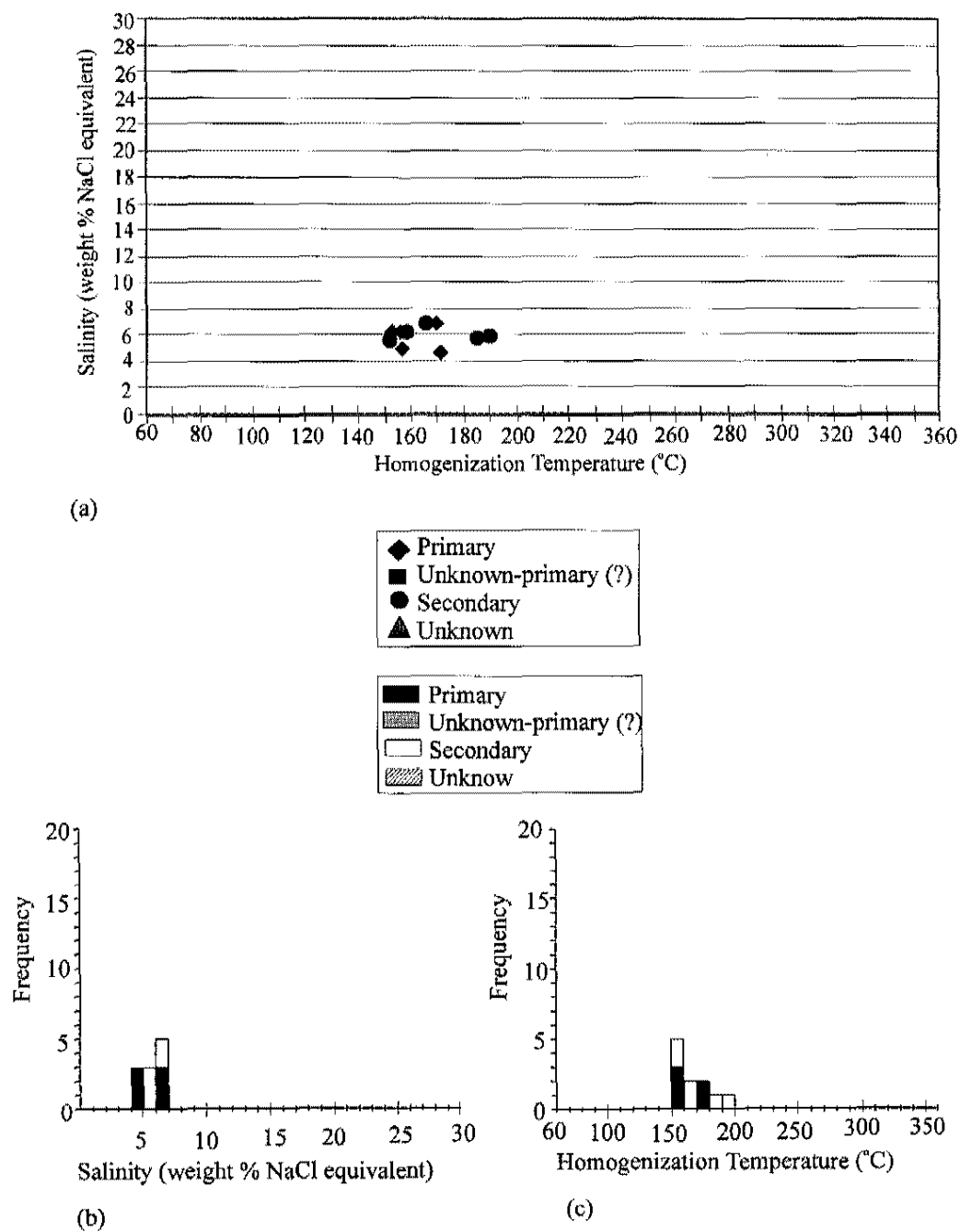


Figure 18. Microthermometric data for fluid inclusions in pre-ore stage quartz in TR 95-95 1760.5.
 (d) Plot of homogenization temperatures versus salinities. Data that do not have both homogenization temperatures and salinities are not shown on this chart.
 (e) Histogram of salinities of fluid inclusions.
 (f) Histograms of homogenization temperatures of fluid inclusions.

% NaCl equivalent (Figure 19a and b). Two inclusions homogenized between 240 ° and 260 °C (Figure 19a and c).

Secondary inclusions in pre-ore stage quartz from TR 94-172 1912.4 have salinities similar to sample TR 95-95 1760.5. Secondary inclusions in quartz from TR 95-95 1760.5 have salinities between 5 and 7 weight % NaCl equivalent (Figure 18a and b), and these inclusions homogenized between 150 ° and 200 °C. Salinities of inclusions from sample TR 94-172 1912.4 ranged from 6 to 10 weight % NaCl equivalent (Figure 19a and b). Homogenization temperatures for sample TR 94-172 1912.4 are higher than those of sample TR 95-95 1760.5 and ranged from 180 ° to 250 ° (Figure 19c).

Unknown inclusions from TR 94-172 1912.4 have salinities from 6 to 11 weight % NaCl equivalent (Figure 19a and b). These inclusions homogenized between 200 ° and 300 °C; and most inclusions homogenized between 250 ° and 300 °C (Figure 19a and c).

Pre-Ore Stage Quartz in Gouge

Fluid inclusions in pre-ore stage quartz in gouge exhibit two ranges of salinities and a wide range of homogenization temperatures (Figure 20a, b, and c). Primary fluid inclusions in pre-ore stage quartz crystals in gouge samples from TR 94-172 1865.5 and 1913 were sparse, and salinities of only two inclusions in 1865.5 were determined. The salinities of the two primary inclusions fell between 21 and 23 weight % NaCl equivalent (Figure 21b). Homogenization temperatures of these inclusions could not be determined.

Unknown-primary (?) inclusions in quartz from TR 94-172 1865.5 have salinities between 18 and 23 weight % NaCl equivalent (Figure 21a and b). Homogenization temperatures of these inclusions range fairly evenly between 140 ° and 220 °C (Figure 21a and c).

Salinities of secondary inclusions in quartz crystals from TR 94-172 1865.5 are consistent ranging from 19 to 22 weight % NaCl equivalent (Figure 21a and b). These inclusions homogenized between 140 ° and 220 °C (Figure 21a and c). Secondary inclusions in quartz crystals from TR 94-172 1913 have a range of salinities from 12 to 16 weight % NaCl equivalent (Figure 22a and b). Homogenization temperatures of these inclusions ranged from 230 ° to 290 °C (Figure 22a and c).

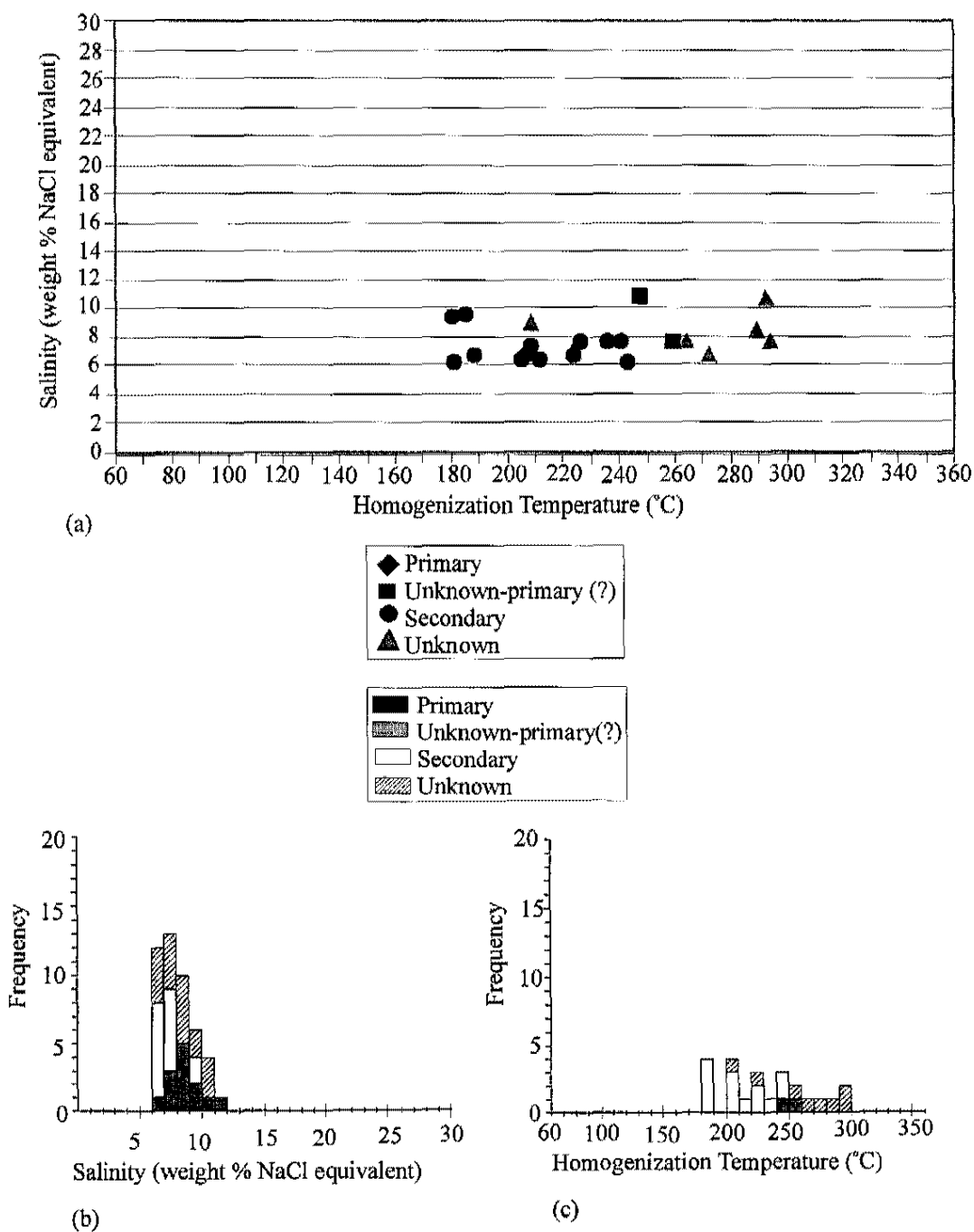


Figure 19. Microthermometric data for fluid inclusions in pre-ore stage quartz in TR 94-172 1912.4.
 (a) Plot of homogenization temperatures versus salinities. Data that do not have both homogenization temperatures and salinities are not shown on this chart.
 (b) Histogram of salinities of fluid inclusions.
 (c) Histograms of homogenization temperatures of fluid inclusions.

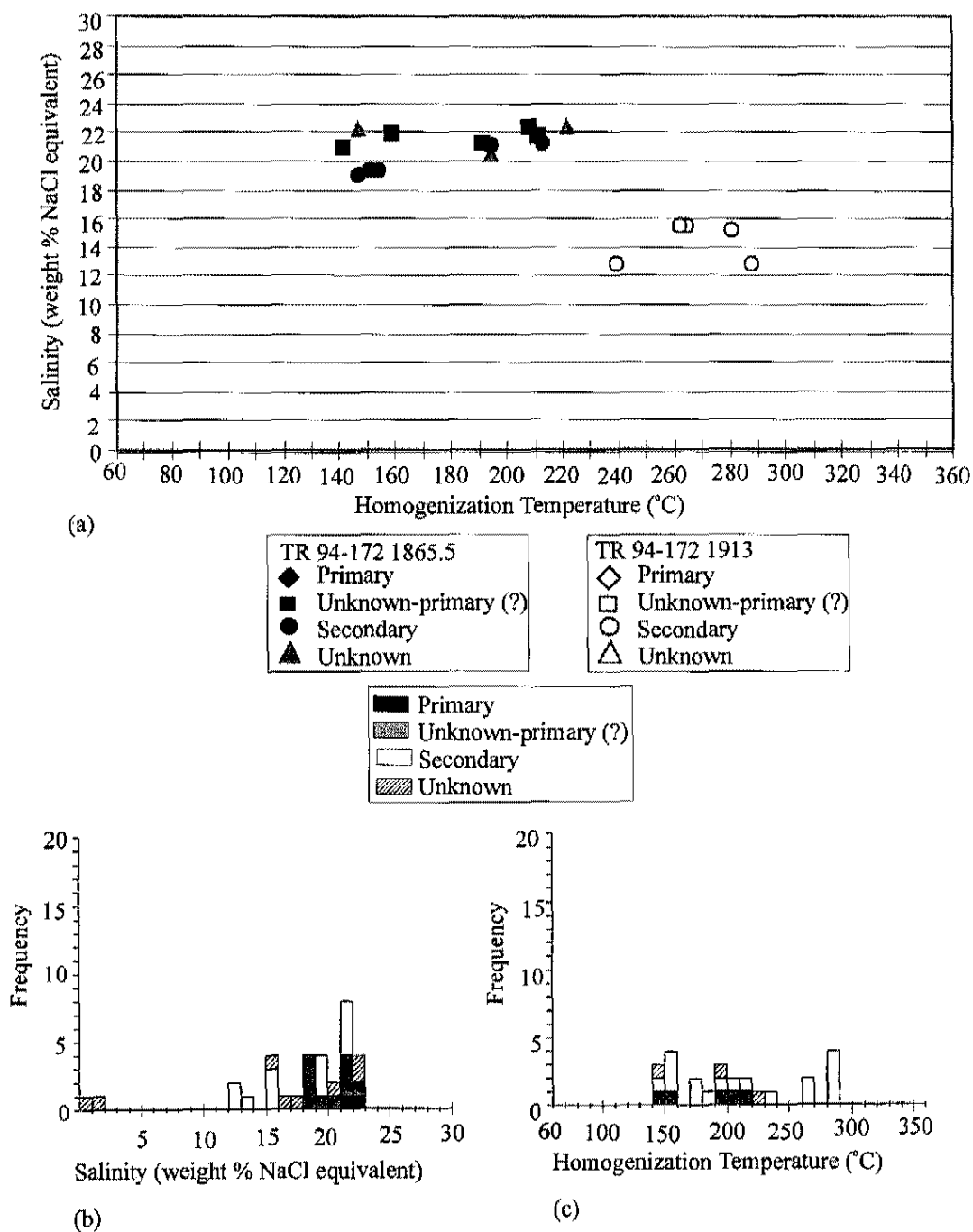


Figure 20. Microthermometric data for fluid inclusions in pre-ore stage quartz in gouge.

- (a) Plot of homogenization temperatures versus salinities. Data that do not have both homogenization temperatures and salinities are not shown on this chart.
- (b) Histogram of salinities of fluid inclusions.
- (c) Histograms of homogenization temperatures of fluid inclusions.

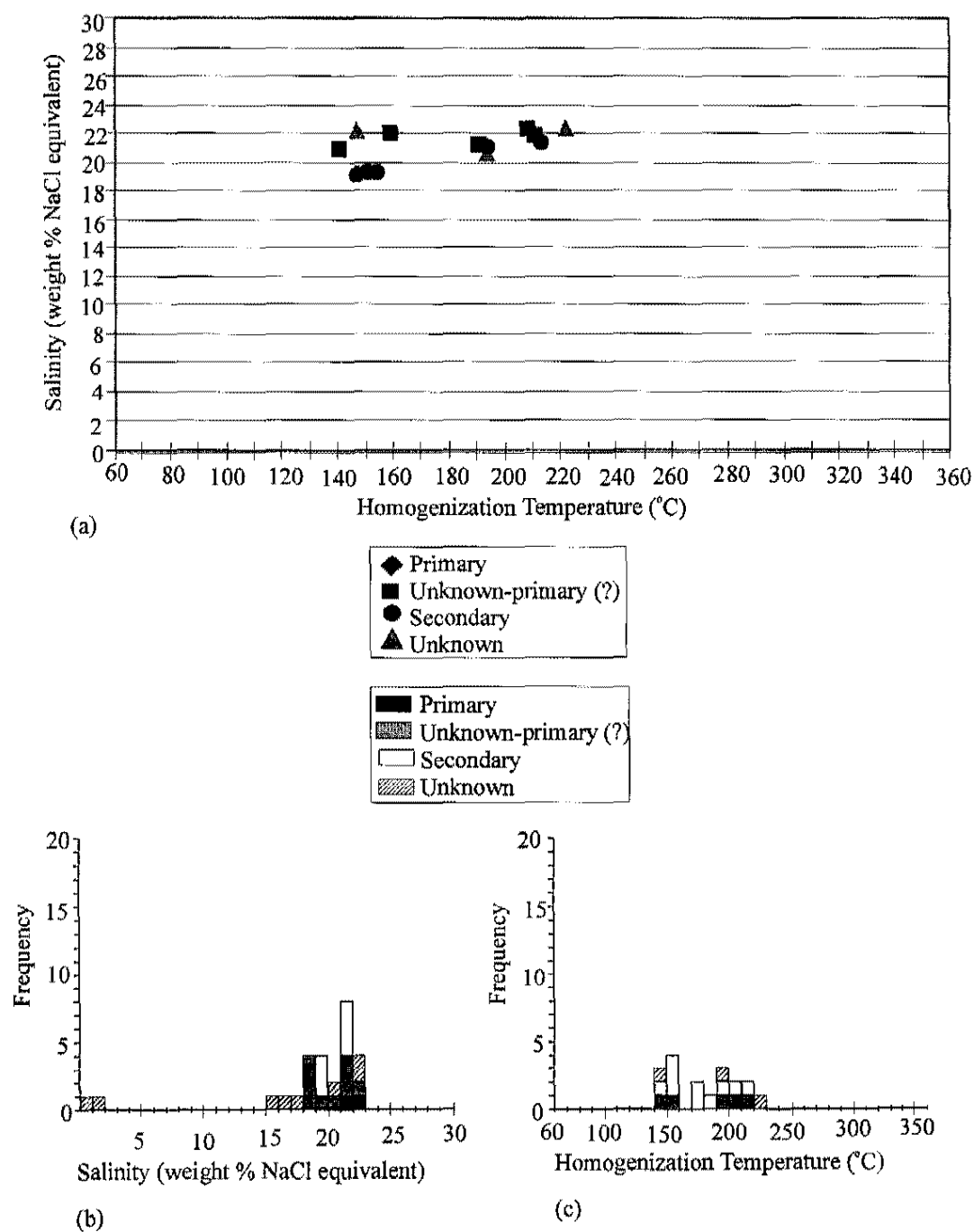


Figure 21. Microthermometric data for fluid inclusions in pre-ore stage quartz in gouge in TR 94-172 1865.5.

- (a) Plot of homogenization temperatures versus salinities. Data that do not have both homogenization temperatures and salinities are not shown on this chart.
- (b) Histogram of salinities of fluid inclusions.
- (c) Histograms of homogenization temperatures of fluid inclusions.

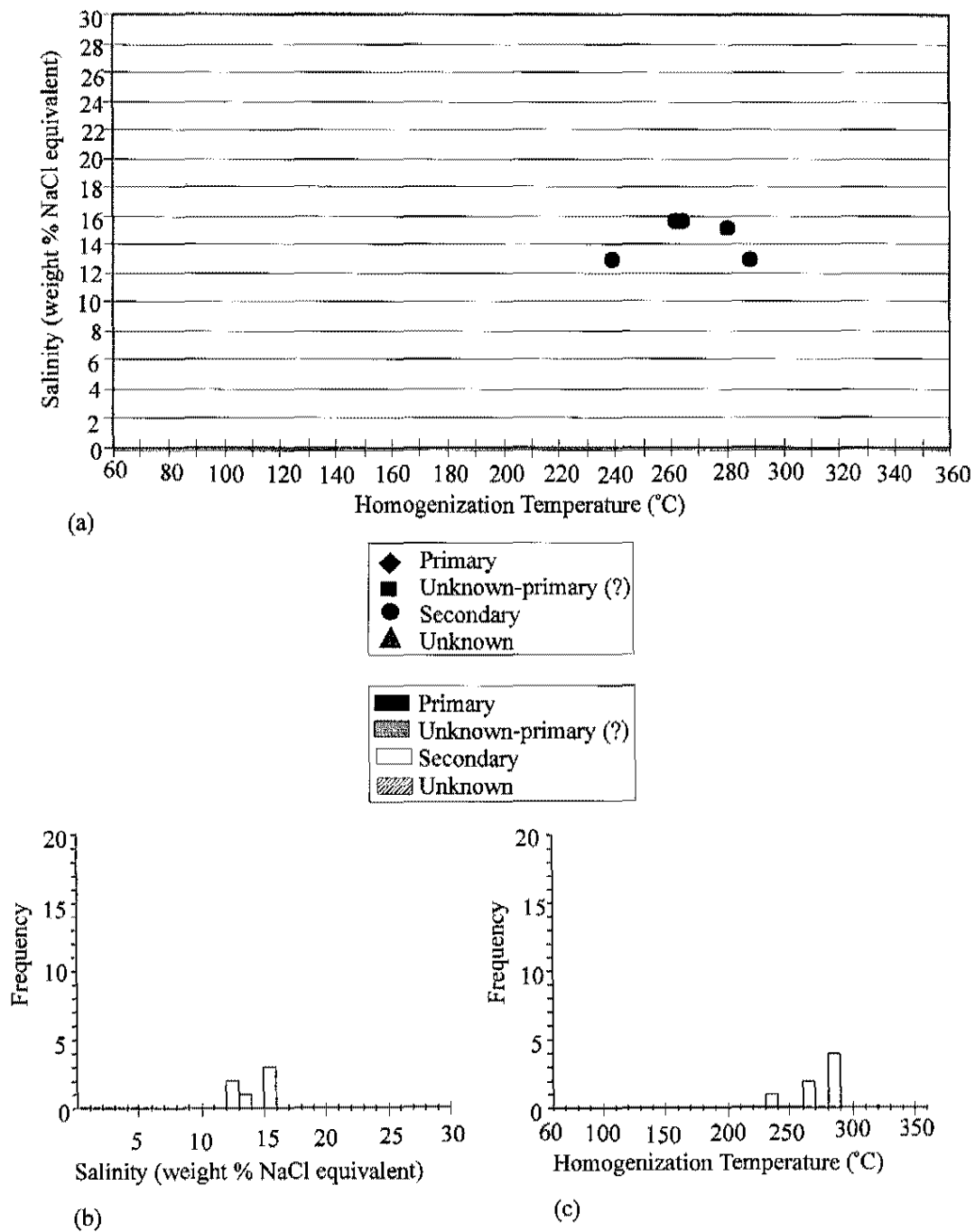


Figure 22. Microthermometric data for fluid inclusions in pre-ore stage quartz in gouge in TR 94-172 1913.

- (a) Plot of homogenization temperatures versus salinities. Data that do not have both homogenization temperatures and salinities are not shown on this chart.
- (b) Histogram of salinities of fluid inclusions.
- (c) Histograms of homogenization temperatures of fluid inclusions.

Unknown inclusions in TR 94-172 1865.5 have salinities ranging from 0.8 to 23 weight % NaCl equivalent, but there are no data points between 2 to 15 weight % NaCl equivalent (Figure 21a and b). These inclusions homogenized between 140 ° and 230 °C (Figure 21a and c).

Pre-Ore Quartz Crosscut by Ore-Stage Minerals

Primary and unknown-primary (?) inclusions in pre-ore stage quartz from TR 95-122 1619.5 that was crosscut by the ore-stage mineral assemblage were not identified. Secondary and unknown inclusions do not exhibit any trend but are spread evenly over a wide range of salinities and homogenization temperatures (Figure 23a).

Secondary inclusions have salinities between 1 and 18 weight % NaCl equivalent (Figure 23a and b). Homogenization temperatures ranged from 140 ° to 270 °C (Figure 23a and c). Salinities of unknown inclusions ranged from 9 to 11 weight % NaCl equivalent and from 17 to 18 weight % NaCl equivalent (Figure 23a and b). These inclusions homogenized between 200 ° and 290 °C (Figure 23a and c).

Discussion of Pre-Ore Stage Quartz Microthermometric Data

Microthermometric data collected from pre-ore quartz exhibit three clusters; one cluster represents two vein quartz samples, the other two clusters represent two gouge samples (Figure 24a). Salinities and homogenization temperatures of inclusions in quartz that is crosscut by ore-stage minerals do not exhibit any regular trend. Each of the three clusters exhibits a restricted range of salinities and a wider range of homogenization temperatures. The first data cluster from inclusions in pre-ore stage vein quartz has salinities between 4 and 11 weight % NaCl equivalent and homogenization temperatures ranging between 150 ° and 290 °C (Figure 24a). The second data cluster from inclusions in one quartz gouge sample has salinities between 18 and 23 weight % NaCl equivalent and homogenization temperatures between 140 ° and 220 °C (Figure 24a). The third cluster from another gouge sample has a range of salinities and homogenization temperatures between 12 and 16 weight % NaCl equivalent and 230 ° and 290 °C, respectively (Figure 24a).

The relatively restricted range of salinities and a wide range of homogenization temperatures of pre-ore stage vein quartz could theoretically indicate (1) fluid boiling, (2) fluid-evolution, (3) mixing of two fluids,

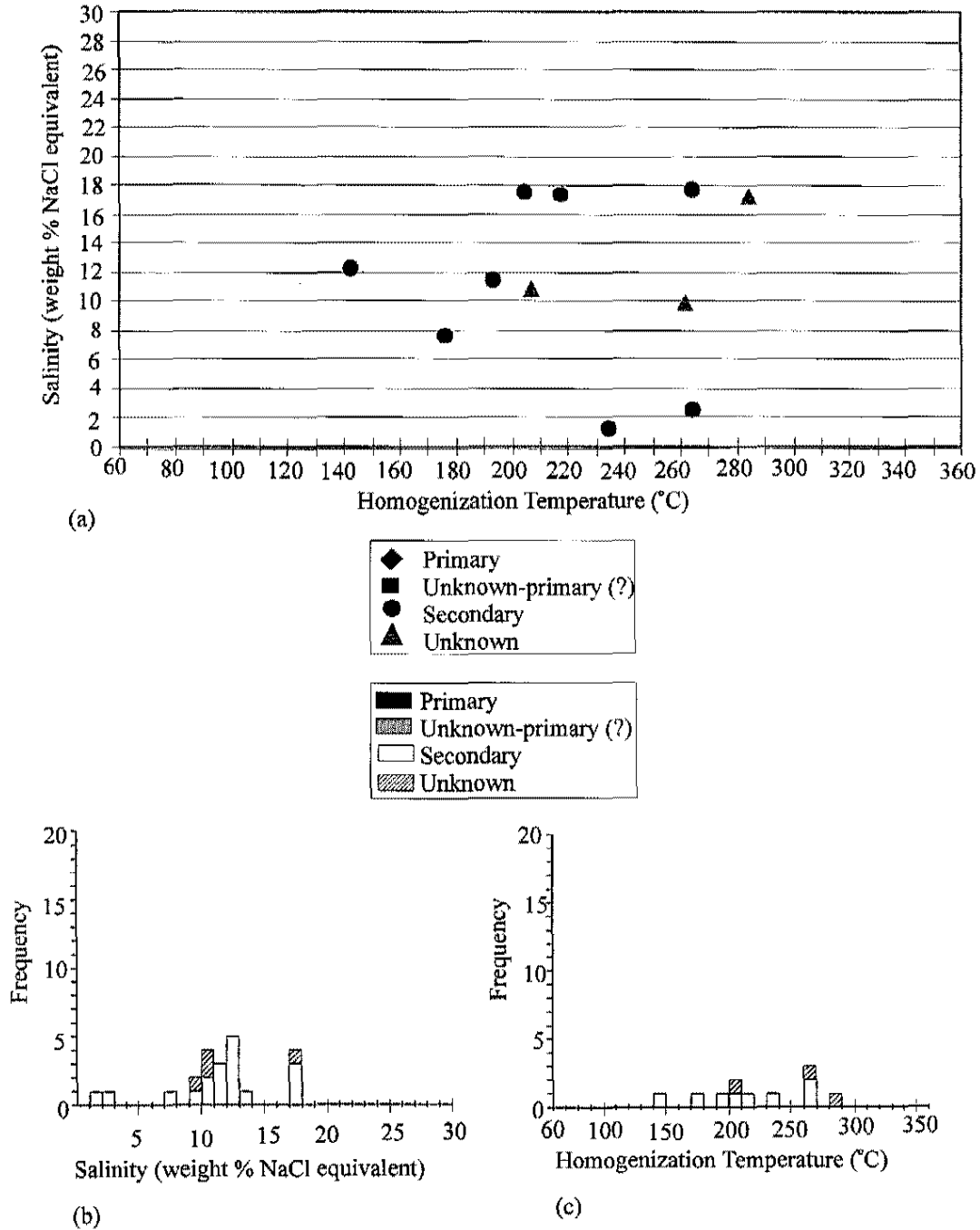


Figure 23. Microthermometric data for fluid inclusions in pre-ore stage quartz that are crosscut by ore-stage mineral assemblage in TR 95-122 1619.5.

- (a) Plot of homogenization temperatures versus salinities. Data that do not have both homogenization temperatures and salinities are not shown on this chart.
- (b) Histogram of salinities of fluid inclusions.
- (c) Histograms of homogenization temperatures of fluid inclusions.

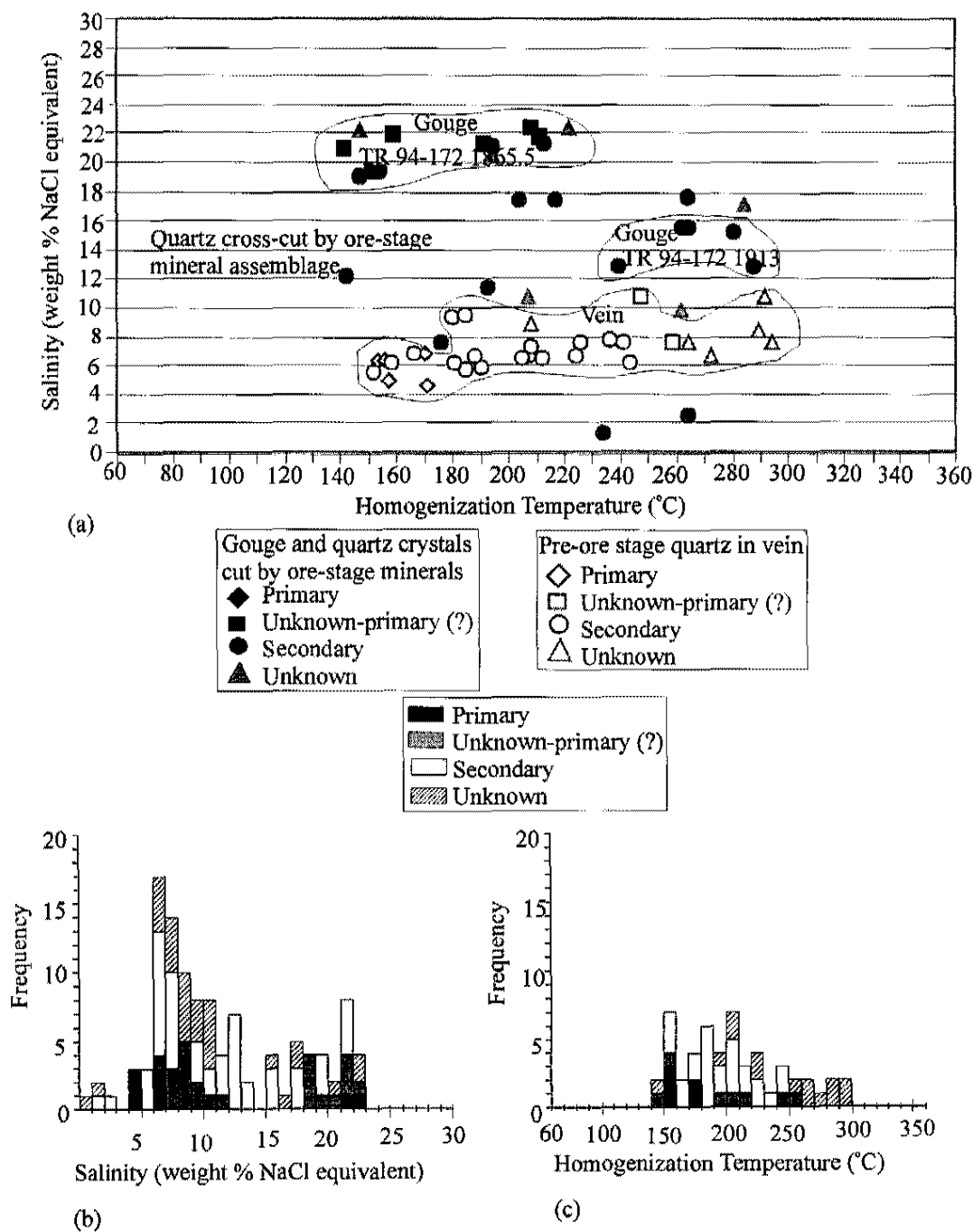


Figure 24. Microthermometric data for all fluid inclusions in pre-ore stage quartz.

- (a) Plot of homogenization temperatures versus salinities. Data that do not have both homogenization temperatures and salinities are not shown on this chart.
- (b) Histogram of salinities of fluid inclusions.
- (c) Histograms of homogenization temperatures of fluid inclusions.

or (4) multiple generations of fluids that were trapped at different times. First, this trend does not support fluid boiling, which would have concentrated salts in the remaining liquid as temperature of the fluid decreased. Second, the wide range of evenly distributed homogenization temperatures may indicate gradual change in temperature of a single fluid. Third, clusters of primary and unknown inclusions may indicate mixing of two different fluids with different temperatures but similar salinities. The secondary and unknown-primary (?) inclusions that plot between the primary and unknown inclusions may represent the mixed fluids. Fourth, as inclusions with different origins have different ranges of homogenization temperatures, inclusions may have trapped different fluids present at different times. In conclusion, salinities and homogenization temperatures of inclusions in pre-ore stage vein quartz indicate three possible fluid paths: (1) fluid evolution, (2) fluid mixing, and (3) multiple generations of fluids.

Salinities and homogenization temperatures exhibited by fluid inclusions in two gouge samples and quartz crystals in an ore-grade sample may reflect the presence of multiple generations of fluids (Figure 24a). Primary and unknown-primary inclusions in quartz in gouge have higher salinities ranging from 18 to 23 weight % NaCl equivalent that are different from primary inclusions in pre-ore quartz vein crystals. The salinity differences may exist because of: (1) fluid boiling during vein formation, (2) mixing of two fluids, or (3) inclusions in gouge and veins trapped different fluids at different times. First, fluid inclusions in the same FIA exhibiting inconsistent phase ratios resulted from fluid boiling was not detected by petrography, and also microthermometric data do not indicate a significant decrease in temperature, which commonly results from boiling. Second, few data points occur between the two clusters of salinities, and there is no distinctive mixing line (Figure 24a). Alternatively, clusters of data may indicate that quartz in gouge and in vein may have trapped different fluids at different times. Salinities and homogenization temperatures of primary and unknown-primary (?) inclusions in gouge samples are not consistent with primary inclusions in vein quartz and may indicate multiple generations of quartz precipitation events. Quartz crystals in gouge and in high-grade vein samples are fractured and crosscut by ore-stage minerals. Therefore, secondary and unknown fluid inclusions that are different from primary inclusions may have been trapped in fractures in pre-ore quartz crystals during some event after the vein formation, possibly during the gold event. Microthermometric data of secondary and unknown inclusions in gouge and ore-grade samples will be evaluated further in Chapter 7.

Fluid Inclusions in Ore-Stage Jasperoid Quartz

Jasperoid quartz contains small inclusions that are usually less than 2.5 micrometers in diameter. They are two-phase, liquid-dominant inclusions and contain vapor bubbles that occupy 5 to 10 volume % of the inclusions. Secondary, empty-looking, one-phase inclusions occur along planes with two-phase inclusions. The presence of inclusions with inconsistent phase ratios suggests that some inclusions have formed by necking. Microthermometric data were collected from a total of three ore-grade samples: two samples from TR 95-122 1617.5, and 1619.5, and one sample of fault gauge from TR 94-172 1913.

Primary fluid inclusions in ore-stage jasperoid quartz crystals have a range of salinities from 6 to 18 weight % NaCl equivalent (Figure 25a). Homogenization temperatures of these inclusions are spread between 130 ° and 200 °C (Figure 25b).

Unknown but possibly primary fluid inclusions have a range of salinities between 6 and 16 weight % NaCl equivalent, but no data points occur from 10 to 14 weight % NaCl equivalent (Figure 26a). These inclusions homogenized between 170 ° and 210 °C (Figure 26b).

Secondary inclusions in ore-stage jasperoid quartz yielded a range of salinities between 3 and 24 weight % NaCl equivalent, with a mode between 8 and 10 weight % NaCl equivalent (Figure 27a). These inclusions exhibit a wide range of homogenization temperatures from 110 ° to 280 °C; a mode is present between 160 ° and 190 °C (Figure 27b).

Unknown inclusions exhibited salinities similar to secondary fluid inclusions. Salinities ranged from 3 to 26 weight % NaCl equivalent (Figure 28a). Homogenization temperatures ranged from 120 ° to 310 °C (Figure 28b). The wide ranges of salinities and homogenization temperatures of fluid inclusions in ore-stage jasperoid quartz may reflect multiple events that were recorded by inclusions in jasperoid quartz crystals (Figure 29a and b). The following discussion presents microthermometric data for each jasperoid quartz sample to examine differences in salinities and homogenization temperatures between the samples.

Ore-Stage Jasperoid Quartz

A single euhedral ore-stage quartz crystal from TR 95-122 1617.5 contains fluid inclusions along discrete growth zones (Figure 30). The crystal is approximately 150 micrometers in diameter. One fracture is present in the crystal, but no fluid inclusions were identified along the fracture plane. Remnants

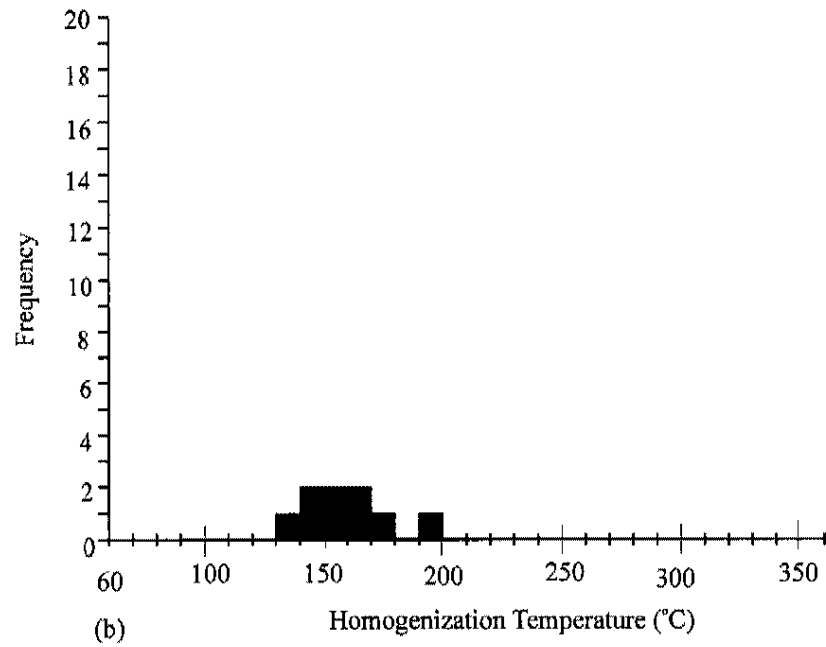
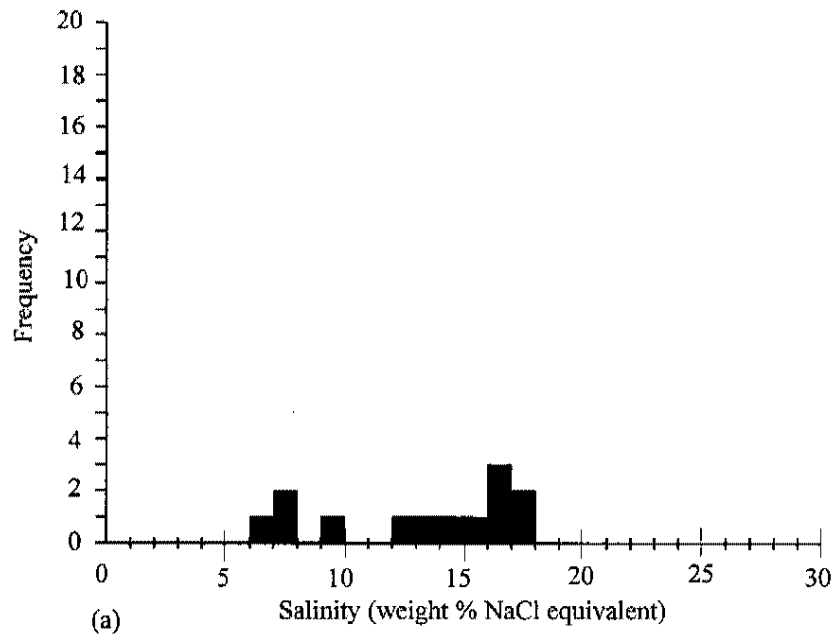


Figure 25. Salinities (a) and homogenization temperatures (b) of primary fluid inclusions in ore-stage jasperoid quartz.

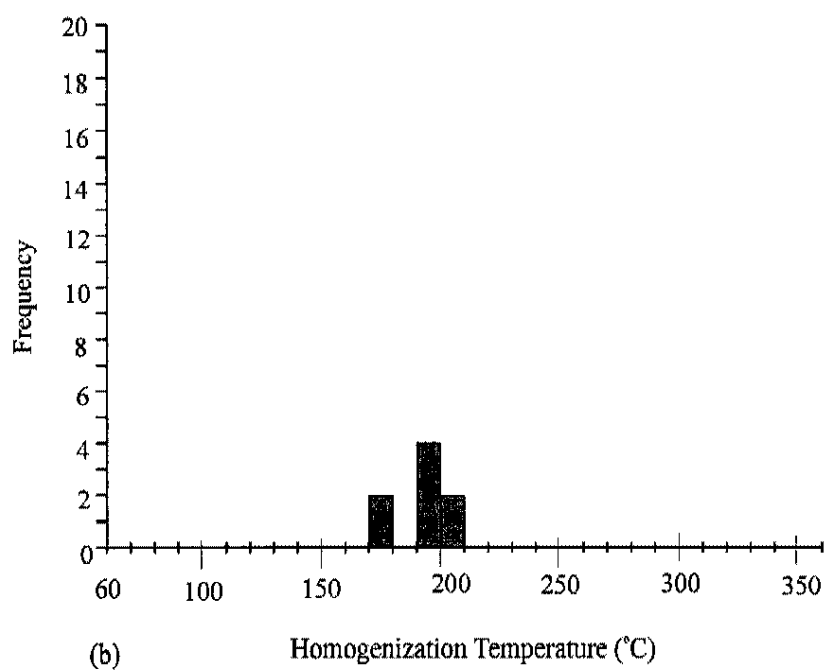
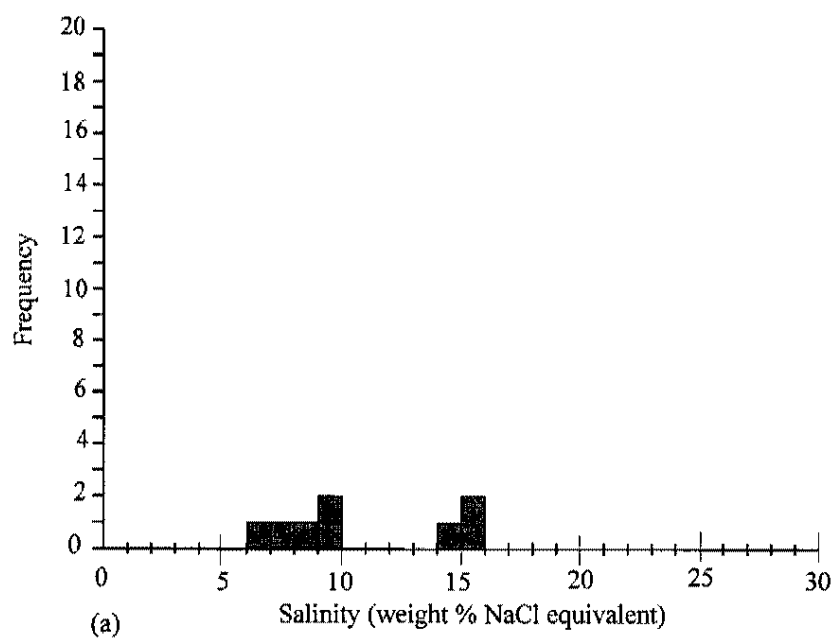


Figure 26. Salinities (a) and homogenization temperatures (b) of unknown-primary (?) fluid inclusions in ore-stage jasperoid quartz.

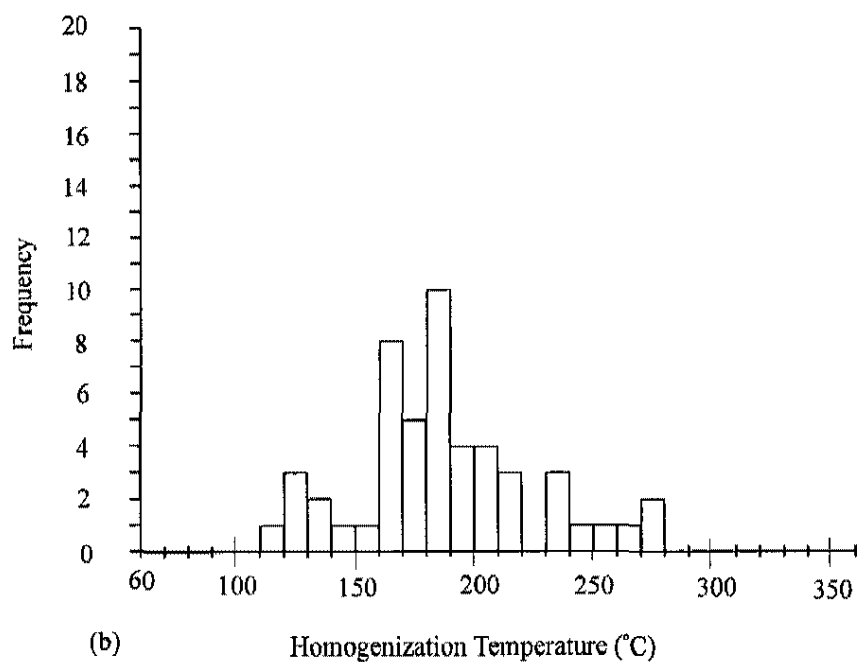
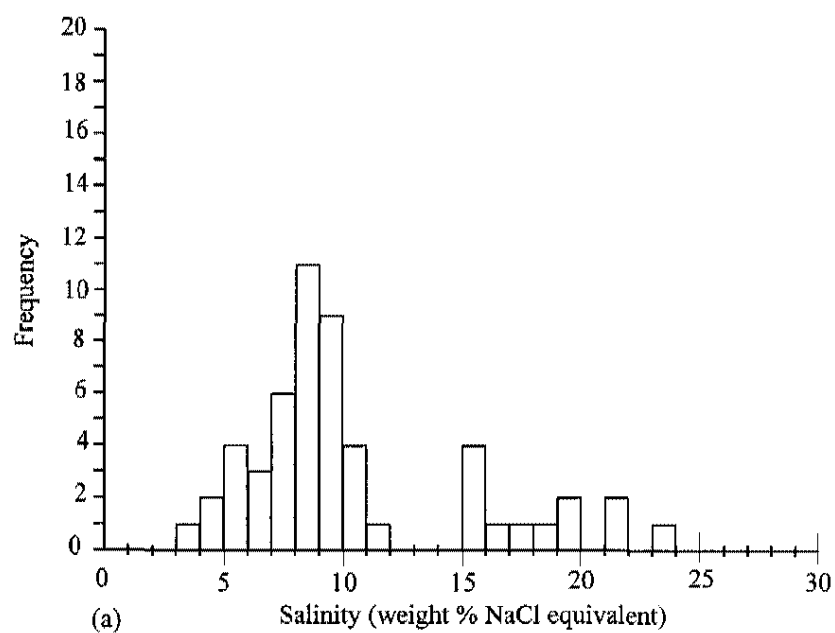


Figure 27. Salinities (a) and homogenization temperatures (b) of secondary fluid inclusions in ore-stage jasperoid quartz.

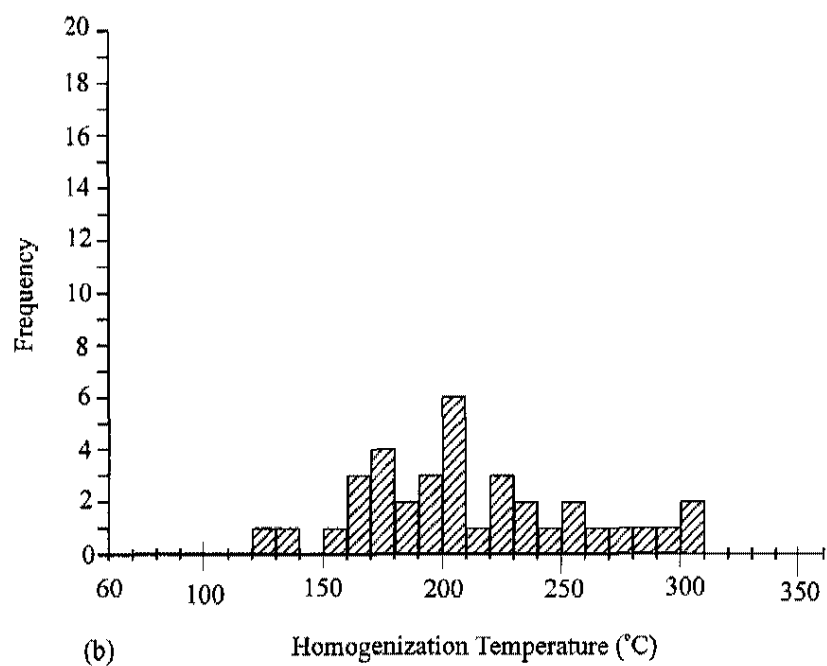
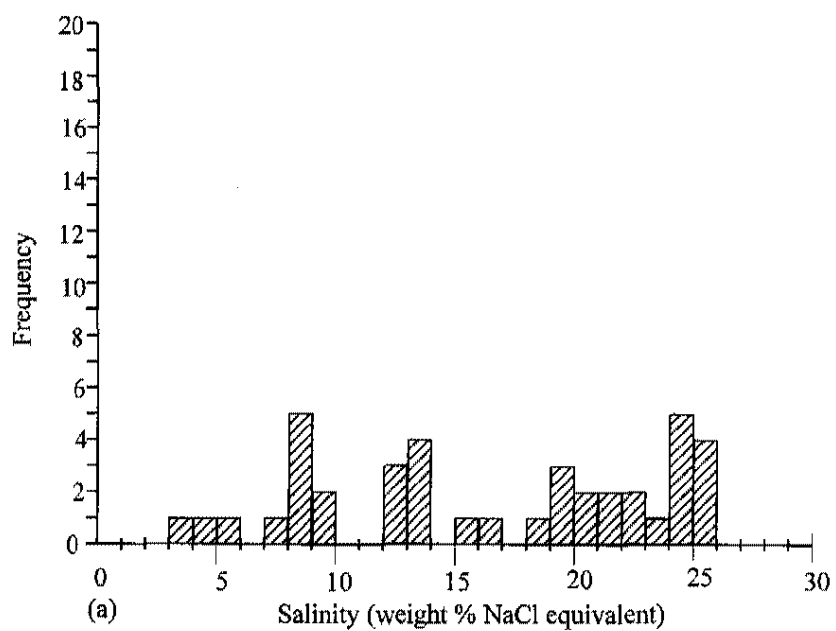


Figure 28. Salinities (a) and homogenization temperatures (b) of unknown fluid inclusions in ore-stage jasperoid quartz.

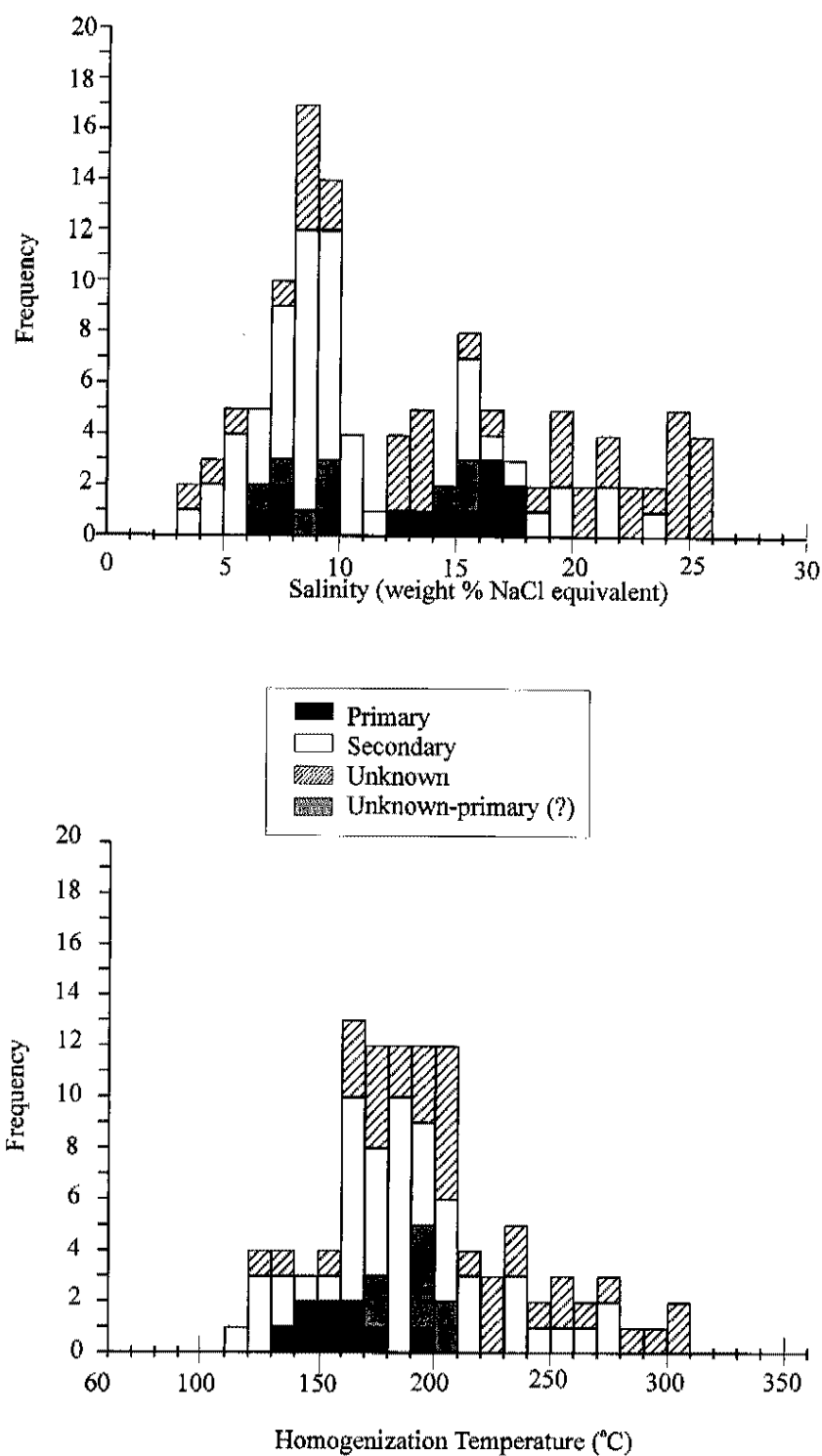


Figure 29. Salinities (a) and homogenization temperatures (b) of all fluid inclusions in ore-stage jasperoid quartz.

of microscopic calcite inclusions were trapped in the crystal indicating replacement of carbonates by the core of the crystal. Fluid inclusions along growth zones are two-phase, liquid-rich, and contain consistent vapor and liquid phase ratios. The vapor phase occupies 10 volume % of fluid inclusion.

Salinities and homogenization temperatures of the primary fluid inclusions along growth zones in the ore-stage jasperoid quartz crystal indicate that salinities varied from 12 to 17 weight % NaCl equivalent (Figure 30a), and these inclusions were trapped at minimum temperatures from 131 ° to 193 °C (Figure 30b). This euhedral crystal also contains gold-bearing pyrite crystals in the core and rim, indicating that this quartz crystal precipitated during the ore-stage event (Figure 31a). Electron microprobe analyses of the pyrite crystals confirmed the presence of gold and associated arsenic. The pyrite grains contain 1100 to 3200 ppm Au, and 10.92 to 15.33 weight % As (Table 2; Figure 31b). The fluid inclusions, therefore, record slight fluctuations in salinity and temperature of fluid during this period of quartz precipitation and trapping of gold-bearing pyrite.

A single fluid inclusion in the core of the crystal indicates that the ore fluid initially had a salinity of 15.9 weight % NaCl equivalent; this inclusion was trapped in the quartz at minimum temperatures of 131 °C (Figure 30). As the crystal grew outward, it encompassed 2 pyrite grains containing 14.13 to 15.33 weight % As and 1100 to 1200 ppm Au (Figure 31b). With continued growth, the quartz crystal trapped additional fluid inclusions. A fluid inclusion assemblage of two inclusions in an inner growth zone has salinities of 12.6 and 13.8 weight % NaCl equivalent and homogenization temperatures of 176 ° and 193 °C. Two nearby fluid inclusions have salinities of 17.3 weight % NaCl equivalent, and were trapped at minimum temperatures of 157 ° and 162 °C. Three fluid inclusions trapped in an outer growth zone indicate that salinities of fluids ranged from 14.7 to 16.9 weight % NaCl equivalent. Fluid inclusions were trapped along this growth zone between 143 ° and 160 °C. As the crystal continued to grow it trapped additional arsenic-rich gold-bearing pyrite grains near the outer rim of the quartz crystal (Figure 31b). A fluid inclusion trapped near the quartz crystal rim has salinity of 16 weight % NaCl equivalent and was trapped at a minimum temperature of 187 °C (Figure 30).

of microscopic calcite inclusions were trapped in the crystal indicating replacement of carbonates by the core of the crystal. Fluid inclusions along growth zones are two-phase, liquid-rich, and contain consistent vapor and liquid phase ratios. The vapor phase occupies 10 volume % of fluid inclusion.

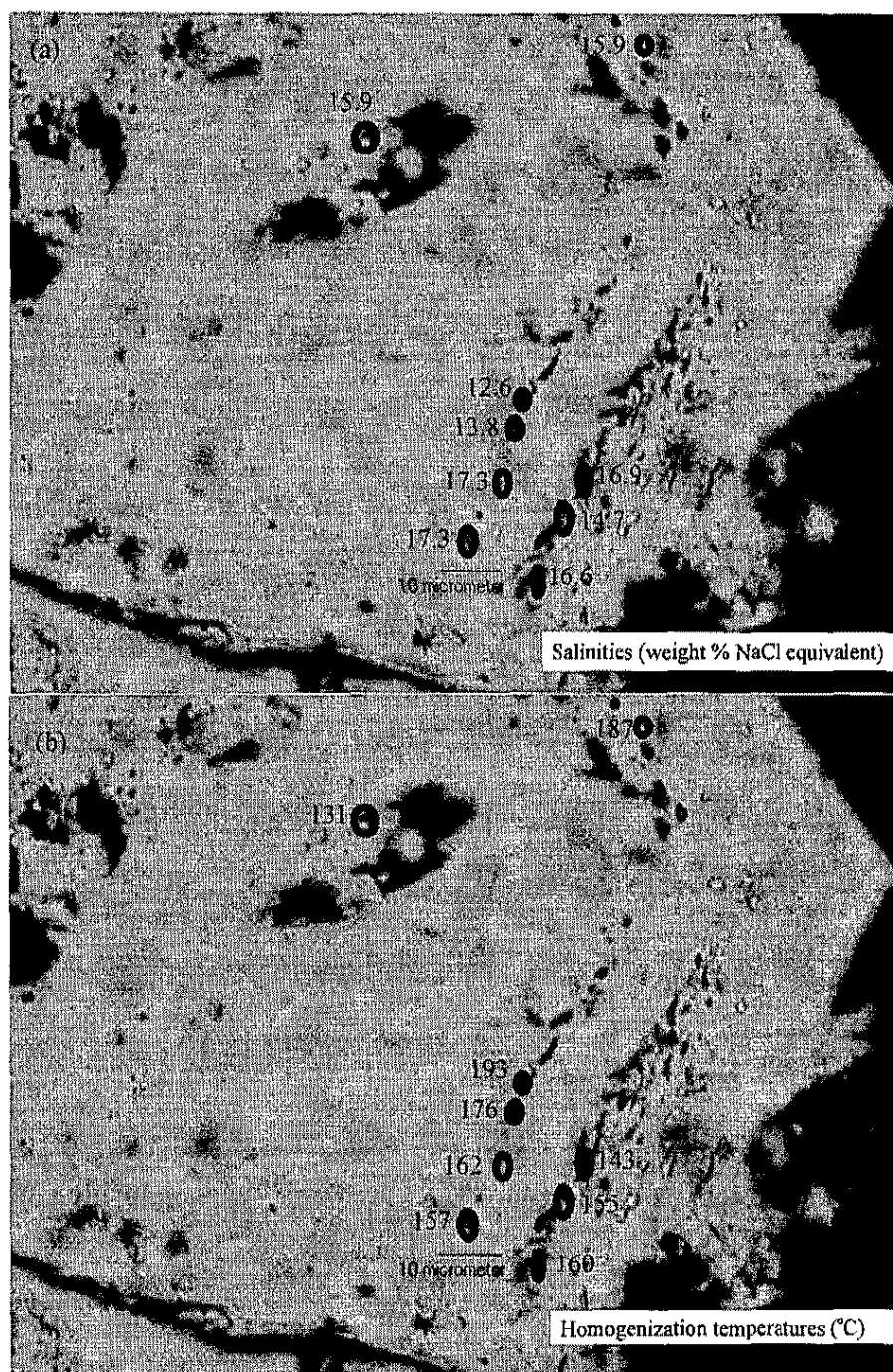


Figure 30. Salinities (a) and homogenization temperatures (b) of primary fluid inclusions in an euhedral ore-stage jasperoid quartz in sample TR 95-122 1617.5. Photomicrographs (a) and (b) were taken under plan polarized light.

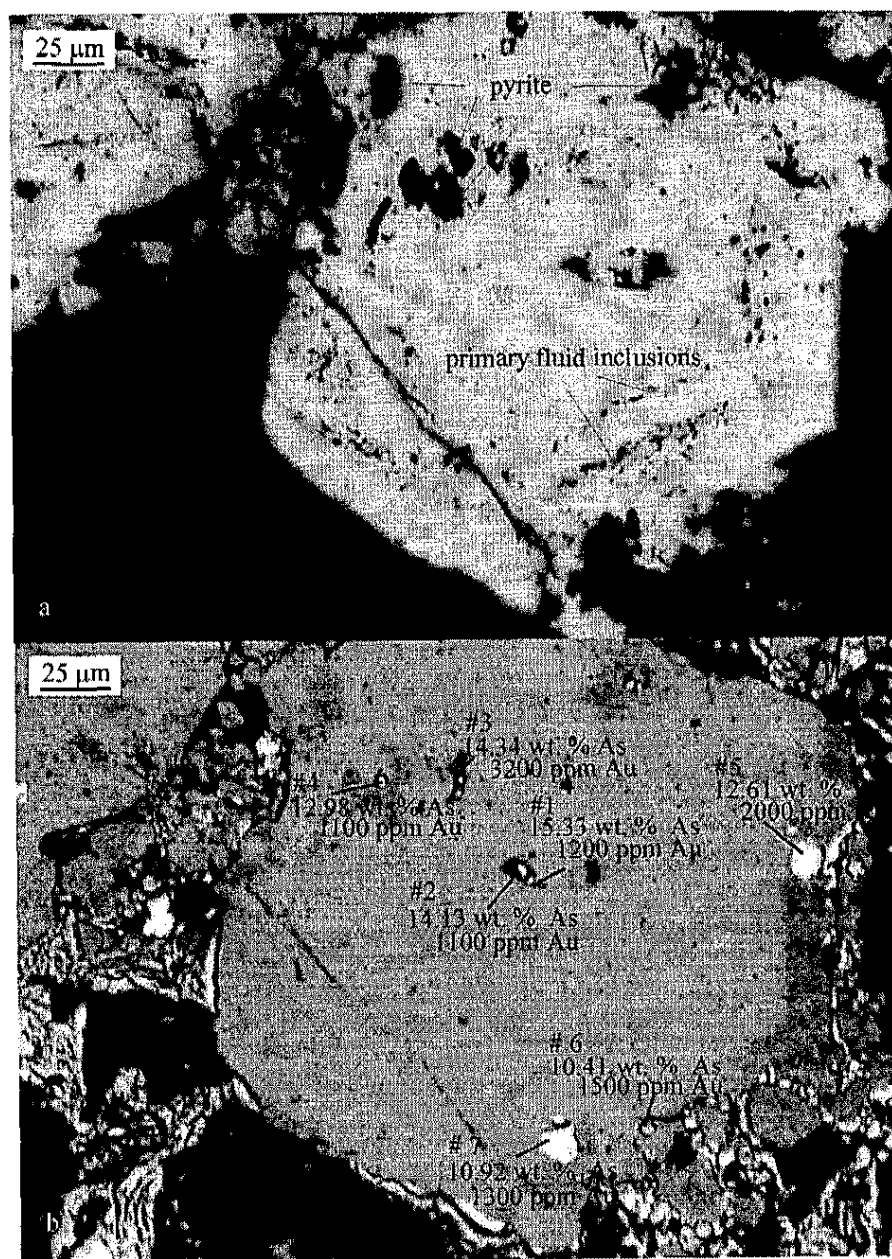


Figure 31. Primary fluid inclusions in growth zones (a) and results of electron microprobe analyses of pyrite crystals in an euhedral ore-stage jasperoid quartz crystal in TR 95-122 1617.5. Photomicrographs (a) and (b) were taken under plane polarized transmitted and reflected light, respectively. Refer to Table 2 for detailed electron microprobe data.

The same sample, TR 95-122 1617.5, contains unknown-primary (?), secondary, and unknown inclusions. Unknown-primary (?) inclusions have salinities ranging from 6 to 16 weight % NaCl equivalent (Figure 32b). These inclusions homogenized from 170 ° to 210 °C (Figure 32c).

Salinities and homogenization temperatures of secondary inclusions exhibit a wide range (Figure 32a). The secondary inclusions have salinities between 6 and 19 weight % NaCl equivalent (Figure 32b). These inclusions homogenized between 110 ° and 280 °C (Figure 32c).

Unknown inclusions yielded variable salinities and homogenization temperatures (Figure 32a). Salinities range from 9 to 26 weight % NaCl equivalent (Figure 32b). Homogenization temperatures of these inclusions ranged between 120 ° and 310 °C (Figure 32c).

Secondary and unknown inclusions in ore-stage jasperoid quartz crystals from TR 95-122 1619.5 exhibit similar salinities and homogenization temperatures (Figure 33a). Salinities of secondary inclusions ranged from 5 to 10 weight % NaCl equivalent, and unknown inclusions have salinities between 3 to 10 weight % NaCl equivalent (Figure 33b). Secondary and unknown inclusions homogenized between 160 ° to 210 °C and 180 ° to 220 °C, respectively (Figure 33c).

Ore-Stage Jasperoid Quartz in Gouge

Jasperoid quartz crystals in gouge from TR 94-172 1913 do not contain pyrite crystals. However, assays indicate the presence of gold in the sampled interval containing sample TR 94-172 1913. Realgar encompasses the quartz crystals and fills spaces between pre-ore stage quartz and jasperoid quartz indicating migration of the hydrothermal fluid through the gouge after fracturing. The inclusions in jasperoid quartz from gouge show two ranges of salinities and a wide range of homogenization temperatures (Figure 34a).

Primary fluid inclusions in ore-stage jasperoid quartz crystals have salinities between 6 to 10 weight % NaCl equivalent (Figure 34b). A homogenization temperature, between 140 ° and 150 °C, was collected from only one primary inclusion (Figure 34b).

Secondary inclusions have salinities ranging from 3 to 24 weight % NaCl equivalent and a small mode between 7 and 10 weight % NaCl equivalent (Figure 34b). Homogenization temperatures exhibit a range from 120 ° to 250 °C and have a mode between 160 ° and 190 °C (Figure 34c).

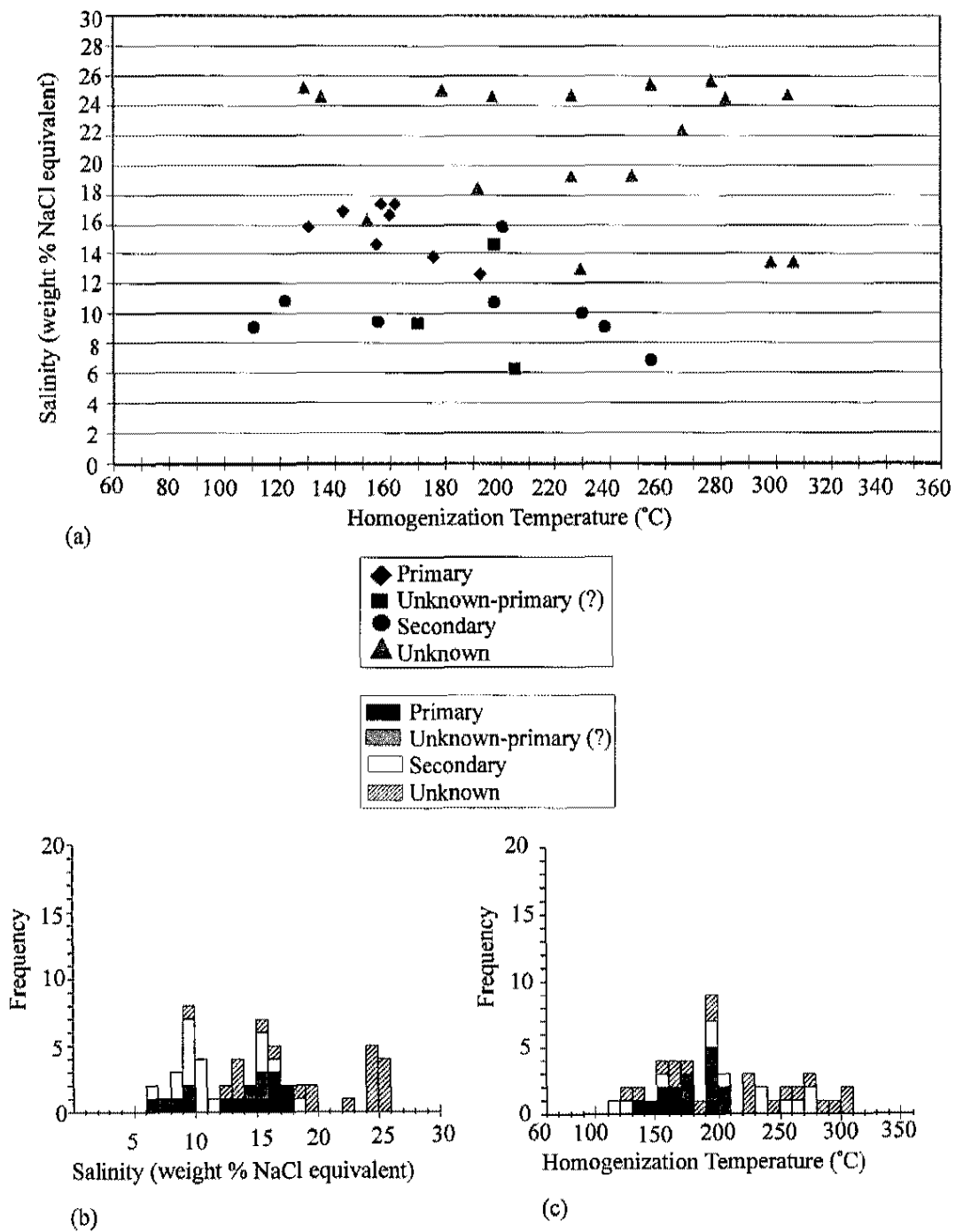


Figure 32. Microthermometric data for fluid inclusions in ore-stage jasperoid quartz in TR 95-122 1617.5.

- (a) Plot of homogenization temperatures versus salinities. Data that do not have both homogenization temperatures and salinities are not shown on this chart.
- (b) Histogram of salinities of fluid inclusions.
- (c) Histograms of homogenization temperatures of fluid inclusions.

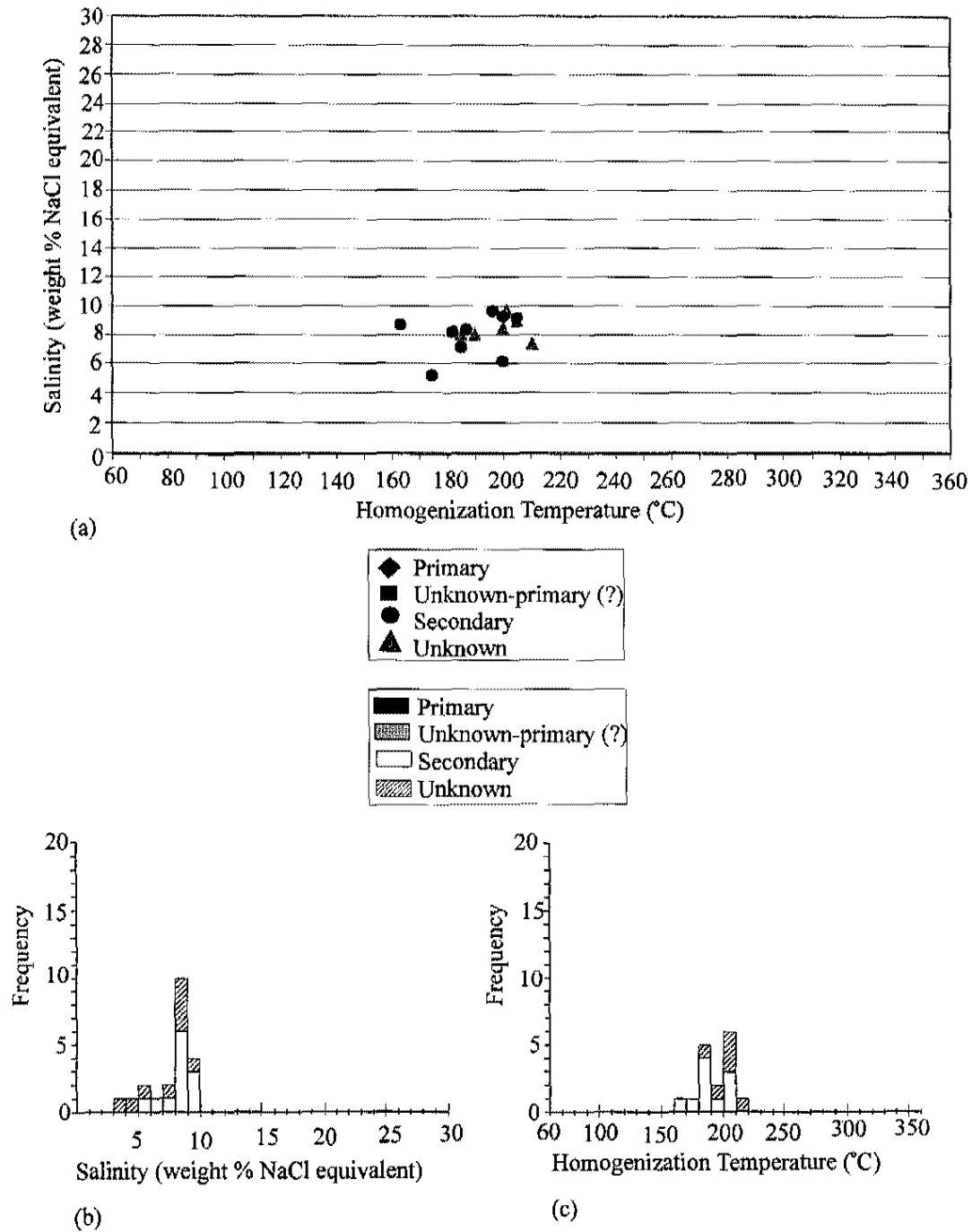


Figure 33. Microthermometric data for fluid inclusions in ore-stage jasperoid quartz in TR 95-122 1619.5.

- (a) Plot of homogenization temperatures versus salinities. Data that do not have both homogenization temperatures and salinities are not shown on this chart.
- (b) Histogram of salinities of fluid inclusions.
- (c) Histograms of homogenization temperatures of fluid inclusions.

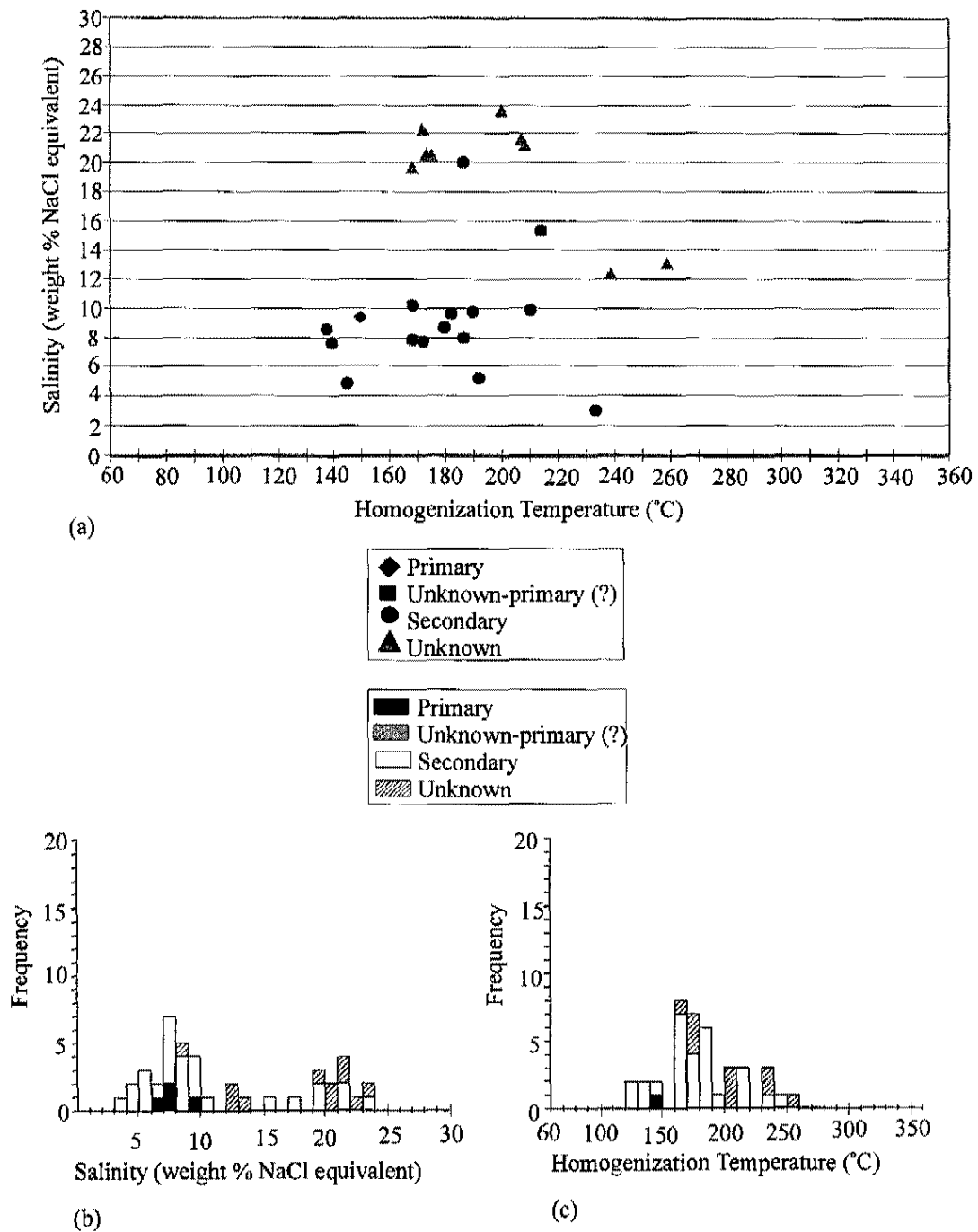


Figure 34. Microthermometric data for fluid inclusions in ore-stage jasperoid quartz in gouge in TR 94-172 1913.

- (a) Plot of homogenization temperatures versus salinities. Data that do not have both homogenization temperatures and salinities are not shown on this chart.
- (b) Histogram of salinities of fluid inclusions.
- (c) Histograms of homogenization temperatures of fluid inclusions.

Unknown inclusions have a range of salinities from 8 to 24 weight % NaCl equivalent (Figure 34b). These inclusions homogenized between 160 ° and 260 °C (Figure 34 c).

Discussion of Ore-Stage Jasperoid Quartz Microthermometric Data

Primary, unknown-primary (?), secondary, and unknown fluid inclusions in ore-stage jasperoid quartz show a wide range of salinities and homogenization temperatures. Inclusions in ore-stage jasperoid quartz crystals exhibit two clusters of salinities (Figure 35a): primary inclusions in TR 95-122 1617.5 form one cluster with a range of salinities from 12 to 18 weight % NaCl equivalent, and secondary and unknown inclusions in TR 95-122 1619.5 form another cluster with a range of salinities from 5 to 10 weight % NaCl equivalent.

Inclusions in jasperoid quartz crystals in gouge from TR 94-172 1913 also show two ranges of salinities (Figure 35a). Primary and secondary inclusions form a ragged cluster of data points with most salinities between 5 and 11 weight % NaCl equivalent; a majority of these inclusion homogenized between ~ 130 °C, and 210 °C. Unknown inclusions form another cluster with salinities between 19 and 24 weight % NaCl equivalent and homogenization temperatures between 160 ° and 220 °C (Figure 35a). This last cluster is consistent with the range of salinities (18 to 26 weight % NaCl equivalent) of unknown inclusions from TR 95-122 1617.5 (Figure 35a).

The groups of salinities and homogenization temperatures may reflect (1) an evolved fluid composition, (2) fluid mixing, (3) fluid boiling, or (4) multiple fluid generations that were trapped at different times. If a fluid evolved through time and gradually changed its temperature and/or composition, data points should be regularly distributed over a range of salinities and homogenization temperatures. The microthermometric data do not exhibit this trend. If two fluids with different salinities mix, the microthermometric data should exhibit two clusters of data points, with additional data points distributed between the two clusters. Data from the Turquoise Ridge deposit do not exhibit such a trend. Boiling of a fluid can cause an increase in salinity, with temperature decrease. This trend is also not indicated by the Turquoise Ridge inclusions. Inclusions in jasperoid quartz from the Turquoise Ridge deposit exhibit different ranges of salinities over a wide range of homogenization temperatures. The groups of salinities, therefore, probably reflect compositions of different fluids that were trapped at different times. One group

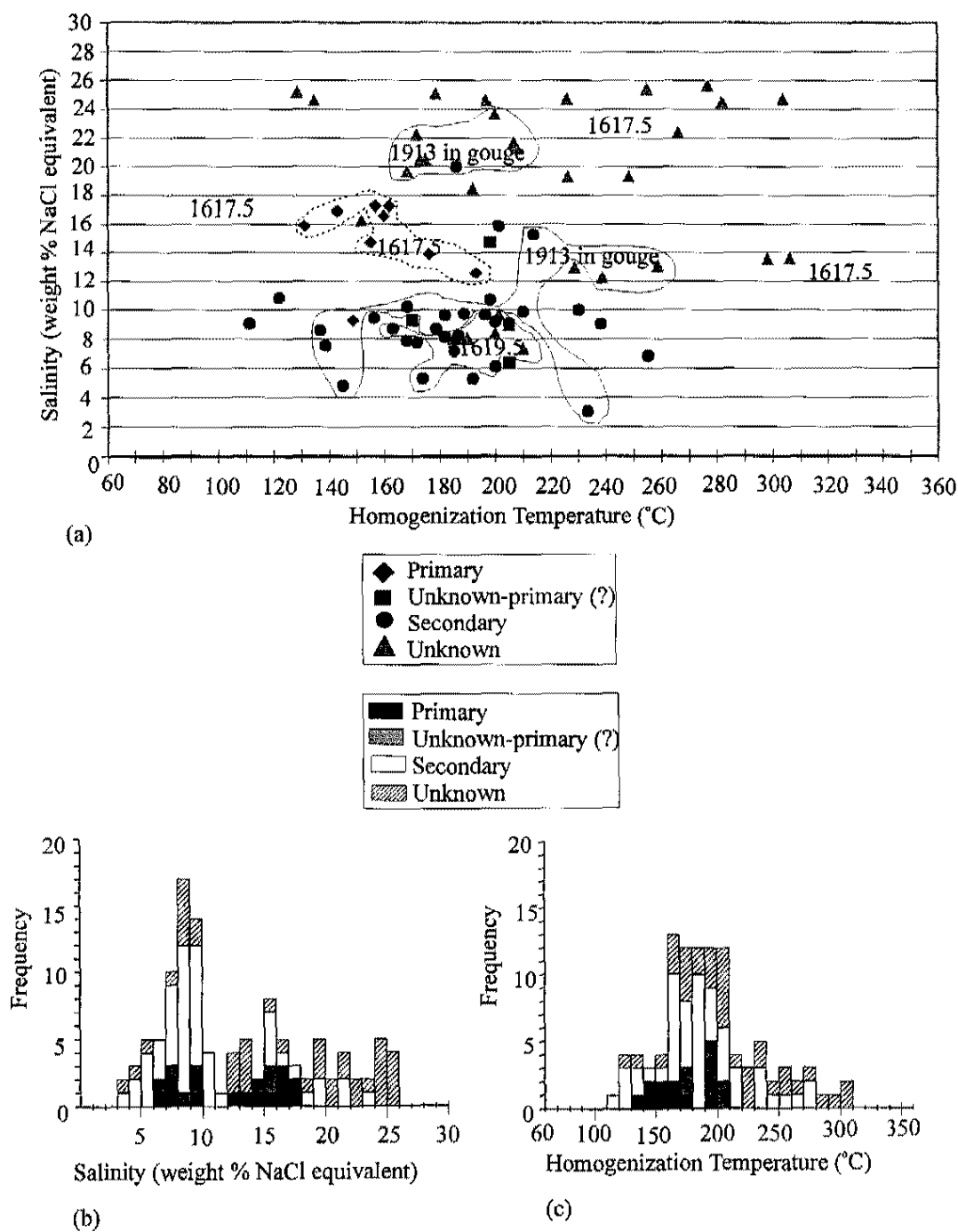


Figure 35. Microthermometric data for all fluid inclusions in ore-stage jasperoid quartz.

- (d) Plot of homogenization temperatures versus salinities. Data that do not have both homogenization temperatures and salinities are not shown on this chart.
- (e) Histogram of salinities of fluid inclusions.
- (f) Histograms of homogenization temperatures of fluid inclusions.

reflects the conditions during the gold mineralizing event, and other groups of fluid inclusions may have been trapped before or after the hydrothermal event.

The salinities, 12 to 17 weight % NaCl equivalent, and homogenization temperatures, 131 ° to 193 °C, of primary fluid inclusions in growth zones in the pyrite-bearing jasperoid quartz crystal suggest that the salinities and temperatures of the ore fluid fluctuated mildly during this period of quartz precipitation and trapping of pyrite crystals.

The jasperoid quartz crystals in gouge do not contain ore-stage pyrite crystals, but are encompassed by realgar. Therefore, the 6 to 10 weight % NaCl equivalent salinities of primary inclusions in gouge may reflect conditions during jasperoid formation prior to ore-stage precipitation. Salinities of 6 to 19 weight % NaCl equivalent, determined for secondary fluid inclusions in jasperoid quartz from TR 95-122 1619.5 and TR 94-172 1913 may reflect fluids that migrated through the fracture zone after the gold hydrothermal event.

Unknown inclusions in TR 95-122 1617.5 and TR 94-172 1913 do not fit in either cluster, and their time of entrapment is unknown. These inclusions have a particularly wide range of homogenization temperatures. Although an attempt was made to analyze only inclusions in fluid inclusion assemblages, high homogenization temperatures may reflect inclusion leaking, and variable temperatures may also be a result of necking of fluid inclusions.

Fluid Inclusions in Late-Ore Stage Minerals

Fluid inclusions are sparse in fluorite, orpiment, realgar, and calcite. Where present, inclusions are generally less than 2.5 micrometers, and the small size and dark internal reflections of inclusions prohibited identification of phases. Most inclusions are located along fracture planes, and are secondary. Orpiment and realgar are generally either free of fluid inclusions, or inclusions are too small to distinguish phases. Rare inclusions are 5 to 10 micrometers in diameter. Calcite primarily contains secondary or unknown fluid inclusions that are generally less than 2 micrometers in diameter; a few are larger than 5 micrometers in diameter. Fluid inclusions in calcite are liquid-rich with approximately 10 volume % occupied by the vapor phase. The presence of one-phase, empty-looking inclusions, and two-phase inclusions along the

same plane indicates inclusion necking. Fluorite is either inclusion-free, or inclusions are too small for phases to be identified.

CHAPTER 6

STABLE ISOTOPE ANALYSES

Oxygen and hydrogen isotopic signatures were determined for fluids released from inclusions in two pre-ore stage quartz samples, two ore-stage jasperoid quartz samples, one late-ore stage realgar sample, and one late-ore calcite sample. One pre-ore stage sample was collected from a vein that crosscuts the black Lower unit. The quartz vein contained abundant euhedral to subhedral quartz crystals. Pre-ore quartz in a sample that was crosscut by ore-stage minerals provided the second sample; realgar was collected from the same drill hole interval. Two ore-stage jasperoid quartz samples were collected approximately 10 meters apart from a drill hole. The Lower unit hosts the ore-stage jasperoid quartz samples. A low-grade sample that primarily contained late ore-stage orpiment and calcite with minor realgar, jasperoid quartz, fluorite, and pyrite crystals provided a calcite sample.

$\delta^{18}\text{O}$ values were determined for quartz and calcite. $\delta^{18}\text{O}_{\text{H}_2\text{O}}$ values of inclusion fluids in equilibrium with quartz and calcite were calculated using formulas provided by Matsuhisa et al., (1979) and Friedman and O'Neil (1977), respectively, that describe the fractionation of oxygen isotopes between quartz or calcite and H_2O as a function of temperature. $\delta^{18}\text{O}_{\text{H}_2\text{O}}$ values of inclusion fluids in realgar, and $\delta\text{D}_{\text{H}_2\text{O}}$ of inclusion fluids in quartz, calcite, and realgar were also determined. Three-phase $\text{CO}_2\text{-H}_2\text{O}$ inclusions at Getchell provided pressure estimates during inclusion trapping at Getchell (Cline, 1999). Pressure corrected microthermometric data from the Getchell deposit (Cline, 1999) and homogenization temperatures from the Turquoise Ridge deposit provided temperatures to determine oxygen isotopic fractionation factors for quartz and calcite. Cline's study (1999) suggests that homogenization temperatures of pre-ore stage quartz from the Getchell deposit that ranged from 160 ° to 200 °C indicate trapping temperatures of 275 ° to 330 °C using a pressure correction of 1.9 kb. Although homogenization temperatures of pre-ore stage quartz from the Turquoise Ridge deposit ranged from 125 ° to 325 °C, a significant number of data points for primary, secondary, and unknown inclusions fall in a range between

150 ° and 230 °C. As the differences in homogenization temperatures from the Turquoise Ridge and Getchell are not large, a temperature range of 250 ° to 350 °C was selected to calculate the fractionation factor for these fluids in pre-ore stage quartz. Fluid inclusions in ore-stage jasperoid quartz from the Getchell deposit homogenized between 160 ° and 200 °C. These inclusions were trapped between 180 ° and 220 °C assuming a confining pressure of 330 bars. Inclusions in ore-stage jasperoid quartz from the Turquoise Ridge deposit homogenized between 130 ° and 230 °C. These numbers are generally consistent with microthermometric data from the Getchell deposit. A temperature range of 160 ° to 240 °C was used to calculate the isotopic fractionation factor. Microthermometric data were not collected from calcite samples from the Turquoise Ridge deposit. However, data from the Getchell deposit suggest that fluid inclusions were trapped in calcite at minimum temperatures between 115 ° and 180 °C, and this range was used to calculate isotopic fractionation factors for calcite.

Experimental results for minerals and fluids are summarized in Table 4 and Figure 36. Results show that inclusions in pre-ore stage vein quartz exhibited $\delta D_{H_2O} = -54 \text{ ‰}$ and $\delta^{18}O_{H_2O} = +13.1 \text{ to } +16.7 \text{ ‰}$. Isotopic signatures of pre-ore stage quartz in an ore-grade sample were $\delta D_{H_2O} = -75 \text{ ‰}$ and $\delta^{18}O_{H_2O} = +10.8 \text{ to } +14.4 \text{ ‰}$. Inclusions in ore-stage jasperoid yielded isotopic signatures of $\delta D_{H_2O} = -33 \text{ ‰}$ and $\delta^{18}O_{H_2O} = +7.1 \text{ to } +12.2 \text{ ‰}$, and $\delta D_{H_2O} = -46 \text{ ‰}$ and $\delta^{18}O_{H_2O} = +5.4 \text{ to } +10.5 \text{ ‰}$. Inclusions in late-ore stage calcite yielded $\delta D_{H_2O} = -110 \text{ ‰}$ and $\delta^{18}O_{H_2O} = +9.64 \text{ to } +14.6 \text{ ‰}$ (Table 4, Figure 36). Isotopic signatures of inclusion fluids in late ore-stage realgar, $\delta D_{H_2O} = -140 \text{ ‰}$ and $\delta^{18}O_{H_2O} = -15.6 \text{ ‰}$, were determined directly from the fluid.

Discussion of Stable Isotope Analysis

Inclusion fluid in pre-ore stage vein quartz (Figure 36, and Table 4) indicates a metamorphic or magmatic fluid source. The spatial association between the intrusion and the quartz veins supports an igneous fluid source. The pre-ore magmatic fluid may have equilibrated with metasedimentary rocks as the fluid moved through the wall-rock. As a result, the magmatic fluid may have shifted to a more metamorphic oxygen isotopic signature (Figure 36). Alternatively, the pressure correction from Getchell, used to correct homogenization trapping temperatures, may not be appropriate for Turquoise Ridge. A lower pressure correction would provide a lower trapping temperature to calculate the fractionation of $\delta^{18}O$

Table 4. Oxygen and hydrogen isotope ratios of inclusion fluids in pre-ore stage quartz, ore-stage jasperoid quartz, and late ore-stage realgar and calcite.

* = measured $\delta^{18}\text{O}$ on quartz and calcite, or on inclusion fluids in realgar.

** = $\delta^{18}\text{O}$ values calculated for the fluid in equilibrium with quartz or calcite for a range of possible temperatures.

Sample #	$\delta^{18}\text{O}^*$	T (°C)	T (K)	Fractionation factor	$\delta^{18}\text{O}_{\text{H}_2\text{O}}^{**}$	δD
TR 95-122 1760.5 pre-ore stage quartz in vein	22	250	523.15	8.9	13.1	-54
		275	548.15	7.8	14.2	
		300	573.15	6.9	15.1	
		325	598.15	6.0	16.0	
		350	623.15	5.3	16.7	
TR 95-122 1617.5 pre-ore stage quartz in ore-grade sample	19.7	250	526.25	8.9	10.8	-75
		275	548.15	7.8	11.9	
		300	573.15	6.9	12.8	
		325	598.15	6.0	13.7	
		350	623.15	5.3	14.4	
TR 95-072 0838 ore-stage jasperoid quartz	19.9	160	433.15	14.5	5.4	-46
		180	453.15	13.0	6.9	
		200	473.15	11.6	8.3	
		220	493.15	10.4	9.5	
		240	513.15	9.4	10.5	
TR 95-072 1878 ore-stage jasperoid quartz	21.6	160	433.15	14.5	7.1	-33
		180	453.05	13.0	8.6	
		200	473.15	11.6	10.0	
		220	493.15	10.4	11.2	
		240	513.15	9.4	12.2	
TR 94-172 1661.5 calcite	25.2	115	388.15	15.6	9.6	-110
		120	393.15	15.1	10.1	
		140	413.15	13.4	11.8	
		160	433.15	11.9	13.3	
		180	453.15	10.7	14.6	
TR 95-122 1617.5 realgar	-15.6					-140

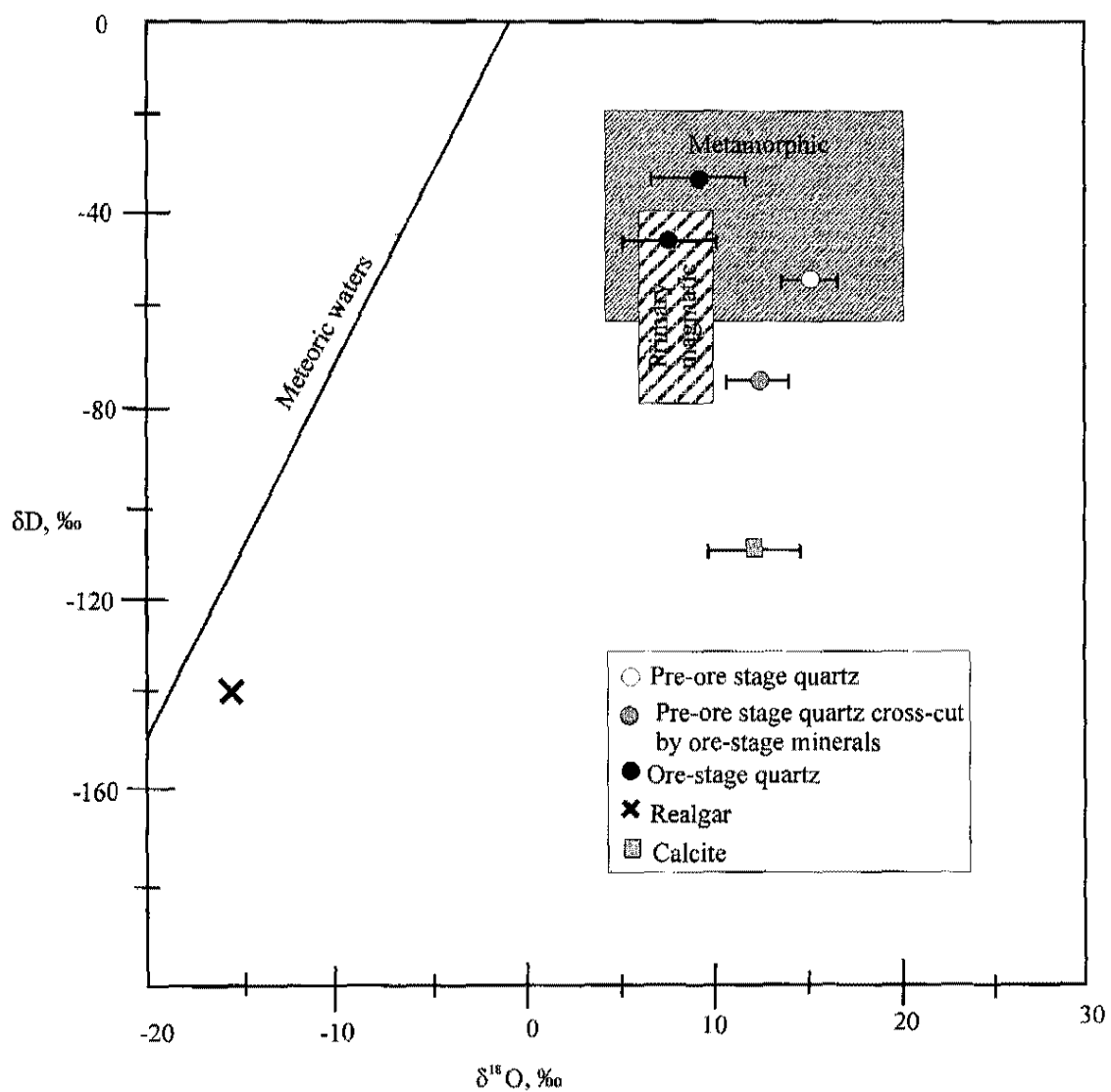


Figure 36. Oxygen and hydrogen isotopic ratios of inclusion fluids in pre-ore, ore, and late-ore stage minerals from the Turquoise Ridge deposit. The bars reflect a range of oxygen isotope ratios over a range of possible temperatures.

between fluid and quartz, and would result in the fluid plotting closer to or within the magmatic water box. The isotopic signature of fluid in pre-ore stage quartz crosscut by ore-stage minerals (Figure 36, and Table 4) exhibits lower δD_{H_2O} and $\delta^{18}O_{H_2O}$ values than the other pre-ore quartz sample. This may result from the presence of secondary ore-stage fluid inclusions in the quartz. The isotopic signatures of inclusion fluids in ore-stage jasperoid quartz exhibit high δD_{H_2O} values, consistent with a metamorphic or magmatic source. Inclusion fluid in late-ore stage calcite exhibits a lower value for δD_{H_2O} , suggesting that the fluid is evolved meteoric water. Late ore-stage realgar (Figure 36, and Table 4) trapped fluid that has a signature close to meteoric water.

Inclusion fluids in ore-stage jasperoid quartz, and late-ore stage realgar and calcite exhibit distinctively different isotopic signatures indicating presence of three different fluids during the precipitation of ore-stage and late-ore stage minerals. Deep fluids were trapped in ore-stage jasperoid quartz and as secondary inclusions in pre-ore stage quartz. Meteoric and evolved meteoric fluids were trapped in late ore-stage realgar and calcite, respectively. Calcite exhibits signatures of more evolved meteoric fluid, which requires greater migration of a fluid over a long time period.

CHAPTER 7

SUMMARY AND DISCUSSION

Two types of variably metamorphosed sedimentary rocks host ore at the Turquoise Ridge deposit: (1) carbonaceous clay-rich and (2) siliceous graphitic sedimentary rocks. The carbonaceous host rock is correlated to the Middle unit, and the siliceous host rock is correlated to the Lower unit throughout this study. Observations of drill core, petrography, and chemical analyses indicate that the Middle and Lower units are variably metamorphosed sedimentary rocks. Relict bedding in the Middle and Lower units indicates that these two host rocks were originally sedimentary rocks and were metamorphosed under low pressure.

Assays show that unaltered Middle and Lower units do not contain gold, but altered units host gold mineralization. Altered host rocks that contain gold are decalcified and replaced by jasperoid quartz. Atkin (1984) suggested that ore grade depends on the degree of decalcification. If so, the carbonaceous Middle unit would be a preferable host rock, as compared to the siliceous Lower unit. Although an extremely high-grade sample was collected from the Middle unit, gold is present in both altered carbonaceous Middle unit and siliceous Lower unit, and variations in the carbonate and silicate content do not appear to affect localization of ore. Depth or proximity to structure rather than rock type may control grade.

Three types of pyrite that have distinctively different morphologies are present in Turquoise Ridge samples. Euhedral to subhedral pyrite crystals conform to bedding in unaltered host rocks and were formed during shallow burial. Subhedral to euhedral pyrite crystals are present in pre-ore stage quartz veins. Finely crystalline porous pyrite is present in high-grade samples. These fine pyrite crystals rim pre-ore cores that exhibit high relief and a good polish. Electron microprobe analyses on seven ore-stage pyrite crystals in TR 95-122 1617.5 showed that they contain 10.41 to 15.33 weight % As and 1100 to 3200 ppm Au. Ore-stage pyrite crystals are consistently present within jasperoid quartz crystals, along pre-ore quartz and ore-stage jasperoid quartz crystal boundaries, and along fractures in pre-ore quartz. The distribution of gold-bearing

pyrite crystals indicates that gold mineralization occurred prior to, and continued during jasperoid quartz precipitation.

Quartz, pyrite, and marcasite in veins that cut the Lower unit constitute a pre-ore mineral assemblage. The veins are spatially associated with a Cretaceous granodiorite intrusion. Assays show that less than 0.001 ounces per ton gold are present in the unaltered Lower unit that contains vein mineral. Pre ore-stage minerals in ore-grade samples are fractured and crosscut by ore-stage minerals. The fractures are absent in ore-stage minerals indicating that fracturing was post vein formation, but occurred prior to the ore-stage event.

Petrographic studies suggest a successive depositional sequence of (1) pyrite with gold, (2) jasperoid quartz, (3) stibnite, (4) fluorite, (5) orpiment, (6) realgar, and (7) calcite during ore-hydrothermal event. The ore-stage mineral assemblage of the Turquoise Ridge deposit is similar to Cline's ore-stage assemblage at Getchell (1999) and Groff's 42 Ma ore-stage mineral assemblage (1996). However, there are differences between the parageneses determined in this and Groff's study (1996). Groff (1996) suggested that both pre-ore and ore-stage realgar precipitation occurred. However, textures indicating pre ore-stage realgar precipitation were not observed in this study.

A relatively restricted range of salinities, 4 to 11 weight % NaCl equivalent, and a wide range of homogenization temperatures, 150 ° to 300 °C, determined for inclusions for pre-ore vein quartz indicate three possible fluid paths: (1) fluid-evolution, (2) fluid mixing, and (3) trapping of multiple generations of fluids. Primary and unknown-primary (?) inclusions in pre-ore stage quartz in gouge have higher salinities and a more restricted range of homogenization temperatures. These data are not consistent with primary inclusions in vein quartz, and pre-ore stage quartz crystals in veins and gouge likely trapped different fluids.

The salinities and homogenization temperatures of inclusion fluids trapped in vein quartz are somewhat consistent with inclusions in pre-ore stage quartz from Getchell. Thus, these pressures and minimum trapping temperatures determined for Getchell inclusions may be applicable for the Turquoise Ridge inclusions.

Microthermometric data for inclusion fluids in ore-stage jasperoid from different locations exhibit somewhat restricted salinities over a range of homogenization temperatures. Although Groff's study (1996) suggested fluid boiling during the ore-stage hydrothermal event, petrography and

microthermometric data from this study do not support fluid boiling. Microthermometric results also do not exhibit a mixing trend or indicate evolution of a single fluid. Results are consistent with trapping of different fluids at different times, or in different locations. Primary inclusions from TR 95-122 1617.5 reflect conditions during the gold hydrothermal event; other groups of fluid inclusions were trapped either before or after the ore stage event, or trapped fluids present in different locations.

Ore-stage fluids have salinities of 12.6 to 17.3 weight % NaCl equivalent and most inclusions homogenized between 143 ° and 193 °C, as indicated by primary fluid inclusions in growth zones in an ore-stage jasperoid quartz crystal. The microthermometric data indicate that salinities and temperatures fluctuated mildly as the crystal grew and trapped gold-bearing pyrite crystals. The presence of pyrite crystals in the quartz core and rim support the close timing of quartz and gold-bearing pyrite precipitation. The salinities and homogenization temperatures indicated by primary fluid inclusions associated with ore-stage pyrite are not consistent with microthermometric data from epithermal, skarn, volcanogenic massive sulfide, or porphyry deposits (Roedder, 1984).

Primary fluid inclusions from Turquoise Ridge have salinities (12 to 17 weight % NaCl equivalent) that are very different from ore-stage jasperoid fluid inclusions from Getchell (salinities between 4 to 5 weight % NaCl equivalent). The different salinities may indicate that different fluids were trapped in the Turquoise Ridge and Getchell samples. However, unknown-primary (?), secondary, and unknown inclusions in ore-stage jasperoid quartz from Turquoise Ridge exhibit strong modes at 7 to 10 weight NaCl equivalent and at 160 ° and 210 °C, similar to Getchell inclusions (Cline, 1999). These results indicate that some fluids trapped at Turquoise Ridge and Getchell were similar. Minimum trapping temperatures of inclusions in Turquoise Ridge samples may be approximately 180 ° to 220 °C as determined for Getchell assuming a confining pressure of 330 bars (Cline, 1999). Salinities of 6 to 19 weight % NaCl equivalent determined for secondary fluid inclusions in jasperoid quartz may reflect the compositions of fluids that migrated through the fracture zone after the gold hydrothermal event. High salinity may result from injection of more saline-rich magmatic or metamorphic fluid.

Oxygen and hydrogen isotope ratios determined for inclusion fluids in pre-ore stage vein quartz, ore-stage jasperoid quartz, and late-ore stage calcite and realgar indicate different fluid sources during different stages. Isotopic signatures of inclusion fluids in pre-ore stage vein quartz reflect a deep fluid source

consistent with fluids exsolving from a granodiorite intrusion. An oxygen isotope ratio higher than primary igneous water may reflect the presence of secondary inclusions. Salinities and homogenization temperatures of primary inclusions in vein quartz crystals are similar to data from epithermal or volcanogenic massive gold sulfide deposits, which are associated with shallow felsic intrusions. Thus, the spatial association between pre-ore stage vein quartz and the Cretaceous granodiorite intrusion, the microthermometric data, and the isotopic signatures of inclusion fluids in pre-ore stage vein quartz support the involvement of magmatic water associated with a granodiorite intrusion. Somewhat lower hydrogen and oxygen isotope ratios determined for inclusion fluids in pre-ore quartz crosscut by ore-stage minerals might reflect analysis of ore-stage fluids trapped in secondary inclusions.

Isotopic signatures of inclusions in ore-stage jasperoid are consistent with a metamorphic or magmatic fluid source, or both. The oxygen values for ore fluids from Turquoise Ridge are similar to oxygen signatures from Getchell and deposits on the Carlin Trend. δD_{H_2O} signatures from Turquoise Ridge are higher than signatures from other Carlin-type gold deposits, but are similar to Getchell values (Cline et al., 1997). Groff's (1996) study determined that δD_{H_2O} ranged between -75.9 and -153 ‰ and $\delta^{18}O_{H_2O}$ ranged between 5.2 and 11.8 ‰ for inclusion fluids in quartz associated with a 83 Ma gold event; $\delta^{18}O_{H_2O}$ ranged from -3.7 to 12.8 ‰ for inclusion fluids in quartz associated with a 42 Ma gold event from the Getchell deposit. Thus, the isotopic signatures of inclusions from the Turquoise Ridge and Getchell deposits indicate a deep fluid source rather than an evolved meteoric fluid source indicated by deposits on the Carlin Trend (Arehart, 1996). These isotopic signatures may reflect differences in fluid source at different Carlin-type gold deposits.

Inclusion fluid in late ore-stage realgar exhibited a near meteoric signature, suggesting trapping of a meteoric fluid. These inclusions are interpreted to have trapped post-hydrothermal fluids. Isotopic signatures of inclusion fluid in late-ore stage calcite suggest trapping of an evolved meteoric fluid. Isotopic signatures of inclusion fluids in calcite from Getchell are similar, but have a wide range of hydrogen values, interpreted to result from the mixing of deep sourced ore fluids with evolved meteoric fluids (Cline et al., 1997). Groff's study determined δD_{H_2O} values of inclusion fluids in calcite for the 42 Ma gold-event between -88 and -134 ‰, and $\delta^{18}O_{H_2O}$ from -9 to 11.3 ‰. These values are generally consistent with isotopic signatures indicated by this study and the study at Getchell (Cline, 1999).

Although the Turquoise Ridge deposit is a Carlin-type gold deposit, it has unique characteristics including high ore-grade, deep ore bodies, high salinity of ore fluids, and a deep ore fluid source. The similarity of mineral assemblages and mineral parageneses at the Turquoise Ridge deposit and the Getchell deposit (Cline, 1999) may suggest that both system have formed as part of a single hydrothermal system. Different microthermometric or isotopic data between Turquoise Ridge and Getchell, and between this study and Groff's study (1996) may reflect local differences such as depth, proximity to structures, or host rock variability. Alternatively, the differences may indicate genetically different systems at Getchell and Turquoise Ridge. Groff (1996) investigated the Getchell, Turquoise Ridge and Twin Creeks deposits and compiled data based on an assumption that these three deposits formed in the same system. However, there is no clear evidence to support that idea. Data from different deposits should be treated differently and compared and contrasted to data from other deposit to determine if the Carlin-type gold system was of a regional scale. Future investigations of other Carlin-type gold deposits will determine whether or not Turquoise Ridge is an unusual, unique Carlin-type system.

CHAPTER 8

CONCLUSIONS

At the Turquoise Ridge deposit, ore develops in metamorphosed carbonaceous and siliceous sedimentary rocks. The carbonaceous unit primarily consists of calcite and dolomite. Quartz is the main constituent of the siliceous unit, and minor microcline, illite, biotite, calcite, and dolomite are present. Assays indicate gold is present in altered host rocks of both types.

Three types of pyrite are present in Turquoise Ridge samples: (1) euhedral to subhedral diagenetic pyrite in unaltered host rocks, (2) euhedral to subhedral pyrite in pre-ore stage quartz veins, (3) finely crystalline pyrite in high-grade samples. Ore-stage pyrite crystals are rich in trace metals, particularly arsenic, and contain gold. Gold-bearing pyrite crystals are consistently present within jasperoid quartz crystals, along pre-ore quartz and ore-stage jasperoid quartz crystal boundaries, and along fractures in ore-stage quartz crystals.

Pre-ore stage mineral assemblage consists of quartz, pyrite, and marcasite in veins that are spatially associated with a Cretaceous granodiorite intrusion. Pre-ore stage minerals in ore-grade samples are fractured and crosscut by ore-stage minerals.

Petrographic studies indicate a precipitation sequence of (1) pyrite with gold, (2) jasperoid quartz, (3) stibnite, (4) fluorite, (5) orpiment, (6) realgar, and (7) calcite during the gold hydrothermal event. The textural and cross-cutting relationships indicate that these minerals precipitated during a single ore hydrothermal event.

Primary fluid inclusions in ore-stage jasperoid quartz have a range of salinities from 12 to 17 weight % NaCl equivalent with a small mode between 16 and 17 weight % NaCl equivalent and were trapped at minimum temperatures from 130 ° to 190 °C. Petrographic studies and microthermometric data do not suggest fluid boiling. Salinities between 6 and 10 weight % NaCl equivalent were indicated by secondary and unknown inclusions in ore-stage jasperoid quartz.

The oxygen and hydrogen isotopic signatures of inclusion fluids in pre-ore stage, ore-stage and late-ore stage minerals indicate that different fluids were trapped in these minerals. The isotopic signatures of pre-ore stage vein quartz indicate a metamorphic or magmatic fluid source. Deep sourced fluids were trapped in ore-stage jasperoid quartz and secondary inclusions in pre-ore stage vein quartz. Meteoric and evolved meteoric fluids were trapped in late ore-stage realgar and calcite, respectively.

APPENDIX I

LIST OF DRILL CORE SAMPLES FROM THE
TURQUOISE RIDGE DEPOSIT

APPENDIX I

LIST OF DRILL CORE SAMPLES FROM THE TURQUOISE RIDGE DEPOSIT

Scale of alteration

Intensive = a sample contains more than 10 % clay-sized minerals

Moderate = a sample contains 5 to 10 % of clay-sized minerals

Weak = a sample contains ~5 % of clay sized minerals

Note: Middle and Lower units are correlated to brown and black hornfels, respectively, in this list. Brown and black hornfels merely refer to their distinctive colors and sedimentary origin.

sample #	assay interval (ore grade oz/ton)	lithology, distinctive mineralization
TR 94-172		
1637.5	1631.5-1638.5 (0.001)	brown hornfels, marble, disseminated py, calcite
1638	1631.5-1638.5 (0.001)	gray shale, disseminated py
1642	1638.5-1643.7 (0.001)	gray shale, coarse rlg
1645.5	1645.5-1649.0 (0.206)	brown hornfels, marble, disseminated py, calcite
1652	1649.0-1655.0 (0.653)	intensively argillized decalcified (except for 1646-47) brown hornfels, pseudo
1655	1649.0-1655.0 (0.653)	intensively argillized, decalcified (except for 1646-47) brown hornfels, coarse rlg
1660.5	1659.2-1665.0 (0.088)	gray marble, coarse orpiment, rlg, calcite
1661.5	1659.2-1665.0 (0.088)	gray marble, coarse orpiment, calcite
1676	1671.0-1676.0 (0.001)	1675-76 intensively argillized brown hornfels + marble, rlg, calcite, disseminated py
1681	1676.0-1681.0 (0.452)	intensively argillized decalcified gray shale, coarse rlg
1686	1681.0-1687.0 (0.942)	intensively argillized decalcified gray shale, coarse rlg
1688.6	1688.6-1695.5 (0.018)	intensively argillized decalcified gray shale, pseudo py
1692.7	1688.6-1695.5 (0.018)	hornfels + marble, coarse calcite
1699.2	1695.5-1701.0 (0.007)	boudinaged hornfels trace rlg, pyrrhotite
1701.7	1701.0-1711.2 (0.001)	boudinaged hornfels, pyrrhotite
1714.5	1711.2-1720.1 (<0.001)	boudinaged hornfels, disseminated py, pyrrhotite
1726	1723.7-1728.5 (0.268)	moderately argillized decalcified brown hornfels, pseudo py
1730.3	1728.5-1733.4 (0.237)	intensively argillized decalcified phyllitic brown hornfels, disseminated py
1735	1733.4-1735.9 (0.001)	boudinaged hornfels, trace rlg, pyrrhotite

1744	1735.9-1745.5 (0.001)	boudinaged hornfels
1746.5	1745.4-1752.9 (<0.001)	boudinaged hornfels, trace rlg, pyrrhotite
1761	1758.9-1768.0 (0.001)	boudinaged hornfels, trace rlg, calcite vein
1767.5	1758.9-1768.0 (0.001)	boudinaged hornfels, coarse calcite, pyrrhotite
1772.6	1768.0-1775.8 (0.021)	mylonitic brown hornfels + marble, calcite vein, py
1776.3	1775.8-1780.5 (0.135)	brown hornfels + marble, calcite, rlg, shearing texture,
1784.5	1780.5-1787.3 (0.563)	argillized decalcified gray shale, rlg, disseminated py, pyrrhotite
1788.6	1780.5-1787.3 (0.563)	brown hornfels + marble, py, rlg, shearing texture,
1795.1	1795.1-2799.1 (0.429)	intensively decalcified argillized hornfels, trace rlg, pseudo py?
1800.6	1799.1-1804.1 (0.103)	moderately argillized decalcified carbonaceous hornfels, disseminated py
1811.5	1811.3-1820.3 (<0.001)	marble + hornfels, not decalcified, coarse calcite, py
1820.5	1820.3-1825.0 (0.001)	decalcified brown hornfels, disseminated py
1831.5	1830.0-1835.4 (<0.001)	intensively argillized decalcified carbonaceous hornfels, py
1835.5	1835.4-1838.9 (0.011)	intensively argillized decalcified carbonaceous hornfels, pseudo py
1841	1838.9-1844.4 (0.120)	intensively argillized decalcified carbonaceous hornfels, pseudo py
1844.4	1844.4-1847.0 (0.058)	intensively argillized decalcified carbonaceous hornfels, pseudo py
1848.7	1847.0-1848.8 (0.009)	intensively argillized decalcified carbonaceous hornfels
1852.8	1852.3-1856.0 (0.001)	limestone
1855.4	1852.3 1856.0 (0.001)	moderately argillized decalcified carbonaceous hornfels, py
1861.3	1861.3-1865.2 (0.018)	moderately argillized carbonaceous hornfels, disseminated py
1865.5	1865.2-1870.1 (0.028)	intensively argillized decalcified carbonaceous hornfels, coarse rlg + py
1867	1865.2-1870.1 (0.028)	intensively argillized decalcified carbonaceous hornfels, orpiment
1875	1870.1-1875.5 (0.023)	intensively argillized decalcified carbonaceous hornfels, orpiment, rlg

1878	1875.5-1880.5 (0.017)	intensively argillized decalcified carbonaceous hornfels, orpiment, rlg
1880	1875.5-1880.5 (0.017)	intensively argillized decalcified carbonaceous hornfels, orpiment, rlg, qtz
1885	1880.5-1885.7 (0.047)	intensively argillized brown hornfels, coarse rlg, qtz
1890.5	1885.7-1890.9 (0.047)	weakly argillized brown hornfels, rlg vein, disseminated py
1897	1895.0-1900.8 (0.006)	intensively argillized decalcified gray shale, coarse rlg
1910	1907.4-1910.4 (0.052)	moderately argillized decalcified graphitic carbonaceous hornfels, coarse rlg, qtz
1912.4	1910.4-1913.6 (0.487)	moderately argillized decalcified graphitic carbonaceous hornfels, qtz
1913	1910.4-1913.6 (0.487)	moderately argillized decalcified graphitic carbonaceous hornfels, coarse rlg
1916.8	1913.6-1922.2 (0.295)	decalcified gray shale, disseminated py
1917.9	1917.7-1922.2 (0.295)	decalcified gray shale, disseminated py, qtz
1926.5	1922.2-1930.8 (0.146)	moderately argillized hornfels + marble, calcite vein, disseminated py
1932	1930.8-1932.2 (0.206)	intensively argillized decalcified hornfels, qtz
1932.5	1930.8-1932.2 (0.206)	intensively argillized decalcified hornfels, qtz
1942	1936.2-1942.2 (0.002)	weakly boudinaged brown hornfels + skarn + marble, py, pyrrhotite, calcite vein
1952.5	1951.0-1955.6 (0.247)	weakly boudinaged brown hornfels + skarn + marble
1955.6	1955.6-1959.6 (0.005)	brown hornfels + skarn + marble, 1961-63 argillized pyrrhotite
1961.7	1959.6-1962.2 (0.036)	brown hornfels + skarn + marble, 1961-63 argillized coarse calcite
1965	1962.2-1967.2 (0.002)	brown hornfels + skarn + marble, 1961-63 argillized coarse calcite vein
1967	1962.2-1967.2 (0.002)	intensively fractured, coarse calcite
1975	1972.5-1982.0 (0.001)	skarn + hornfels + marble, pyrite, mylonitic texture, tension crack
1977	1972.5-1982.0 (0.001)	boudinaged hornfels
1985	1982.0-1992.0 (0.001)	boudinaged hornfels, pyrite

1993	1992.0-1997.0 (0.001)	decalcified carbonaceous hornfels, tension crack + mylonitic texture
1995.1	1992.0-1997.0 (0.001)	decalcified carbonaceous hornfels
1999.8	1997.0-200.2.0 (0.257)	argillized shaly carbonaceous hornfels, disseminated py
2002.3	2002.0-2017.0 (0.458)	argillized shaly carbonaceous hornfels, qtz, disseminated py
2007	2002.0-2017.0 (0.458)	argillized shaly carbonaceous hornfels, disseminated py-rich
2011	2002.0-2017.0 (0.458)	argillized shaly carbonaceous hornfels, disseminated py-rich,
2014	2002.0-2017.0 (0.458)	argillized shaly carbonaceous hornfels, disseminated py-rich
2016.8	2002.0-2017.0 (0.458)	argillized shaly carbonaceous hornfels, disseminated py-rich, qtz
2021	2017.0-2021.1 (0.683)	argillized shaly carbonaceous hornfels, disseminated py-rich, qtz
2026	2021.1-2026.0 (0.052)	light gray dacite, py vein
2030.5	no assay data	greenish dacite
2034.8	no assay data	greenish dacite, calcite
TR 95-39		
1575.6	1575-1580 (0.071)	intensively argillized decalcified brown hornfels, pseudo py, rlg
1590.5	1585-1595.0 (0.093)	intensively argillized brown hornfels, disseminated py, rlg
1595	1595.0-1600.0 (0.133)	intensively argillized, py masses, rlg
1601.5	1600.0-1605.0 (0.831)	intensively decalcified argillized brown hornfels, decalcified qtz, rlg
1603	1600.0-1605.0 (0.831)	intensively argillized shaly brown hornfels, disseminated py
1607	1605.0-1610.0 (0.266)	shaly limestone, calcite,
1611	1610.0-1620.0 (0.105)	intensively argillized brown hornfels, rlg, pseudo py
1620	1620.0-1625.0 (0.105)	moderately argillized black hornfels, rlg, qtz, pseudo py
1621	1620.0-1625.0 (0.105)	intensively argillized decalcified brown hornfels, rlg
1626	1625.0-1630.0 (0.052)	intensively argillized decalcified brown hornfels, rlg
1631	1630.0-1635.0 (0.578)	intensively argillized decalcified brown hornfels, pseudo py, trace rlg
1637.5	1635.0-1639.5 (0.181)	intensively argillized hornfels, coarse rlg, qtz

1643	1639.5-1645.9 (0.598)	intensively argillized decalcified brown hornfels, py masses
1643.5	1639.5-1645.9 (0.598)	intensively argillized brown hornfels, rlg, pseudo masses
1652.5	1650.5-1653.7 (0.187)	intensively argillized decalcified brown hornfels, trace rlg, massive py
1655.5	1653.7-1657.4 (0.222)	intensively argillized brown hornfels, trace rlg, py masses
1661.5	1657.4-1664.6 (0.005)	boudinaged hornfels, trace rlg, calcite masses
1666	1664.6-1670.8 (0.075)	intensively argillized decalcified shaly gray hornfels, qtz, rlg
1670.5	1664.6-1670.8 (0.075)	intensively argillized decalcified shaly gray hornfels, qtz, rlg
1676.7	1670.8-1677.0 (0.034)	intensively argillized decalcified gray shale, qtz, rlg
1804.5	1801.0-1804.5 (0.044)	intensively argillized decalcified carbonaceous hornfels, rlg, disseminated py, qtz
1809.5	1804.5-1810.0 (0.024)	decalcified carbonaceous hornfels, massive py, tension crack
1812	1810.0-1815.4 (0.016)	decalcified carbonaceous hornfels, qtz, massive py, coarse rlg, tension crack
1821.9	1819.6-1823.5 (0.111)	decalcified carbonaceous hornfels, py masses, trace rlg
1828.4	1828.0-1834.0 (0.318)	decalcified carbonaceous hornfels, trace rlg
1833	1828.0-1834.0 (0.318)	intensively argillized decalcified carbonaceous hornfels, qtz, rlg, py
1839	1838.2-1842.2 (0.053)	argillized decalcified carbonaceous hornfels, coarse rlg, tension crack
1842.2	1842.2-1846.5 (0.440)	argillized decalcified carbonaceous hornfels, qtz, rlg, tension crack
1843.5	1842.2-1846.5 (0.440)	argillized decalcified carbonaceous hornfels, qtz, rlg, py, tension crack
1847	1846.5-1850.8 (0.575)	argillized decalcified carbonaceous hornfels, qtz, coarse rlg, tension crack
1850.5	1846.5-1850.8 (0.575)	argillized decalcified carbonaceous hornfels, qtz, coarse rlg, tension crack
1853.5	1850.8-1855.4 (0.411)	argillized decalcified carbonaceous hornfels, qtz, coarse rlg, tension crack
1855.4	1855.4-1859.2 (0.268)	argillized decalcified carbonaceous hornfels, qtz, coarse rlg, tension crack
1861.6	1859.2-1864.9 (0.458)	argillized decalcified carbonaceous hornfels, trace rlg, calcite, tension crack

1866.5	1864.9-1868.0 (0.288)	argillized decalcified carbonaceous hornfels, rlg, py masses, tension crack
1875.4	1868.0-1876.4 (0.009)	boudinaged brown hornfels + marble, calcite, py masses
1881	1878.8-1883.5 (0.164)	argillized decalcified hornfels, disseminated py
1886.3	1883.5-1889.0 (0.070)	limestone, trace rlg
1885	1883.5-1889.0 (0.070)	limestone, pseudo py
1891.8	1891.0-1895.0 (<0.027)	limestone, trace py
1893	1891.0-1895.0 (<0.027)	shaly limestone, trace rlg
1899.2	1898.2-1908.0 (0.003)	shaly limestone, trace rlg
1905	1898.2-1908.0 (0.003)	shaly limestone, py
1910.5	1908.0-1916.0 (0.043)	shaly limestone, calcite, tension crack
1917	1916.0-1918.3 (<0.001)	shaly limestone, py, calcite vein, tension crack
1923.3	1918.3-1928.5 (0.024)	shaly limestone, rlg, tension crack
1928.5	1928.5-1932.3 (0.059)	silicified carbonaceous hornfels, qtz, py masses
1935	1932.3-1935.2 (0.004)	silicified carbonaceous hornfels, pseudo py
1937	1935.2-1940.0 (0.370)	silicified carbonaceous hornfels, rlg, disseminated py
1944	1940.0-1945.0 (0.020)	weakly argillized decalcified carbonaceous hornfels, qtz, rlg
1948	1945.0-1950.0 (0.347)	weakly argillized decalcified carbonaceous hornfels, qtz, pseudo py, rlg
1951.5	1950.0-1956.8 (0.280)	moderately silicified carbonaceous hornfels, disseminated py
1954	1950.0-1956.8 (0.280)	intensively silicified carbonaceous hornfels
1957.8	1956.8-1962.0 (0.400)	moderately silicified carbonaceous hornfels, qtz, pseudo py
1961	1956.8-1962.0 (0.400)	moderatey silicified carbonaceous hornfels
1962	1962.0-1967.1 (0.458)	intensively silicified carbonaceous hornfels,
1966	1962.0-1967.1 (0.458)	moderately silicified carbonaceous hornfels, rlg, py
1966.7	1962.0-1967.1 (0.458)	weakly argillized carbonaceous hornfels
1967.1	1967.1-1970.9 (0.327)	intensively argillized decalcified carbonaceous hornfels, disseminated py
1970	1967.1-1970.9 (0.327)	intensively argillized decalcified carbonaceous hornfels, disseminated py, qtz

1972.5	1970.9-1974.7 (0.247)	moderately silicified carbonaceous hornfels, qtz
1976.7	1974.7-1980.0 (0.583)	moderately silicified carbonaceous hornfels, qtz
1977.5	1974.7-1980.0 (0.583)	moderately silicified carbonaceous hornfels, qtz
1984.3	1980.0-1985.0 (0.175)	weakly argillized decalcified carbonaceous hornfels disseminated py
1984.8	1980.0-1985.0 (0.175)	weakly argillized decalcified carbonaceous hornfels
1989	1985.0-1990.0 (0.047)	moderately argillized decalcified brown hornfels, py
1992.7	1990.0-2000.0 (0.001)	brown hornfels, py vein
1998.5	1990.0-2000.0 (0.001)	brown hornfels, pink marble, py
2009.8	2007-2010.0 (0.013)	moderately argillized brown hornfels, coarse calcite, pseudo py
2014.5	2010.0-2016.0 (<0.001)	brown hornfels, py masses, coarse calcite
TR 95-46		
1611.5	1602.1-1612.6 (0.041)	weakly argillized dacite porphyry, trace rlg
1616	1612.6-1620.0 (0.586)	moderately argillized decalcified carbonaceous hornfels, coarse rlg
1621.5	1620.0-1624.2 (0.481)	moderately argillized decalcified carbonaceous hornfels, coarse rlg
1623	1620.0-1624.2 (0.481)	moderately argillized decalcified brown hornfels
1630	1624.2-1630.3 (0.324)	moderately argillized decalcified carbonaceous hornfels, massive rlg, qtz
1633	1630.3-1635.0 (0.581)	moderately argillized, decalcified carbonaceous hornfels, rlg, qtz,
1634	1630.3-1635.0 (0.581)	moderately argillized, decalcified carbonaceous hornfels, rlg, qtz
1636	1635.0-1640.3 (0.750)	intensively argillized decalcified carbonaceous hornfels, rlg, qtz
1639	1635.0-1640.3 (0.750)	intensively argillized decalcified carbon-rich brown hornfels, rlg, disseminated py, qtz
1643.5	1640.3-1645.0 (0.432)	intensively argillized decalcified carbonaceous hornfels, rlg, disseminated py, qtz
1645.5	1645.0-1649.5 (0.627)	moderately argillized decalcified brown hornfels, rlg, disseminated py, qtz

1647.5	1645.0-1649.5 (0.627)	intensively argillized decalcified carbonaceous hornfels, py, trace rlg, calcite
1655	1654.7-1660.0 (0.096)	weakly argillized brown hornfels
1662.5	1660.0-1667.4 (0.009)	moderately argillized brown hornfels, rlg, calcite, py masses
1668.3	1667.4-1677.4 (<0.001)	brown hornfels + marble + skarn, calcite, rlg
1747	1745.2-1750.5 (0.028)	intensively argillized brown hornfels, decalcified
1756.5	1755.0-1759.9 (0.071)	intensively argillized brown hornfels, py
1758.5	1755.0-1759.9 (0.071)	intensively argillized decalcified hornfels, py
1762	1759.9-1767.0 (0.400)	intensively argillized decalcified hornfels, py, rlg
1763.7	1759.9-1767.0 (0.400)	intensively argillized decalcified carbonaceous hornfels, rlg, pseudo py
1767.3	1767.0-1772.0 (0.206)	intensively argillized brown hornfels, disseminated py
1772.5	1772.0-1777.0 (0.006)	brown hornfels + marble, tension crack
1779	1777.0-1782.3 (0.194)	brown hornfels + marble, tension crack
1781	1777.0-1782.3 (0.194)	brown hornfels + marble, tension crack
1783	1782.3-1788.6 (0.496)	weakly argillized decalcified carbonaceous hornfels, rlg
1783.5	1782.3-1788.6 (0.496)	moderately argillized decalcified brown hornfels, trace rlg, disseminated py
1789.6	1788.6-1791.7 (0.173)	intensively argillized decalcified brown hornfels, disseminated py
1797	1777.0-1782.3 (0.194)	brown hornfels
1798.2	1791.7-1798.3 (0.136)	brown hornfels
1805	1801.1-1805.4 (0.096)	intensively argillized decalcified carbonaceous brown hornfels, rlg
1809.5	1805.4-1810.0 (0.017)	intensively argillized decalcified carbonaceous hornfels, rlg, pseudo py, qtz or flr
1811.5	1810.0-1815.1 (0.016)	intensively argillized decalcified carbonaceous hornfels, py cube, rlg
1818.5	1815.1-1821.6 (0.012)	intensively argillized decalcified carbonaceous hornfels, rlg, qtz, calcite
1823.5	1821.6-1824.7 (0.008)	intensively argillized decalcified carbonaceous hornfels, rlg, qtz

1827	1824.7-1828.1 (0.022)	intensively argillized decalcified carbonaceous hornfels, coarse rlg
1829.7	1828.1-1833.5 (0.452)	intensively argillized decalcified carbonaceous hornfels, rlg, orpiment
1838	1833.5-1838.5 (0.712)	argillized decalcified carbonaceous hornfels, fissile, rlg, qtz
1842.8	1841.4-1846.0 (0.017)	argillized decalcified carbonaceous hornfels, rlg, orp
1844.5	1841.4-1846.0 (0.017)	argillized decalcified carbonaceous hornfels, rlg, orp
1847.5	1846.0-1851.7 (0.007)	argillized decalcified carbonaceous hornfels, rlg, orp
1850.5	1846.0-1851.7 (0.007)	argillized decalcified carbonaceous hornfels, rlg, orp
1851.5	1846.0-1851.7 (0.007)	argillized decalcified carbonaceous hornfels, rlg, orp
1851.7	1851.7-1856.2 (0.010)	argillized decalcified carbonaceous hornfels, rlg, orp
TR 95-49		
1518.5	1514.5-1520.0 (0.047)	moderately argillized decalcified brown hornfels, rlg, qtz
1523.7	1520.0-1526.6 (0.053)	intensively argillized decalcified hornfels, qtz, rlg
1527.5	1526.6-1533.0 (0.044)	brown hornfels, calcite, py
1534	1533.0-1535.7 (0.417)	intensively argillized decalcified brown hornfels, rlg, py masses
1536.5	1535.7-1540.7 (0.218)	intensively argillized decalcified brown hornfels, disseminated py
1549	1548.5-1555.5 (0.141)	intensively argillized brown hornfels, trace rlg, qtz
1558	1555.5-1561.0 (0.060)	moderately argillized brown hornfels, massive and disseminated py
1906	1906.5-1910.5 (0.052)	weakly argillized decalcified carbonaceous hornfels, qtz, rlg
1916	1915.0-1920.0 (0.429)	weakly argillized decalcified carbonaceous hornfels, qtz, rlg, disseminated py
1916.5	1915.0-1920.0 (0.429)	weakly argillized decalcified carbonaceous hornfels, qtz, trace rlg, disseminated py
1923	1920.0-1925.0 (0.260)	weakly argillized decalcified carbonaceous hornfels, qtz, rlg, disseminated py
1925.5	1925.0-1928.5 (0.222)	silicified carbonaceous hornfels, coarse rlg, qtz
1931	1928.5-1933.5 (0.214)	silicified carbonaceous hornfels, disseminated py

1934	1933.5-1937.5 (0.102)	silicified carbonaceous hornfels, coarse rlg, qtz
1936.5	1933.5-1937.5 (0.102)	silicified carbonaceous hornfels, coarse rlg, qtz
1939.5	1937.5-1943.0 (0.060)	decalcified graphitic carbonaceous hornfels, qtz
1946.5	1943.0-1947.0 (0.066)	decalcified graphitic carbonaceous hornfels, calcite vein, py
1949.6	1947.0-1952.0 (0.001)	brown hornfels + marble, py
TR 95-71		
1743	1739.0-1749.0 (<0.0001)	brown hornfels + skarn + marble, py, calcite vein
1752.5	1749.0-1756.0 (0.0006)	brown hornfels + skarn + marble, py
1761	1761.0-1766.0 (0.194)	moderately argillized decalcified phyllitic hornfels, disseminated py
1765	1761.0-1766.0 (0.194)	moderately argillized decalcified phyllitic hornfels, rlg, py
1774	1771.0-1776.3 (0.132)	intensively argillized decalcified hornfels, rlg, pseudo py
1776	1776.3-1780.0 (0.250)	moderately argillized brown hornfels, coarse rlg
177.5	1776.3-1780.0 (0.250)	moderately argillized brown hornfels, coarse rlg
1784	1780.8-1785.0 (0.583)	weakly argillized brown hornfels, py
1787.8	1785.0-1788.3 (0.360)	weakly argillized brown hornfels, py
1793	1791.0-1798.0 (0.323)	moderately argillized phyllitic brown hornfels, py
1798	1798.0-1802.0 (0.088)	moderately argillized phyllitic brown hornfels, py
1810	1804.0-1810.3 (0.078)	intensively argillized brown hornfels, py, trace rlg
1813	1810.3-1814.0 (0.108)	intensively argillized brown hornfels, py, trace rlg
1817	1814.0-1817.5 (0.132)	argillized carbonaceous hornfels, coarse calcite, py
1819	1817.5-1820.0 (0.326)	argillized carbonaceous hornfels, coarse rlg, qtz
1822.5	1823.3-1827.0 (0.949)	intensively argillized decalcified brown hornfels, rlg,
1824	1823.3-1827.0 (0.949)	intensively argillized decalcified hornfels, coarse rlg
1828	1827.0-1830.0 (1.150)	intensively argillized decalcified hornfels, coarse rlg
1840	1837.2-1842.0 (0.002)	boudinaged brown hornfels, py, rlg, calcite vein
1848	1842.0-1851.5 (0.022)	boudinaged brown hornfels
1852.5	1851.5-1855.0 (0.709)	weakly argillized decalcified shaly gray hornfels, disseminated py

1855	1855.0-1860.3 (0.150)	weakly argillized decalcified shaly gray hornfels, disseminated py
1861.5	1860.3-1865.0 (0.944)	moderately argillized brown hornfels, py
1866.5	1865.0-1870.0 (0.082)	intensively argillized brown hornfels, rlg
1870	1870.0-1872.0 (0.136)	intensively argillized carbonaceous hornfels rlg, calcite, py
1876	1876.5-1878.5 (0.064)	silicified decalcified carbonaceous hornfels,
1883	1883.5-1885.0 (0.040)	silicified decalcified carbonaceous hornfels, qtz, rlg
1884.8	1883.5-1885.0 (0.040)	weakly silicified decalcified carbonaceous hornfels, qtz, rlg
1888	1885.0-1888.3 (0.034)	weakly silicified decalcified carbonaceous hornfels, qtz, rlg
1941	1940.0-1945.0 (0.186)	silicified decalcified carbonaceous hornfels, qtz, rlg, stibnite
1943	1940.0-1945.0 (0.186)	silicified carbonaceous hornfels, coarse rlg
1945	1945.0-1950.0 (0.154)	argillized decalcified carbonaceous hornfels, massive and cubic py
1955.5	1954.0-1958.2 (0.106)	silicified carbonaceous hornfels, massive py, coarse rlg
1961.2	1958.2-1963.5 (0.061)	silicified carbonaceous hornfels, massive py, coarse rlg
1966.5	1963.5-1967.5 (0.2360)	intensively argillized carbonaceous hornfels, coarse rlg
1970	1967.5-1972.5 (0.629)	intensively argillized carbonaceous hornfels, rlg, py specs
1971	1967.5-1972.5 (0.629)	intensively argillized carbonaceous hornfels, qtz
1976	1975.0-1977.0 (0.843)	intensively argillized carbonaceous hornfels, rlg, calcite, qtz, py cube
1977.6	1977.0-1978.3 (0.118)	intensively argillized carbonaceous hornfels, qtz
1982	1978.3-1985.0 (0.054)	brown hornfels + skarn, trace rlg, py
1991.5	1989.5-1994.5 (0.019)	marble, hornfels, py, calcite
1996.5	1994.5-1999.5 (<0.0001)	brown hornfels, clay-rich, calcite
2001.5	1999.5-20004.5 (0.005)	brown hornfels, trace rlg, py
2011.8	2009.7-2015.0 (0.0004)	brown hornfels, py, coarse calcite
2021.8	2015.0-2020.0 (0.0008)	brown hornfels, py, coarse calcite

2031	2030.0-2035.0 (0.066)	intensively argillized carbonaceous hornfels, calcite, trace rlg
2032.5	2030.0-2035.0 (0.066)	argillized carbonaceous hornfels, calcite, trace rlg
2037.3	2035.0-2040.0 (0.0120)	weakly argillized brown hornfels, py, calcite
2045	2040.0-2045.0 (0.377)	moderately argillized carbonaceous hornfels, trace rlg
2046.5	2045.0-2047.5 (0.170)	moderately argillized carbonaceous hornfels, py masses
2051.5	2047.5-2052.5 (0.356)	intensively argillized carbonaceous hornfels, rlg, calcite
2056	2052.5-2057.5 (0.009)	brown hornfels, py, calcite
TR 95-72		
1526	1526.0-1528.5 (0.021)	intensively argillized brown hornfels, coarse rlg
1530.5	1528.5-1532.3 (0.019)	intensively argillized brown hornfels, rlg
1533	1532.3-1536.7 (0.003)	brown hornfels + marble, py
1537.5	1536.7-1541.3 (0.102)	intensively argillized brown hornfels, py, trace rlg
1542	1541.3-1545.7 (0.365)	intensively argillized hornfels, disseminated py, coarse rlg
1550.5	1545.7-1551.9 (0.799)	intensively argillized brown hornfels, coarse rlg, pseudo py
1556.3	1551.9-1557.2 (0.750)	intensively argillized carbonaceous hornfels, rlg
1558	1557.2-1562.0 (0.003)	brown hornfels, trace rlg, calcite vein, py
1564.7	1562.0-1566.3 (0.020)	fractured hornfels
1572	1572.0-1574.5 (0.046)	weakly argillized brown hornfels + skarn, py, rlg, calcite
1575.3	1574.5-1577.0 (0.140)	moderately argillized shaly hornfels, disseminated py
1835.2	1835.2-1840.4 (0.150)	moderately argillized decalcified carbonaceous hornfels, qtz, trace rlg, disseminated py
1838	1835.2-1840.4 (0.150)	moderately argillized decalcified carbonaceous hornfels, qtz, trace rlg, disseminated py
1841	1840.4-1844.5 (0.218)	intensively argillized decalcified gray hornfels, coarse rlg
1852.5	1851.4-1854.5 (0.126)	weakly argillized boudinaged brown hornfels, skarn, rlg in vein, disseminated py
1855.8	1854.5-1856.8 (0.286)	weakly argillized carbonaceous hornfels, trace rlg
1859.8	1856.8-1860.8 (0.125)	intensively argillized carbonaceous hornfels, disseminated py
1867.8	1866.0-1871.4 (0.084)	argillized brown hornfels, rlg, disseminated py

1868.5	1866.0-1871.4 (0.084)	argillized carbonaceous hornfels, qtz, rlg
1869	1866.0-1871.4 (0.084)	argillized carbonaceous hornfels, qtz, coarse rlg
1875	1871.4-1876.8 (0.261)	silicified carbonaceous hornfels, massive rlg
1878	1876.8-1882.2 (0.253)	silicified carbonaceous hornfels, massive rlg
1883.5	1882.2-1887.5 (0.224)	intensively argillized carbonaceous hornfels, qtz, rlg
1889	1887.5-1892.5 (0.365)	intensively argillized carbonaceous hornfels, qtz, rlg
1890	1887.5-1892.5 (0.365)	silicified carbonaceous hornfels, qtz, rlg, pseudo py
1892.7	1892.5-1896.0 (1.46)	silicified carbonaceous hornfels, qtz, rlg, and pseudo py
1895	1892.5-1896.0 (1.46)	silicified carbonaceous hornfels, coarse rlg
1899	1896.0-1901.4 (0.890)	silicified carbonaceous hornfels, qtz, rlg, pseudo py
1901.5	no assay	argillized carbonaceous hornfels, qtz, rlg
1903.5	no assay	marble, calcite, trace rlg
1911.5	no assay	brown hornfels, py-vein
TR 95-76		
1410.8	1405.0-1413.0 (0.0002)	diabase, brown, weakly argillized, weakly reacts with HCl py
1416	1413.0-1419.6 (0.0002)	weakly argillized brown hornfels + marble. calcite vein
1424.5	1419.6-1426.8 (0.048)	moderately argillized brown hornfels, py, shearing texture
1426.8	1426.8-1428.7 (0.809)	intensively argillized decalcified shaly gray hornfels, trace rlg, py masses
1428	1426.8-1428.7 (0.809)	intensively argillized decalcified shaly gray hornfels, rlg
1433	1428.7-1434.0 (0.172)	moderately argillized decalcified shaly gray hornfels, rlg disseminated and massive py
1440.5	1464.0-1442.0 (0.009)	moderately argillized decalcified shaly gray hornfels, rlg disseminated py
1443.5	1442.0-1453.0 (0.010)	moderately argillized decalcified shaly gray hornfels, rlg disseminated py, stibnite
1450.7	1442.0-1453.0 (0.010)	shaly brown hornfels, calcite vein
1457.3	1453.0-1462.0 (0.333)	moderately argillized brown hornfels, qtz
1457.5	1453.0-1462.0 (0.333)	moderately argillized shaly gray hornfels, qtz

1465	1462-1466.5 (0.789)	intensively argillized dacite, trace rlg
1468.8	1466.5-1472.0 (0.278)	intensively argillized dacite, trace rlg
1473	1472.0- 1477.5 (0.266)	weakly argillized dacite, rlg, py-vein
1483.5	1482.0-1487.5 (0.963)	intensively argillized brown hornfels + dacite, qtz, rlg
1488.5	1487.5-1492.0 (1.187)	intensively argillized brown hornfels + dacite, qtz, rlg
1490.5	1487.5-1492.0 (1.187)	weakly argillized brown hornfels, rlg, py masses
1493.8	1492.0-1494.8 (0.439)	intensively argillized brown hornfels, coarse rlg
1494.5	1492.0-1494.8 (0.439)	intensively argillized brown hornfels, coarse rlg
1496	1494.8-1502.0 (0.546)	argillized brown hornfels, disseminated py
1499	1494.8-1502.0 (0.546)	intensively argillized decalcified gray shale, qtz, rlg
1507.5	1507.0-1512.0 (0.212)	intensively argillized decalcified gray shale, qtz, rlg
1515.5	1512.0-1519.5A (0.142) B(0.001)	weakly argillized brown hornfels, decalcified disseminated py
1520.5	1519.5-1526.0 (0.224)	intensively argillized brown hornfels, qtz, disseminated py
1521.5	1519.5-1526.0 (0.224)	intensively argillized brown hornfels, rlg, disseminated py
1527.7	1526.0-1528.1 (0.188)	weakly argillized dacite, disseminated py
1531.5	1528.1-1535.1 (0.098)	dacite + brown hornfels, disseminated py
1534	1528.1-1535.1 (0.098)	brown hornfels + skarn + marble, massive py
1545	1543.0-1550.6 (0.005)	basalt, calcite, trace rlg
1550.5	1543.0-1550.6 (0.005)	basalt, calcite-vein, py-cube
1557.8	no assay	intensively argillized hornfels, py-vein
TR 95-95		
1536.5	1535.0-1545.0 (0.007)	boudinaged brown hornfels, py
1542.5	1535.0-1545.0 (0.007)	boudinaged brown hornfels, py, calcite
1547.5	1545.0-1549.3 (0.124)	moderately silicified carbonaceous hornfels, qtz, py
1550.5	1549.3-1553.4 (0.534)	intensively argillized shaly gray hornfels, trace rlg, disseminated py
1556.0	1553.4-1558.2 (0.118)	silicified carbonaceous hornfels, qtz, trace rlg, pseudo py
1556.2	1553.4-1558.2 (0.118)	argillized carbonaceous hornfels, qtz, rlg

1556.5	1553.4-1558.2 (0.118)	argillized carbonaceous hornfels, qtz, rlg
1559.5	1558.2-1572.0 (0.102)	argillized carbonaceous hornfels, qtz, rlg, disseminated py
1563	1558.2-1572.0 (0.102)	moderately silicified carbonaceous hornfels, qtz, rlg,
1564.5	1558.2-1572.0 (0.102)	moderately silicified carbonaceous hornfels, qtz, rlg,
1569	1558.2-1572.0 (0.102)	moderately silicified carbonaceous hornfels, qtz, rlg,
1573.8	1572.0-1575.0 (0.164)	moderately silicified carbonaceous hornfels, qtz, rlg, disseminated py
1579.8	1575.0-1580.0 (0.088)	weakly silicified carbonaceous hornfels, qtz, rlg, disseminated py
1581.5	1580.0-1583.4 (0.384)	intensively silicified carbonaceous hornfels, qtz, rlg, pseudo py
1584.5	1583.4-1586.0 (0.430)	argillized carbonaceous hornfels, qtz, rlg
1584.7	1583.4-1586.0 (0.430)	intensively carbonaceous hornfels, qtz, rlg
1587	1586.0-1591.0 (0.200)	intensively carbonaceous hornfels, qtz, rlg
1596.0	1591.0-1598.2 (0.061)	argillized carbonaceous hornfels, qtz, rlg
1597	1591.0-1598.2 (0.061)	silicified carbonaceous hornfels, qtz, rlg
1599	1598.2-1605.0 (0.009 or 0.0005)	silicified brown hornfels, qtz, py masses
1599.5	1598.2-1605.0 (0.009 or 0.0005)	silicified brown hornfels, qtz, py masses
1602.5	1598.2-1605.0 (0.009 or 0.0005)	argillized carbonaceous hornfels, qtz, rlg
1603.5	1598.2-1605.0 (0.009 or 0.0005)	argillized hornfels, qtz, py masses
1612.7	1610.0-1615.0 (0.0006)	brown hornfels + marble + skarn, calcite, disseminated py
1617.5	1615.0-1620.0 (0.0006)	moderately argillized shaly gray hornfels, rlg, calcite
1622	1620.0-1624.1 (0.103)	argillized carbonaceous hornfels, qtz
1626.5	1624.1-1628.8 (0.416)	argillized carbonaceous hornfels, qtz, disseminated py
1628	1624.1-1628.8 (0.416)	argillized brown hornfels, qtz, disseminated py
1629.5	1628.8-1634.0 (0.570)	argillized brown hornfels, qtz, disseminated py
1633	1628.8-1634.0 (0.570)	argillized carbonaceous hornfels, clay-rich, qtz
1633.8	1628.8-1634.0 (0.570)	argillized carbonaceous hornfels, qtz
1636.5	1634.0-1638.1 (0.100)	carbonaceous hornfels, py-cube

1641.5	1638.1-1645.1 (0.073)	carbonaceous hornfels, disseminated py
1648	1645.1-1650.3 (0.166)	carbonaceous hornfels, disseminated py
No samples available interval 1650-1747		
1751	1750.0-1753.0 (0.156)	intensively argillized carbonaceous hornfels, qtz, disseminated py
1756	1753.0-1760.1 (0.062, 0.063, or <0.001)	weakly argillized carbonaceous hornfels, qtz, rlg
1756.5	1753.0-1760.1 (0.062, 0.063, or <0.001)	weakly argillized carbonaceous hornfels, qtz, rlg
1758.3	1753.0-1760.1 (0.062, 0.063, or <0.001)	weakly argillized carbonaceous hornfels, qtz, rlg, qtz, py
1759.8	1753.0-1760.1 (0.062, 0.063, or <0.001)	weakly argillized carbonaceous hornfels, qtz, rlg, qtz, py
1759.9	1753.0-1760.1 (0.062, 0.063, or <0.001)	weakly argillized carbonaceous hornfels, qtz, rlg, qtz, py
1760.3	1760.1-1764.4 (0.178)	weakly argillized decalcified carbonaceous hornfels, euhedral qtz, tension crack
1760.5-1	1760.1-1764.4 (0.178)	weakly argillized decalcified carbonaceous hornfels, euhedral qtz vein, tension crack
1760.5-2	1760.1-1764.4 (0.178)	weakly argillized decalcified carbonaceous hornfels, euhedral qtz vein, tension crack
1760.5-3	1760.1-1764.4 (0.178)	weakly argillized decalcified carbonaceous hornfels, euhedral qtz vein, tension crack
1768	1764.4-1768.8 (0.090)	moderately silicified decalcified carbonaceous hornfels, rlg, py, tension crack
1772.8	1768.8-1773.0 (0.023)	moderately silicified decalcified carbonaceous hornfels, rlg, py, tension crack
1774	1773.0-1777.5 (0.041)	moderately silicified decalcified carbonaceous hornfels, tension crack
1780.5	1777.5-1782.7 (0.113)	intensively silicified decalcified carbonaceous hornfels, qtz, rlg, py, tension crack
1786.7	1482.7-1787.1 (1.47)	moderately silicified decalcified carbonaceous hornfels, qtz, rlg, py, tension crack
1786	1482.7-1787.1 (1.47)	moderately silicified decalcified carbonaceous hornfels, rlg, py, tension crack

1790.5	1787.7-1791.5 (0.475)	moderately silicified decalcified carbonaceous hornfels, qtz masses, rlg, py, tension crack
1792.2	1791.5-1795.0 (0.001)	boudinaged brown hornfels + marble, py
1798.5	1795.0-1800 (0.001)	boudinaged brown hornfels + marble, calcite in tension crack
TR 95-113		
1477.9	1477.9-1483.0 (0.046)	intensively argillized brown hornfels, trace rlg, disseminated py, clay bands
1480.5	1477.9-1483.0 (0.046)	intensively argillized brown hornfels, trace rlg, disseminated py, clay bands
1481.0	1477.9-1483.0 (0.046)	intensively argillized brown hornfels, trace rlg, disseminated py, clay bands
1488.5	1483.0-1493.0 (0.013)	intensively argillized shaly brown hornfels, trace rlg, disseminated py
1491.5	1483.0-1493.0 (0.013)	intensively argillized shaly brown hornfels, trace rlg, disseminated py
1500	1498.4-1503.8 (0.200)	intensively argillized shaly brown hornfels, coarse rlg, pseudo py
1504	1503.8-1508.8 (0.233)	intensively argillized phyllitic brown hornfels, coarse rlg, py
1507.8	1503.8-1508.8 (0.233)	gray shale, pyrrhotite, rlg in cracks, calcite vugs, disseminated py
1509.5	1508.8-1514.2 (1.08)	weakly argillized gray shale
1510.8	1508.8-1514.2 (1.08)	intensively argillized carbonaceous hornfels, pseudo py, coarse rlg
1512	1508.8-1514.2 (1.08)	intensively argillized carbonaceous hornfels, pseudo py, coarse rlg
1512	1508.8-1514.2 (1.08)	intensively argillized carbonaceous hornfels, pseudo py, coarse rlg
1514.2	1514.2-1519.6 (0.592)	intensively argillized brown hornfels, disseminated py, coarse rlg
1516	1514.2-1519.6 (0.592)	gray shale, pseudo py, intensively fractured
1517	1514.2-1519.6 (0.592)	weakly argillized gray shale, pseudo py
1518	1514.2-1519.6 (0.592)	intensively argillized phyllitic brown hornfels, coarse rlg
1522.6	1519.6-1524.8 (0.266)	intensively argillized phyllitic brown hornfels, coarse rlg
1523.8	1519.6-1524.8 (0.266)	intensively argillized phyllitic brown hornfels, trace rlg

1524.8	1524.8-1528.8 (0.074)	moderately argillized gray shale
1527.8	1524.8-1528.8 (0.074)	moderately argillized gray shale
TR 95-122		
1531.7	1529.1-1532.0 (<0.001)	brown hornfels + skarn, calcite and py vein
1533	1532.0-1540.3 (0.001)	pink-white marble + brown hornfels + argillized limestone
1537	1532.0-1540.3 (0.001)	pink-white marble + brown hornfels + argillized limestone calcite vein
1540.0	1532.0-1540.3 (0.001)	marble>brown hornfels, weakly argillized limestone, rlg, calcite
1544.4	1544.4-1551.0 (0.012)	greenish brown hornfels, calcite, pyrrhotite
1545	1544.4-1551.0 (0.012)	shuffled carbonaceous hornfels and dacite, pyrrhotite, intensively fractured
1545.5	1544.4-1551.0 (0.012)	shuffled carbonaceous hornfels and dacite, pyrrhotite, intensively fractured
1546.5	1544.4-1551.0 (0.012)	shuffled carbonaceous hornfels and dacite, biotite, pyrrhotite, calcite
1552	1551.0-1560.3 (0.013)	shuffled carbonaceous hornfels and dacite, biotite, pyrrhotite, calcite
1553.8	1551.0-1560.3 (0.013)	brownish dacite porphyry, pyrrhotite
1555.5	1551.0-1560.3 (0.013)	gray dacite porphyry
1560.4	1560.3-1564.2 (0.063)	shuffled dacite and hornfels, trace rlg
1561	1560.3-1564.2 (0.063)	brown hornfels + dacite, pyrrhotite
1563	1560.3-1564.2 (0.063)	intensively argillized brown hornfels + dacite, pyrrhotite
1564.2	1564.2-1569.7 (0.569)	intensively argillized shaly brown hornfels, rlg, intensively fractured
1564.5	1564.2-1569.7 (0.569)	intensively argillized gray shale, pyrrhotite, intensively fractured
1565	1564.2-1569.7 (0.569)	intensively argillized brown hornfels, pyrrhotite, intensively fractured
1569.5	1564.2-1569.7 (0.569)	intensively argillized gray shale, rlg, intensively fractured
1572	1569.7-1574.8 (0.400)	intensively argillized gray shale, trace rlg
1573	1569.7-1574.8 (0.408)	intensively argillized gray shale, trace rlg

1574.5	1569.7-1574.8 (0.408)	intensively argillized gray shale, trace rlg
1576	1574.8-1579.9 (0.207)	intensively argillized gray shale, trace rlg
1578.5	1574.8-1579.9 (0.207)	intensively argillized gray shale, trace rlg
1583	1579.0-1585.5 (1.00)	intensively argillized decalcified gray shale, coarse rlg
1585.3	1579.0-1585.5 (1.00)	intensively argillized decalcified gray shale, coarse rlg
1588	1585.8-1589.8 (0.458)	dacite> argillized greenish-carbonaceous hornfels, py-vein, coarse rlg
1590	1589.8-1595.0 (0.118)	weakly argillized dacite and brown hornfels, py vein, trace rlg
1599.5	1595.0-1599.9 (0.350)	moderately argillized dacite, pseudo py
1604.5	1599.0-1605.0 (0.546)	intensively argillized brownish dacite, qtz vein, py, coarse rlg
1610.5	1610-1613.5 (2.33)	intensively argillized brown hornfels, rlg-rich
1611.5	1610-1613.5 (2.33)	moderately argillized brown hornfels, rlg-rich
1614.5	1613.5-1617.5 (1.64)	intensively argillized brown hornfels, disseminated py, rlg
1617.5	1617.5-1622.2 (4.71)	intensively argillized shaly brown hornfels, calcite-rich, coarse rlg, py
1619.5	1617.5-1622.2 (4.71)	intensively argillized shaly brown hornfels, calcite-rich, coarse coarse rlg, py, calcite
1623	1622.6-1626.5 (1.28)	intensively argillized shaly brown hornfels, calcite-rich, coarse coarse rlg, py, calcite
1625.5	1622.6-1626.5 (1.28)	moderately argillized shaly brown hornfels, calcite veinlets, rlg
1629.5	1626.5-1633.5 (0.578)	intensively argillized brown hornfels
1633.5	1633.5-1643.5 (0.071)	marble + hornfels, calcite, py
1643	1633.5-1643.5 (0.071)	marble + hornfels, biotite, calcite
1647.5	1643.5-1649.0 (0.116)	gray shale + hornfels
1653	1649.0-1656.0 (0.014)	brown hornfels + marble
TR 95-124		
1476.4	1479.5-1483.1 (0.052)	intensively argillized decalcified gray shale, qtz, coarse rlg
1478.3	1479.5-1483.1 (0.052)	intensively argillized gray shale, qtz, pseudo py, rlg
1485.7	1483.1-1487.3 (<0.001)	weakly argillized brown hornfels

1486	1483.1-1487.3 (<0.001)	brown hornfels, pyrrhotite, py-cube, calcite vein
1492.5	1492.5-1497.5 (0.158)	weakly argillized gray shale, coarse rlg, pseudo py
1498	1497.5-1502.5 (0.954)	weakly argillized gray shale, coarse rlg, pseudo py
1503	1502.5-1507.5 (0.276)	weakly argillized gray shale, calcite, trace rlg, pseudo py
1506.5	1502.5-1507.5 (0.276)	medium-light gray shale, qtz, coarse rlg
1507.3	1502.5-1507.5 (0.276)	medium-light gray shale, py-vein, trace rlg
1514	1512.7-1519.0 (0.449)	intensively argillized gray shale, decalcified, trace rlg, py
1520	1519.0-1524.2 (0.686)	medium-light gray shale, pseudo py, trace rlg
1527.5	1524.2-1529.5 (0.706)	medium-light gray shale, trace rlg
1531.5	1529.5-1534.5 (0.709)	medium-light gray shale, trace rlg
1534.5	1534.5-1539.0 (0.540)	medium-light gray shale, trace rlg, py-vein
1543.5	1539.0-1544.0 (0.350)	brown hornfels, trace rlg, py
1551.5	1544.0-1547.0 (0.105)	weakly argillized brown hornfels, calcite, pseudo py
1552.5	1547.0-1553.5 (0.001)	intensively argillized brown hornfels, trace rlg, pseudo py
1554.5	1553.5-1562.5 (0.001)	moderately argillized brown hornfels, rlg
1557	1553.5-1562.5 (0.001)	brown hornfels, pyrrhotite, marble
1562	1553.5-1562.5 (0.001)	boudinaged brown hornfels, rlg, orpiment
1567	1566.2-1577.2 (0.001)	boudinaged brown hornfels, py-vein, pyrrhotite, calcite vein
TR 95-126		
1790.5	no assay	intensively argillized carbonaceous hornfels, disseminated py, py vein
1795.5	no assay	weakly argillized carbonaceous hornfels, calcite vein
1804.5	1805-1809.3 (0.352)	intensively argillized carbonaceous hornfels, coarse rlg, qtz
1810.5	1809.3-1814.6 (0.346)	carbonaceous hornfels, qtz, coarse rlg, fissile, carbonaceous
1811	1809.3-1814.6 (0.346)	carbonaceous hornfels, py masses, fractured
1814.6	1814.6-1819.8 (0.564)	carbonaceous hornfels, coarse rlg, disseminated py, qtz, fissile
1819.8	1819.8-1825.8 (0.334)	carbonaceous hornfels, coarse rlg, disseminated py, qtz, fissile
1825.9	1825.8-1832.4 (0.132)	carbonaceous hornfels, fractured, fissile, py-cube, coarse rlg

1838	1832.4-1839.5 (0.090)	moderately argillized carbonaceous hornfels, calcite vein, disseminated py
1838.7	1832.4-1839.5 (0.090)	moderately argillized carbonaceous hornfels, calcite in tension crack, massive py
1843.8	1839.5-1844 (0.146)	moderately argillized carbonaceous hornfels, coarse rlg, disseminated py, qtz, calcite
1869.5	1861-1870.5 (0.114)	moderately argillized carbonaceous hornfels, massive py, calcite in tension crack
1881.5	1881-1883 (0.238)	weakly argillized carbonaceous hornfels, disseminated py, calcite
1893	1892-1896.5 (0.146)	intensively argillized brown hornfels, coarse rlg, calcite, qtz, massive and disseminated py
1897.5	1896.5-1901 (0.012)	weakly argillized brown hornfels + marble, py, trace rlg
1902.5	1901-1911.3 (<0.001)	weakly argillized brown hornfels, pyrrhotite, py, trace rlg
1906	1901-1911.3 (<0.001)	brown hornfels + marble, py, pyrrhotite, tension crack
1913	1911.3-1916 (<0.001)	brown hornfels + marble, py, pyrrhotite, tension crack
1920	1916-1921.2 (<0.001)	weakly argillized brown hornfels, massive py
TR 95-136		
1847	1851.0-1855.0 (0.202)	weakly argillized brown hornfels, massive py, qtz
1867	1864.0-1868.0 (0.048)	weakly argillized carbonaceous hornfels, rlg, massive py, qtz, calcite
1867.5	1864.0-1868.0 (0.048)	weakly argillized carbonaceous hornfels, massive rlg, calcite, qtz
1869.5	1868.0-1871.5 (0.044)	weakly argillized carbonaceous hornfels, massive rlg, calcite, qtz
1875.7	1871.5-1877.0 (0.168)	weakly argillized carbonaceous hornfels, disseminated py, calcite
1879	1877.0-1882.0 (0.080)	weakly argillized brown hornfels, py masses, calcite, rlg
1885.5	1882.0-1887.0 (0.210)	weakly argillized brown hornfels, py specs
1896.5	1892.0-1897.0 (0.326)	intensively argillized brown hornfels, massive rlg, calcite, py
1898.5	1897.0-1902.0 (0.522)	intensively argillized carbonaceous hornfels, disseminated py, rlg
1904.8	1902.0-1907.0 (0.498)	intensively argillized brown hornfels, disseminated py
1906.5	1902.0-1907.0 (0.498)	intensively argillized carbonaceous hornfels, trace rlg

1909	1907.0-1912.0 (0.626)	moderately carbonaceous hornfels, pseudo py
1918.5	1917.0-1922.0 (0.710)	moderately argillized phyllitic brown hornfels, calcite
1920.5	1917.0-1922.0 (0.710)	moderately argillized phyllitic brown hornfels, calcite, disseminated py
1926.2	1922.0-1927.0 (0.531)	moderately argillized phyllitic brown hornfels, calcite, disseminated py
1931.0	1931.0-1935.7 (0.068)	weakly argillized brown hornfels, disseminated py
1932.5	1931.0-1935.7 (0.068)	weakly argillized gray shale, disseminated py
1937.5	1935.7-1939.2 (0.032)	weakly argillized hornfels, disseminated py
1939.5	1939.2-1945.4 (<0.001)	brown hornfels + marble, disseminated py
TR 96-22		
1347.7	no assay	brown hornfels + marble + skarn, disseminated py
1359.5	1358.0-1368.0 (0.008)	brown hornfels + marble + skarn, disseminated py
1365	1358.0-1368.0 (0.008)	weakly argillized mylonitic brown hornfels, disseminated py, rlg, calcite
1368	1368.0-1373.0 (0.852)	intensively argillized mylonitic brown hornfels, disseminate py
1381	1378.0-1381.7 (0.048)	intensively argillized brown hornfels, disseminated py, calcite
1386	1381.7-1386.5 (0.056)	moderately argillized hornfels, coarse rlg
1391	1386.5-1391.3 (0.004)	marble>brown hornfels, disseminated py, trace rlg,
1399.5	1396.5-1401.0 (-0.002)	brown hornfels, marble, disseminated py, trace rlg
1401.5	1401.0-1411.3 (-0.002)	marble> brown hornfels, disseminated py
TR 96-24		
1340.5	1330.8-1641.0 (-0.002)	brown hornfels > marble, disseminated py, py veins
1350.5	1341.8-1351.5 (-0.002)	massive marble > brown hornfels, disseminated py, calcite vein
1354.5	1351.5-1356.5 (0.118)	weakly argillized brown hornfels, trace rlg, disseminated py, calcite in fracture
1355.5	1351.5-1356.5 (0.118)	weakly argillized brown hornfels, trace rlg, fissile
1356.4	1351.5-1356.5 (0.118)	weakly argillized hornfels, disseminated py, fissile
1359.3	1356.5-1361.3 (0.314)	weakly argillized gray shale, trace rlg, py

1362.5	1361.3-1366.3 (0.294)	weakly argillized brown hornfels, coarse rlg, disseminated py
1369.5	1366.3-1372.2 (0.518)	weakly argillized brown hornfels, massive py
1377	1372.2-1378.0 (0.262)	intensively argillized brown hornfels, coarse rlg, pseudo py
1378	1378.0-1380.0 (0.524)	weakly argillized brown hornfels + dacite, coarse rlg
1380	1380.0-1384.2 (0.096)	weakly argillized brown hornfels + dacite
1383	1380.0-1384.2 (0.096)	intensively argillized dacite/shale (?), disseminated py, trace rlg
1388	1384.2-1389.0 (0.084)	intensively argillized dacite/shale (?), disseminated py, trace rlg
1390	1389.0-1393.6 (0.062)	weakly argillized dacite/ shale (?), qtz
1392	1389.0-1393.6 (0.062)	moderately argillized brown hornfels, disseminated py
1397	1393.6-1397.5 (0.126)	intensively argillized brown hornfels, disseminated py
1401	1397.5-1402.0 (0.276)	intensively argillized shaly brown hornfels, rlg, pseudo py
1406	1402.0-1407.0 (0.292)	intensively argillized carbonaceous hornfels, rlg, qtz
1409.5	1407.0-1412.0 (0.544)	intensively argillized carbonaceous hornfels, massive rlg
1410	1407.0-1412.0 (0.544)	intensively argillized carbonaceous hornfels, rlg, pseudo py
1422	1417.0-1423.0 (0.158)	intensively argillized carbonaceous hornfels, rlg
1425.5	1423.0-1429.0 (0.440)	intensively argillized carbonaceous hornfels, rlg, disseminated py
1431	1429.0-1436.0 (0.256)	limestone, marble, disseminated py
1434.5	1429.0-1436.0 (0.256)	limestone, marble
1438.8	1436.0-1442.0 (0.220)	intensively argillized brown hornfels, pseudo py
1446.5	1442.0-1447.0 (0.080)	gray shale, rlg, calcite vein, disseminated py
1447	1447.0-1455.8 (0.004)	moderately argillized carbonaceous hornfels, coarse calcite
1447.5	1447.0-1455.8 (0.004)	moderately argillized carbonaceous hornfels, coarse calcite
1451	1447.0-1455.8 (0.004)	moderately argillized carbonaceous hornfels, disseminated py, trace rlg
1452.5	1447.0-1455.8 (0.004)	weakly argillized boudinaged brown hornfels + skarn, disseminated py, calcite vein
1459.8	1455.8-1461.3 (-0.002)	intensively argillized brown hornfels, clay-rich, disseminated py, coarse calcite

1467	1461.3-1471 (-0.002)	boudinaged brown hornfels + skarn, disseminated py, coarse calcite
1471	1471 -1475 (-0.002)	weakly argillized brown hornfels, disseminated py, trace rlg
TR 96-58		
1149.5	1144.0-1154.2 (-0.002)	brown hornfels, marble, calcite, py, pyrrhotite
1155.8	1154.2-1162.7 (0.002)	brown hornfels, marble, trace rlg, py
1163	1162.7-1164.2 (0.096)	weakly argillized brown hornfels, coarse rlg, pseudo py
1166.7	1164.2-1169.9 (0.526)	intensively argillized brown hornfels, coarse rlg, pseudo py
1169.4	1164.2-1169.9 (0.526)	intensively argillized brown hornfels, coarse rlg, pseudo py
1178	1174.3-1179.7 (0.536)	intensively argillized brown hornfels, coarse rlg, pseudo py
1181	1179.7-1185.0 (0.292)	intensively argillized brown hornfels, coarse rlg
1186.6	1185.0-1196.0 (0.856)	intensively argillized brown hornfels, rlg
1193	1191.2-1196.0 (0.604)	intensively argillized brown hornfels, coarse rlg
1197	1196.0-1201.0 (0.604)	moderately argillized brown hornfels, coarse rlg
1198	1196.0-1201.0 (0.604)	intensively argillized brown hornfels, coarse rlg
1199.5	1196.0-1201.0 (0.604)	intensively argillized brown hornfels, trace rlg, disseminated py
1209	1207.0-1213.5 (0.312)	intensively argillized brown hornfels, disseminated py, coarse rlg
1216	1213.5-1218.6 (0.278)	moderately argillized brown hornfels, disseminated py, coarse rlg
1218.5	1213.5-1218.6 (0.278)	moderately argillized brown hornfels, coarse rlg
1223	1218.6-1224.2 (0.136)	weakly argillized diabase sill, trace rlg, disseminated py
1221.5	1218.6-1224.2 (0.136)	weakly argillized diabase sill, massive py
1226.5	1224.2-1228.5 (-0.210)	moderately argillized diabase sill, massive rlg, py masses
1227.9	1224.2-1228.5 (-0.210)	weakly argillized diabase sill, calcite, py
1230.8	1228.5-1236.0 (-0.002)	weakly argillized diabase sill, py, calcite vein
1327.9	1325.6-1335.6 (-0.002)	diabase + mylonitic brown hornfels + marble, qtz
1338.8	1335.6-1344.3 (0.008)	weakly argillized diabase + brown hornfels, py vein

1345	1344.3-1351.0 (-0.002)	weakly argillized diabase + brown hornfels, py vein
1351	1351.0-1354.0 (-0.002)	weakly argillized, disseminated py, rlg, calcite
TR96-61		
816.5	814.9-826.5 (0.010)	brown hornfels, pseudp
825	814.9-826.5 (0.010)	brown hornfels, pseudo py
830.5	826.5-834.1 (0.008)	weakly argillized brown hornfels, disseminated py
833.3	826.5-834.1 (0.008)	intensively argillized carbonaceous hornfels, qtz
839	834.1-842.6 (0.002)	intensively argillized carbonaceous hornfels, disseminated py, qtz
846.5	842.6-850.7 (0.002)	weakly argillized brown hornfels, qtz, disseminated py
851	850.7-854.3 (0.204)	moderately argillized carbonaceous hornfels, disseminated py
853	850.7-854.3 (0.204)	intensively argillized carbonaceous hornfels, disseminated py
853.8	850.7-854.3 (0.204)	intensively argillized carbonaceous hornfels
854	850.7-854.3 (0.204)	moderately argillized brown hornfels, qtz, disseminated py
855.5	854.3-860.6 (0.002)	intensively argillized brown carbonaceous hornfels, pseudo py
859	854.3-860.6 (0.002)	moderately argillized carbonaceous hornfels, disseminated py
861	860.6-864.3 (0.040)	moderately argillized carbonaceous hornfels, calcite, pseudo py
863.5	860.6-864.3 (0.040)	moderately argillized carbonaceous hornfels
865.8	864.3-868.2 (0.204)	intensively argillized carbonaceous hornfels, qtz, pseudo py
867.5	864.3-868.2 (0.204)	intensively argillized carbonaceous hornfels, disseminated py
868.2	868.2-871.6 (0.112)	moderately argillized carbonaceous hornfels, disseminated py
884	880.1-885.3 (0.024)	moderately argillized carbonaceous hornfels, disseminated py, shearing texture
887.5	885.3-890.0 (0.060)	moderately argillized carbonaceous hornfels, disseminated py shearing texture
TR 96-66		
1669.8	1668.8-1680.8 (-0.002)	brown hornfels + marble, massive rlg
1673.5	1668.8-1680.8 (-0.002)	weakly argillized brown hornfels, py

1680.8	1680.8-1689.0 (0.182)	brown hornfels, disseminated py, calcite in tension crack
1682.5	1680.8-1689.0 (0.182)	weakly argillized carbonaceous hornfels, disseminated py tension crack
1686.7	1680.8-1689.0 (0.182)	weakly argillized carbonaceous hornfels, disseminated py
1690.5	1689.0-1694.0 (0.174)	moderately argillized carbonaceous hornfels, disseminated py, qtz
1696.5	1694.0-1698.0 (0.082)	carbonaceous hornfels, massive py
1697.5	1694.0-1698.0 (0.082)	carbonaceous hornfels, py
1701.5	1698.0-1704.0 (0.030)	carbonaceous hornfels, py masses
1705	1704.0-1708.6 (0.010)	weakly silicified carbonaceous hornfels, py masses, calcite
1708	1704.0-1708.6 (0.010)	weakly argillized boudinaged brown hornfels, massive py, trace rlg
1713.3	1712.5-1718.0 (0.102)	weakly argillized brown hornfels, marble, trace rlg, pseudo py
1718.2	1718.0-1722.8 (0.186)	weakly argillized carbonaceous hornfels, disseminated py
1725.5	1722.8-1726.5 (1.640)	intensively argillized brown hornfels, trace rlg, pseudo py
1729.5	1726.5-1732.5 (0.452)	moderately argillized brown hornfels, massive rlg, calcite
1734	1732.5-1737.3 (0.008)	boudinaged hornfels, marble, trace rlg, py masses,
1739.8	1732.5-1737.3 (0.008)	moderately argillized hornfels + marble, trace rlg, disseminated py

APPENDIX II

LIST OF DOUBLY POLISHED THICK SECTIONS,
POLISHED THIN SECTIONS,
AND QUICK PLATES

APPENDIX II

List of Doubly Polished Thick Sections

note: Sample # indicates drill hole # followed by the depth of the sample.

Drill holes are near vertical.

Sample #	grade (oz/ton)	drill hole angle (degree)	surface elevation (feet)	surface elevation (meters)
TR 94-172 1655	0.653	88.36	5472.52	16417.56
TR 94-172 1660.5	0.088	88.36	5472.52	16417.56
TR 94-172 1661.5	0.088	88.36	5472.52	16417.56
TR 94-172 1676	0.452	88.36	5472.52	16417.56
TR 94-172 1686	0.942	88.36	5472.52	16417.56
TR 94-172 1730.3	0.237	88.38	5472.52	16417.56
TR 94-172 1776.3	0.135	88.26	5472.52	16417.56
TR 94-172 1855.4	0.001	88.15	5472.52	16417.56
TR 94-172 1865.5	0.028	88.15	5472.52	16417.56
TR 94-172 1912.4	0.487	88.04	5472.52	16417.56
TR 94-172 1913	0.487	88.04	5472.52	16417.56
TR 94-172 1917.9	0.295	88.04	5472.52	16417.56
TR 94-172 1999.8	0.257	88.02	5472.52	16417.56
TR 94-172 2016.8	0.458	88.15	5472.52	16417.56
TR 94-172 2026	0.052	88.15	5472.52	16417.56
TR 95-039 1958	0.28	86.94	5525.73	16577.19
TR 95-046 1634	0.581	88.04	5547.01	16641.03
TR 95-072 1892.7	1.46	85.01	5473.23	16419.69
TR 95-076 1483.5	0.963	78.81	5538.45	16615.35
TR 95-095 1760.5	0.178	89.13	5426.55	16279.65
TR 95-095 1786.7	1.47	89.13	5426.55	16279.65
TR 95-122 1617.5-1	4.71	83.53	5463.75	16391.25
TR 95-122 1617.5-2	4.71	83.53	5463.75	16391.25
TR 95-122 1617.5-3	4.71	83.53	5463.75	16391.25
TR 95-122 1619.5-1	4.71	83.53	5463.75	16391.25
TR 95-122 1619.5-2	4.71	83.53	5463.75	16391.25
TR 96-066 1725.5	1.64	85.53	5446.46	16339.38

List of Polished Thin Sections

TR 94-172 1637.5	0.001	88.51	5472.52	16417.56
TR 94-172 1645.5	0.206	88.51	5472.52	16417.56
TR 94-172 1688.6	0.025	88.36	5472.52	16417.56
TR 94-172 1699.2	0.007	88.36	5472.52	16417.56
TR 94-172 1788.6	0.015	88.26	5472.52	16417.56
TR 94-172 1811.5	<0.001	88.34	5472.52	16417.56
TR 94-172 1977	0.001	88.02	5472.52	16417.56
TR 94-039 1809.5	0.024	86.98	5547.01	16641.03

List of Quick Plates

sample #	fluid inclusion host mineral
TR 95-39 1607	calcite
TR 95-39 1620	quartz
TR 95-39 1661.5	pre-ore stage quartz
TR 95-39 1809.5	pre-ore stage quartz
TR 95-39 1828.4	quartz
TR 95-39 1839	realgar
TR 95-39 1842.2	vein quartz
TR 95-39 1850	calcite
TR 95-39 1886.3	calcite
TR 95-39 1948	pre-ore stage quartz
TR 95-39 1954	jasperoid quartz
TR 95-39 1966	pre-ore stage quartz
TR 95-39 1977.5	no inclusions > 3 μ m
TR 95-39 2014.5	no inclusions > 3 μ m
TR 95-46 1634	no inclusions > 3 μ m
TR 95-46 1647.5	calcite
TR 95-46 1850.5	no inclusions > 3 μ m
TR 95-49 1549	pre-ore stage quartz
TR 95-49 1925.5	no inclusions > 3 μ m
TR 95-71 1883	quartz
TR 95-71 2051.5	jasperoid quartz
TR 95-72 1892.7	no inclusions > 3 μ m
TR 95-76 1443.5	jasperoid quartz
TR 95-76 1483.5	no inclusions > 3 μ m
TR 95-76 1545	calcite
TR 95-95 1599.5	pre-ore stage quartz
TR 95-95 1758.3	pre-ore stage quartz
TR 95-95 1760.3	no inclusions > 3 μ m
TR 95-95 1786.7	calcite
TR 95-113 1512.8	no inclusions > 3 μ m
TR 95-113 1518	no inclusions > 3 μ m
TR 95-122 1611.5	no inclusions > 3 μ m
TR 95-122 1625.5	calcite
TR 95-124 1498	no inclusions > 3 μ m
TR 95-126 1814.6	jasperoid quartz
TR 95-122 1881.5	pre-ore stage quartz
TR 96-22 1368	no inclusions > 3 μ m
TR 96-24 1409.5	realgar
TR 96-24 1431	calcite
TR 96-61 854	jasperoid quartz
TR 96-66 1690.5	no inclusions > 3 μ m
TR 96-66 1725.5	jasperoid quartz

APPENDIX III

RESULTS OF X-RAY DIFFRACTION ON
TWO TYPES OF UNALTERED
HOST ROCKS

Appendix III

Results of X-ray Diffraction on TR 94-172 1637.5

TR 94-172 1637.5

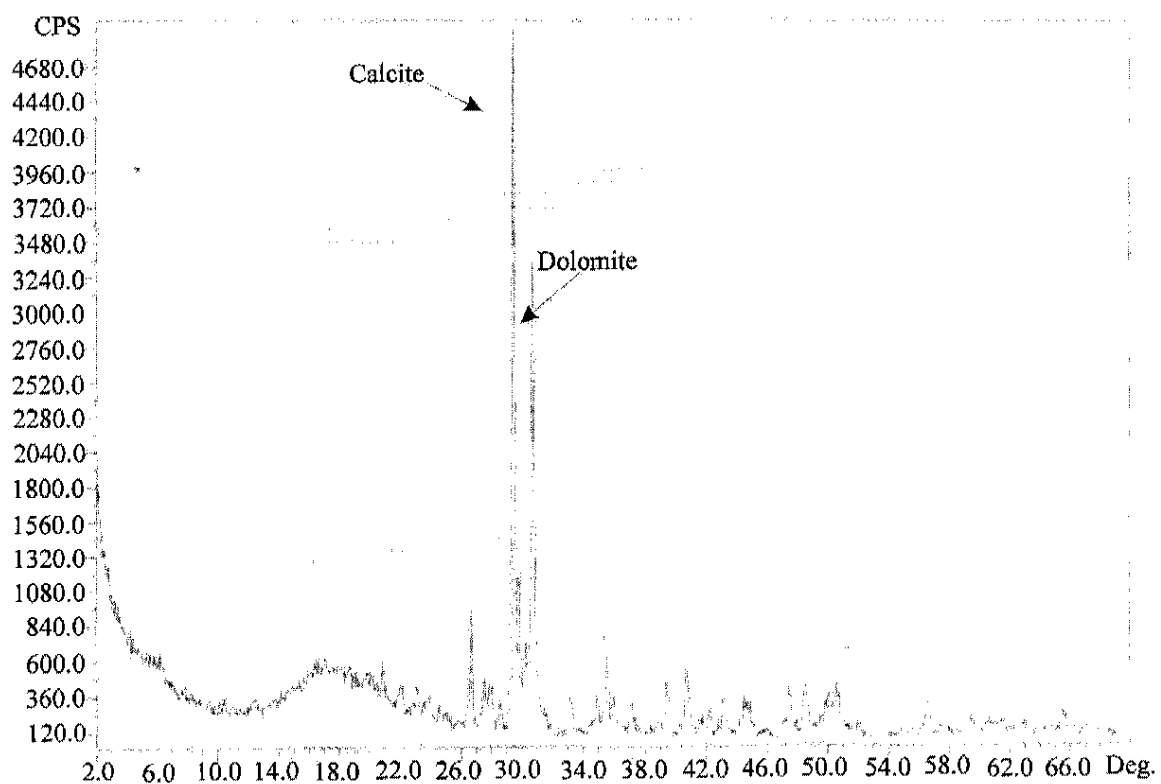
Scan Type: Normal, Start Angle: 2 deg., Stop angle: 70 deg., Num Points: 1361, Step size: 0.05 deg.

Peaks:

Position (Dsp)	Intensity (cps)	FWHM (Deg)	Area (cps.-deg.)	Source	Curve
3.0305	3700	0	1416.9	Peak Finder	None
2.9145	2572	0	19698.9	Peak Finder	None
2.9908	710	0	2718.9	Peak Finder	None
3.3422	620	0.1	4748.6	Peak Finder	None
2.2098	344	0.15	2634.7	Peak Finder	None
2.5266	338	0	3887.7	Peak Finder	None
2.2823	298	0.05	2282.4	Peak Finder	None
1.9107	250	0.1	957.4	Peak Finder	None
1.8736	250	0.05	1914.7	Peak Finder	None
2.9521	236	0.15	1807.5	Peak Finder	None
3.2408	216	0.05	1654.3	Peak Finder	None
4.2569	212	0	811.9	Peak Finder	None
1.6248	206	0.1	1577.7	Peak Finder	None
2.0278	204	0.1	781.2	Peak Finder	None
2.7081	204	0.1	1562.4	Peak Finder	None
3.2065	202	0.5	1547.1	Peak Finder	None
3.1784	200	0.5	765.9	Peak Finder	None
2.0924	182	0.5	1393.9	Peak Finder	None
14.1298	180	0.5	0	Peak Finder	None
1.8028	170	0.1	3272	Peak Finder	None
2.4927	160	0.1	1225.4	Peak Finder	None
1.8175	150	0.05	574.4	Peak Finder	None
2.1349	148	0.1	1133.5	Peak Finder	None
2.015	140	0.1	0	Peak Finder	None
2.4244	134	0.15	2052.6	Peak Finder	None
3.7201	126	0.2	482.5	Peak Finder	None
2.5651	126	0.1	965	Peak Finder	None
4.0369	118	0	903.8	Peak Finder	None
13.9075	108	0.1	0	Peak Finder	None
1.8243	108	0.1	413.6	Peak Finder	None
3.8502	107	0.1	1230.4	Peak Finder	None
3.1293	106	0.1	405.9	Peak Finder	None
3.6231	90	0.1	0	Peak Finder	None
4.4249	88	0.05	0	Peak Finder	None
1.7571	84	0	0	Peak Finder	None
1.5043	80	0.05	306.4	Peak Finder	None
1.4221	79.15	0.1	909.3	Peak Finder	None
4.7162	72	0.05	827.2	Peak Finder	None
1.5547	66	0.05	0	Peak Finder	None
4.9513	64	0.25	0	Peak Finder	None
2.8378	60	0	229.8	Peak Finder	None
4.3393	60	0.1	229.8	Peak Finder	None
4.8836	52	0	398.3	Peak Finder	None
1.4385	48	0.05	183.8	Peak Finder	None
2.0408	46	0.05	352.3	Peak Finder	None

Position (Dsp)	Intensity (cps)	FWHM (Deg)	Area (cps.-deg.)	Source	Curve
1.4105	44	0.15	337	Peak Finder	None
2.3902	42	0.1	0	Peak Finder	None
29.45	3700	0	14169.1	Peak Finder	None
30.65	2572	0	19698.9	Peak Finder	None
29.85	710	0	2718.9	Peak Finder	None
26.65	620	0.1	4748.6	Peak Finder	None
40.8	344	0.15	2634.7	Peak Finder	None
35.5	338	0	3887.7	Peak Finder	None
39.45	298	0.05	2282.4	Peak Finder	None
47.55	250	0.1	957.4	Peak Finder	None
48.55	250	0.05	1914.7	Peak Finder	None
30.25	236	0.15	1807.8	Peak Finder	None
27.5	216	0.05	1654.3	Peak Finder	None
20.85	212	0	811.9	Peak Finder	None
56.6	206	0.1	1577.7	Peak Finder	None
44.65	204	0.1	781.2	Peak Finder	None
33.05	204	0.1	1562.4	Peak Finder	None
27.8	202	0.05	1547.1	Peak Finder	None
28.05	200	0.05	765.9	Peak Finder	None
43.2	180	0.05	1393.9	Peak Finder	None
6.25	180	0.05	0	Peak Finder	None
50.5881	170	0.1	3272	Peak Finder	None
36	160	0.1	1225.4	Peak Finder	None
50.15	150	0.05	574.4	Peak Finder	None
42.3	148	0.1	1133.5	Peak Finder	None
44.95	140	0.1	0	Peak Finder	None
37.05	134	0.15	2052.6	Peak Finder	None
23.9	126	0.2	482.5	Peak Finder	None
34.95	126	0.1	965	Peak Finder	None
22	118	0	903.8	Peak Finder	None
6.35	108	0.1	0	Peak Finder	None
49.95	108	0.1	413.6	Peak Finder	None
23.0812	107	0.1	1230.4	Peak Finder	None
28.5	106	0.1	405.9	Peak Finder	None
24.55	90	0.1	0	Peak Finder	None
20.05	88	0.05	0	Peak Finder	None
52	84	0	0	Peak Finder	None
61.6	80	0.05	306.4	Peak Finder	None
65.5919	79	0.1	909.3	Peak Finder	None
18.8	72	0.05	827.2	Peak Finder	None
59.4	66	0.05	0	Peak Finder	None
17.9	64	0.25	0	Peak Finder	None
31.5	60	0	229.8	Peak Finder	None
20.45	60	0.1	229.8	Peak Finder	None
18.15	52	0	398.3	Peak Finder	None
64.75	48	0.05	183.8	Peak Finder	None
44.35	46	0.05	352.3	Peak Finder	None
66.2	44	0.15	337	Peak Finder	None
37.6	42	0.1	0	Peak Finder	None

Step: 0.050 °
Count Time: 0.500 sec.
Range: 2.00 - 70.00 (deg)
Scan Rate: 6.00 Deg/min.



Results of x-ray diffraction analysis on the Middle unit from TR 94-172 1637.5.

Results of X-ray Diffraction on TR 94-172 1993

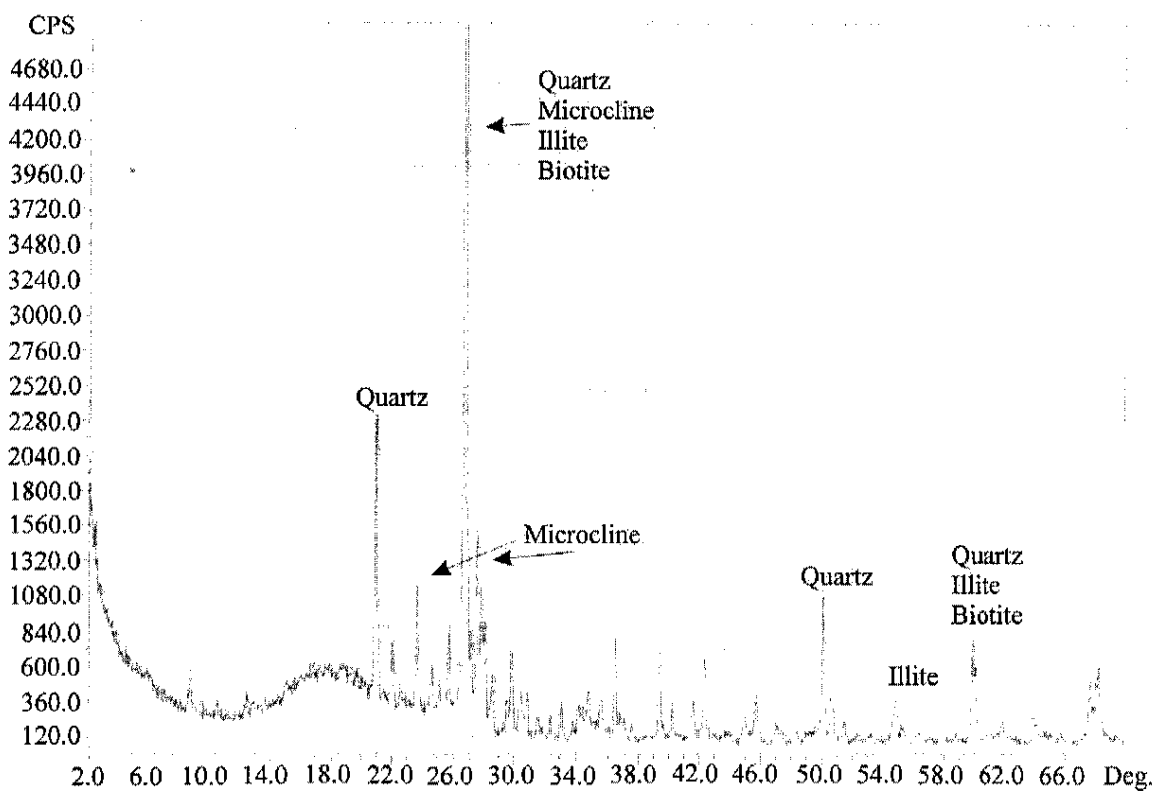
TR 94-172 1993

Scan Type: Normal, Start Angle: 2 deg., Stop angle: 70 deg., Num Points: 1361, Step size: 0.05 deg.

Peaks:

Position (Dsp.)	Intensity (cps)	FWHM (Deg.)	Area (cps.-deg.)	Source	Curve
3.3422	8946	0.5	34258.6	Peak Finder	None
4.2569	1732	0.1	13265.3	Peak Finder	None
1.8175	928	0.05	7170.5	Peak Finder	None
3.2374	832	0.1	9564.1	Peak Finder	None
3.7746	748	0.1	5728.9	Peak Finder	None
3.2065	672	0.05	5146.8	Peak Finder	None
1.5417	644	0.05	4932.4	Peak Finder	None
2.4564	572	0.1	4380.9	Peak Finder	None
3.1784	560	0.05	2144.5	Peak Finder	None
2.2795	558	0	2136.9	Peak Finder	None
2.1277	504	0.15	3860.1	Peak Finder	None
3.4635	396	0.1	3033	Peak Finder	None
3.2877	394	0.05	0	Peak Finder	None
2.9957	390	0.1	2987	Peak Finder	None
4.0369	360	0.15	1378.6	Peak Finder	None
1.832	332	0.1	2542.8	Peak Finder	None
1.375	316	0.2	6062.1	Peak Finder	None
1.9795	260	0.2	1991.3	Peak Finder	None
3.1293	258	0.05	1976	Peak Finder	None
1.6724	246	0.05	942.1	Peak Finder	None
1.7991	244	0.05	1868.8	Peak Finder	None
2.1624	228	0.05	1746.2	Peak Finder	None
10.0975	226	0.05	865.5	Peak Finder	None
3.6231	216	0.1	827.2	Peak Finder	None
2.7081	214	0.05	819.5	Peak Finder	None
2.2361	212	0.1	1623.7	Peak Finder	None
2.5758	186	0.05	1424.6	Peak Finder	None
2.5198	178	0.05	681.6	Peak Finder	None
2.9005	166.57	0.1	2551.5	Peak Finder	None
2.9398	162.56	0.1	2491.5	Peak Finder	None
3.5449	150	0.1	574.4	Peak Finder	None
2.6234	146	0.1	559.1	Peak Finder	None
2.7693	130	0.05	497.8	Peak Finder	None
1.4526	122	0.1	934.4	Peak Finder	None
3.0293	121.57	0.1	1396.6	Peak Finder	None
1.9279	114	0.1	436.6	Peak Finder	None
2.4371	112	0.05	428.9	Peak Finder	None
2.6085	110	0.1	421.2	Peak Finder	None
1.7114	106	0.15	811.9	Peak Finder	None
1.4963	101.1	0.1	1161.5	Peak Finder	None
2.8373	100	0.1	382.9	Peak Finder	None
3.957	100	0.25	765.9	Peak Finder	None

Step: 0.050 °
Count Time: 0.500 sec.
Range: 2.00 - 70.00 (deg)
Scan Rate: 6.00 Deg/min.



Results of x-ray diffraction analysis on the Lower unit from TR 94-172 1993.

APPENDIX IV

SUMMARY OF PETROGRAPHY AND ORE MICROSCOPY OF DOUBLY POLISHED THICK SECTIONS AND POLISHED THIN SECTIONS

APPENDIX IV

Doubly Polished Thick Section from a Drill Hole TR 94-172

Sample #: TR 94-172 1655

This sample dominantly contains clasts of original brown hornfels, crystalline quartz, jasperoid quartz and realgar. The size of clasts ranges from 5 by 10 millimeter in widths and 10 to 20 millimeters in lengths. The clasts shapes are angular to semi-angular tabular. Fine iron sulfide crystals are present in the clasts. Marcasite laths form spherical masses that average 20 micrometers in size. Tabular or cubic shaped crystals are 1.5 x 5 micrometer in size. These crystals exhibit anisotropy. Marcasite grains contain porous cores with clear laths on rims. The aggregates form horizontal bedding, which reaches up to 1.2 millimeter in length. Individual marcasite crystals are scattered throughout clasts and are also present between crystalline quartz crystal boundaries. Masses of crystalline quartz are present in clasts of protolith. Quartz crystals are generally equigranular and average 50 micrometers. However, crystal size can range from 20 to 700 micrometers in size. Feathery crystals are present. They exhibit high interference colors. They are overgrown by jasperoid quartz and realgar. Jasperoid quartz is present in open spaces between clasts. Jasperoid quartz ranges from 7 to 50 micrometers and average 15 micrometers in size. Grain shapes vary from xenomorphic to idiomorphic. Reticulate crystals range from 5 to 40 micrometers in widths and from 12 to 80 micrometers in lengths. Subhedral and anhedral crystals exhibit jigsaw puzzle texture. Euhedral jasperoid quartz crystals are over grown by realgar. Subhedral and anhedral realgar fills open spaces between clasts and clusters of jasperoid quartz. Subhedral crystals range from 30 by 50 to 800 by 800 micrometers in size. Realgar contains individual jasperoid quartz crystals and fills fractures in clusters of jasperoid quartz. Euhedral stibnite crystals are present in jasperoid quartz, and particularly realgar. Stibnite forms needle-like crystals, which are average 4 by 40 micrometers in size. Crystals, however, can grow up to 30 by 150 micrometers. They are concentrated along spaces between realgar and clasts.

Sample #: 94-172 1660.5

Orpiment, realgar, and calcite form coarse crystals in this sample. Jasperoid quartz and fluorite are minor constituents. Clasts of hornfels are also present. Jasperoid quartz is either masses of or individual crystals. Euhedral and subhedral crystals average 50 micrometer and range from 10 to 80 micrometers in diameter. A reticulate texture is also present. Quartz crystals range from 15 to 60 micrometers in width and 40 to 180 micrometers in length. Approximately 10 % of jasperoid quartz are coated by clay. The feathery crystals form radial aggregates. The size of clay crystals ranges from 10 by 40 to 140 by 300 micrometers. Rims of clay are overgrown by orpiment. Jasperoid crystals are overgrown by rare fluorite crystals. The cubic fluorite crystals range from 3 by 3 to 30 by 30 micrometers. Fluorite crystals have a clean appearance, but are rimmed by fine pyrite crystals on their rims. Oval-shaped crystals that exhibit yellow-green to pink interference colors are present in fluorite. Orpiment formed on fluorite. Orpiment is the most abundant mineral in this particular section. Coarse crystals reach approximately 900 micrometers in length and 300 micrometers in width. Orpiment contains fine iron sulfide crystals, which are perhaps, marcasite. Orpiment fills fractures in masses of protolith. Subhedral and anhedral realgar filled open spaces between orpiment crystals. Single realgar crystals fill open spaces as large as 220 by 320 micrometers. Very few fine iron-sulfide crystals are present in realgar. Realgar is overgrown on calcite. Calcite formed on orpiment and realgar crystal faces. Subhedral and anhedral crystals filled open space that is 7500 micrometers. Pyrite is present in jasperoid quartz, particularly along jasperoid quartz crystal boundaries. Orpiment also contains pyrite, but very few pyrite crystals are present in realgar. Rounded to cubic pyrite crystals average 4 micrometers in size. They are porous and have fuzzy crystal boundaries. Some pyrite crystals are overgrown by marcasite. Lath-shaped marcasite crystals are overgrown by quartz and orpiment. Coarse laths and aggregates of fine crystals are present. They range from 3 by 8 to 10 by 35 micrometers in size.

Sample #: 94-172 1661.5

Coarsely crystalline orpiment, calcite, and realgar are distinctive in this sample. Realgar filled fractures in orpiment and forms on jasperoid quartz and orpiment crystal faces. Realgar ranges from 10 by 25 to 600 by 2000 micrometers in size. Realgar locally formed on calcite, but dominantly calcite forms on realgar. Calcite forms crystals up to 1000 by 2000 micrometers. Calcite fills fractures in orpiment, and also forms on pre-ore quartz and jasperoid quartz. Calcite contains 2.5-micrometer iron-sulfide crystals, which are,

perhaps, marcasite. Calcite exhibits no or few fractures. Crystal faces of jasperoid quartz are overgrown by calcite. Approximately 5 % of jasperoid quartz are rimmed by clay minerals that show various interference colors that range from first order gray and yellow to second order pink and blue in the thick section. The grains have feathery texture suggesting they are chalcedony. Jasperoid quartz crystals average 60 micrometers and range from 40 to 300 micrometers in size. Subhedral and anhedral crystals are interlocked and exhibit a jigsaw puzzle texture. Barite is locally present with jasperoid quartz, and it contains jasperoid quartz. Barite forms up to 150 by 400-micrometer crystals, which contain calcite inclusions and fine pyrite crystals in rims. Barite is overgrown by orpiment and realgar. Pre-ore stage quartz is fractured. Individual crystals are present as masses. Subhedral grains average 50 by 50 micrometers and range from 25 by 25 to 500 by 1000 micrometers. Fine-grained pyrite is concentrated along jasperoid quartz crystal boundaries and encompassed by jasperoid quartz. Pyrite crystals are present along pre-ore quartz crystal boundaries and fractures in pre-ore quartz. Pyrite crystals average 3 micrometer in size. Spherical and cubic crystals are made of aggregates of needle-like crystals that have the appearance of marcasite but do not show anisotropism.

Sample #: 94-172 1676

Calcite, realgar, jasperoid quartz, crystalline quartz, and pyrite are present in brown hornfels that exhibits mylonitic texture and boudinaged texture. Jasperoid quartz exhibits typical jigsaw-puzzle texture and contains calcite inclusions. Some jasperoid quartz does not contain many calcite inclusions. Jasperoid quartz crystals are anhedral and rounded. The size of crystals ranges from 25 to 100 micrometers and averages 50 micrometers. Approximately 10 % of this quartz are coated with clay, which exhibits feathery texture. Fractured euhedral and subhedral quartz crystals are also present. The coarse mineralization and presence of fractures are similar to the characteristics of pre-ore stage quartz. However, the quartz crystals in this sample do not contain abundant inclusions that are larger than 5 micrometers in diameter. Fluid inclusions are generally less than 2.5 micrometers in diameter, and phases cannot be identified. Fractures in quartz are filled with realgar. Calcite crystals are anhedral or subhedral, and they form on jasperoid quartz and crystalline quartz. They also fill web-like veins. Calcite range from 80 by 50 to 800 by 1200 micrometers in width and length. Realgar formed on calcite crystals that are present in fractures in pyrite. Realgar preferentially formed on pyrite crystal surfaces. Realgar formed anhedral to subhedral crystals that average 15 micrometers in size. Marcasite laths are scattered throughout altered brown hornfels. Euhedral crystals are also enclosed by realgar. The size of laths averages 3 by 15 micrometers and ranges from less than 2.5 to 25 micrometers in dimension. Marcasite exhibits a porous texture. Pyrrhotite is anhedral and is fractured but takes a good polish. Strained crystals form discontinuous horizontal plane, which ranges from 15 by 15 micrometers to 3000 by 3000 millimeters. Some crystals have a bright yellow part in their cores, which exhibit anisotropy indicating the cores are pyrite.

Sample #: TR 94-172 1686

This sample consists of pre-ore quartz, jasperoid quartz, realgar, marcasite, pyrite, and a clay mineral in hornfels. Pre-ore quartz is a minor constituent in this section. It is less than approximately 5 % of the whole sample. Subhedral and euhedral crystals are fractured and randomly present. They average 50 by 50 and range from 25 by 25 to 200 by 400 micrometers. Jasperoid quartz exhibits a jigsaw puzzle texture. Anhedral and subhedral crystals average 25 by 25 and range from 5 by 5 to 30 by 50 micrometers in size. Realgar forms on pre-ore quartz and jasperoid quartz. Realgar ranges from 25 by 25 to 100 by 500 in size. Open spaces between marcasite laths create porous appearance. Marcasite laths average 5 by 10 and range from 2.5 by 5 to 25 by 100 in size. They are scattered throughout hornfels and are also present in quartz. Euhedral well-polished pyrite crystals are present in pre-ore quartz, jasperoid quartz, and realgar. Subhedral and euhedral pyrite cubes average 10 by 10 micrometers and range from less than 2.5 to 25 micrometers in diameter. They take a good polish but are locally fractured. Pyrite and marcasite tend to form clusters. Marcasite laths range from 3 by 20 to 90 by 170 micrometers. They form masses as large as 50 by 500 micrometers.

Sample #: TR 94-172 1730.3

This sample consists of pre-ore quartz, jasperoid quartz, and pyrite in fractured brown hornfels. Jasperoid quartz exhibits a granular texture. Subhedral and euhedral grains average 30 by 30 micrometers and range from 10 by 10 to 50 by 50 micrometers in size. Jasperoid quartz crystals are clustered. Subhedral pre-ore quartz is fractured. Crystals average 30 by 30 micrometers and range from 50 by 50 to 300 by 500

micrometers in size. Pyrite crystals are present in pre-ore quartz and are concentrated along jasperoid quartz crystal boundaries. Anhedral and subhedral cubic pyrite crystals average 10 by 10 micrometers and range from less than 2.5 to 250 micrometers. They take a good polish and are rimmed with marcasite laths. Marcasite forms on pyrite and also forms spherical masses that reach 130 micrometers across. Marcasite laths range from 2.5 by 5 to 20 by 30 micrometers in size.

Sample #: TR 94-172 1776.3

Approximately 30 % of this sample consists of realgar and calcite. The rest is hornfels that contains pyrite, marcasite, (non-jasperoid) quartz and pre-ore quartz. Pre-ore quartz composes less than 5 % of this sample. Subhedral crystals range from 10 by 50 to 250 by 500 micrometers, and average 50 by 75 micrometers. Crystals are fractured and present in masses of individual crystals. Jasperoid quartz exhibits granular texture and is present as clasts. Anhedral, subhedral, and euhedral crystals average 15 by 15 micrometers and range from 10 by 10 to 50 by 50 micrometers in size. Marcasite laths average 2.5 by 5 micrometers. They form clusters that average 15 by 15 micrometers and range from 2.5 by 2.5 to 100 by 250 micrometers. Pyrite crystals are rimmed with marcasite laths. Some marcasite clusters do not contain pyrite crystals in their cores. They are scattered throughout jasperoid quartz and are also overgrown by jasperoid quartz. Subhedral realgar forms on quartz crystals. Realgar crystals range from 10 by 10 to 400 by 400 micrometers, and average 200 by 200 micrometers in size. They are fractured and over-grown by calcite. Calcite filled open spaces between realgar crystals and also forms on jasperoid quartz. A single calcite crystal reaches to 400 by 1200 micrometers in size. Fine pyrite crystals are present in pre-ore quartz and realgar. Anhedral and subhedral pyrite crystals are average 10 by 10 micrometers and range from 7.5 by 7.5 to 30 by 50 micrometers in size.

Sample #: TR 94-172 1855.4

Calcite, pre-ore quartz, crystalline quartz, marcasite, and pyrite fill fractures in black hornfels. Subhedral and euhedral pre-ore quartz crystals average 50 by 50 micrometers and range from 25 by 25 to 75 by 75 micrometers in size. They are locally fractured. Calcite is a dominant constituent of vein fill and forms over pre-ore quartz. Subhedral crystals range from 25 by 25 to 400 by 800 micrometers and average 100 by 200 micrometers in size. A single subhedral realgar crystal is present in a calcite vein. The crystal faces of realgar were overgrown by calcite. The size of the crystal is approximately 900 by 500 micrometers. Massive pyrite crystals in veins are overgrown by pre-ore quartz and calcite. The vein is approximately 500 micrometers in width and 1500 micrometers in length. Pyrite is present in the pre-ore quartz and calcite vein. Pyrite is also present in black hornfels. Pyrite crystal shapes vary from anhedral to cubic. They average 25 by 25 micrometers and range from 2.5 by 2.5 to 200 by 200 micrometers in size. Some large pyrite cubes are aggregates of fine pyrite crystals. Open spaces between crystals create porous appearance. Pyrite crystals also form horizontal layers in black hornfels. Marcasite is present throughout black hornfels and veins. Marcasite laths average 5 by 15 micrometers and range from 2.5 by 10 to 10 by 50 micrometers. Masses of laths occur in veins. Crystal faces of marcasite were overgrown by pre-ore quartz and calcite.

Sample #: TR 94-172 1865.5

This sample consists of pre-ore quartz, jasperoid quartz, crystalline quartz, pyrite, and realgar in black hornfels gouge. Crystalline quartz was over grown by pre-ore quartz. Crystalline quartz crystals are equigranular and average 25 by 25 micrometers in size. They compose approximately 50 % of this sample. Pre-ore quartz crystals range from 50 by 100 to 400 by 700 micrometers and average 50 by 150 micrometers in size. Subhedral and anhedral crystals are fractured. Individual crystals are randomly present in this sample. Jasperoid quartz crystals range from 10 by 10 to 150 by 150 micrometers in size. They tend to form masses and exhibit a xenomorphic texture. They do not contain many calcite inclusions, which are most common near crystal rims. Jasperoid quartz, pre-ore quartz and crystalline quartz were over-grown by realgar. Realgar filled open spaces between crystalline quartz crystals that range from 25 by 30 to 200 by 4000 micrometers. Marcasite crystals are encompassed by crystalline quartz and formed on euhedral crystalline quartz. They are overgrown by realgar. Laths average 10 by 10 micrometers and range from less than 2.5 to 10 by 20 micrometers. They are concentrated along crystalline quartz crystal boundaries. Stibnite crystals are present in jasperoid quartz and realgar. The laths average 100 by 100 micrometers and range from 50 by 50 to 100 by 250 micrometers. Laths form spherical masses. Subhedral to euhedral grains formed on realgar, and grew over pre-ore quartz and crystalline quartz.

Sample #: TR 94-172 1912.4

A vein that is 15-millimeter in width is present in this sample. Calcite, pre-ore quartz, realgar, and pyrite compose the vein. Anhedra and subhedra pyrite crystals average 15 by 15 micrometers and range from 5 by 5 to 25 by 25 micrometers in size. Feathery crystals that exhibit high interference color are present between pre-ore quartz and black hornfels. Euhedra and subhedra marcasite, and spherical marcasite aggregates are present. The marcasite is porous and fractured. Marcasite laths range from 1 by 5 to 25 by 50 micrometers and average 5 by 10 micrometers. The laths form clusters. Marcasite masses are present in black hornfels and also pre-ore quartz veins. In black hornfels marcasite grows over quartz. Pre-ore quartz forms on pyrite and marcasite crystals. Pre-ore quartz ranges from 25 by 25 to 1.2 by 2.0 millimeters and averages 200 by 200 micrometers in size. Crystal shapes are varied and are xenomorphic to equigranular. Large crystals are fractured. Realgar forms on quartz. Subhedra realgar crystals range from 60 by 100 by to 300 by 1200 micrometers and average 200 by 300 micrometers in size.

Sample #: TR 94-172 1913

This sample consists of pre-ore quartz, apatite, pyrite, stibnite, and realgar in black hornfels gouge. Pre-ore quartz crystals range from 25 by 25 to 400 by 800 micrometers and average 50 by 50 in size. Subhedra and anhedra crystals are fractured. Individual pre-ore quartz crystals are randomly present in black hornfels in this sample. Realgar grows on them. Realgar filled fractures in black hornfels and pyrite. Pyrite crystals range from 2.5 by 5 to 250 by 500 micrometers. Aggregates of fine subhedra and euhedra pyrite crystals are overgrown by realgar. Stibnite laths average 2.5 by 7.5 micrometers and are present in realgar. Jasperoid quartz crystals are equidimensional and present in realgar. Crystals average 15 by 15 micrometers. They do not contain pyrite and marcasite. Pyrite and marcasite crystals are concentrated along quartz crystal boundaries.

Sample #: TR 94-172 1917.9

This section exhibits little paragenetic information because of the high clay content. Marcasite and pyrite are present in black hornfels. Pyrite crystals are fractured and strained. They range from 25 by 25 to 150 by 800 micrometers and average 30 by 30 micrometers in size. Well-polished marcasite laths average 5 by 7.5 micrometers in size. The laths form discontinuous horizontal layers in black hornfels.

Sample #: TR 94-172 1999.8

This sample consists of pre-ore quartz, (non-jasperoid) quartz, massive pyrite and clay in fractured black hornfels. Pre-ore quartz is fractured and forms masses. Subhedra and euhedra crystals average 100 by 150 micrometers and reach 800 by 1200 micrometers in size. Quartz crystals grow on euhedra pyrite. Euhedra pyrite and marcasite precipitated on pre-ore quartz. Pyrite forms subhedra and euhedra cubic crystals, which average 5 by 5 micrometers. Open spaces between pyrite crystals create a porous appearance. Marcasite laths range from 1 by 2.5 to 2.5 by 50 micrometers, and average 2.5 by 7 micrometers in size. They form masses and layers. Some grains contain bright yellow cores, which may be pyrite. Marcasite crystals are disseminated in black hornfels and are present with feathery clays.

Sample #: TR 94-172 2016.8

Strained pre-ore quartz veins are present in black hornfels that exhibits a mylonitic texture. Veins also consist of pyrite, marcasite, quartz, and jasperoid quartz. Subhedra and anhedra pre-ore quartz crystals are fractured. The crystals average 50 by 50 micrometers and range from 25 by 25 micrometers to 1 by 3 millimeters in size. Jasperoid quartz is anhedra and contains calcite inclusions. Jasperoid quartz crystals range from 20 by 25 to 75 by 100 micrometers and average 25 by 25 micrometers in size. A third type of quartz forms euhedra and subhedra quartz crystals that neither exhibit a jigsaw puzzle texture nor contain calcite inclusions. The crystals average 25 by 25 micrometers and range from 15 by 15 to 50 by 50 micrometers in size. This type of quartz contains realgar. Isolated realgar crystals are present, which are 10 by 25 micrometers. Realgar is overgrown by marcasite. Pre-ore quartz and jasperoid quartz contain euhedra marcasite crystals. Subhedra and euhedra marcasite laths average 5 by 12.5 micrometers and range from 2.5 by 7.5 to 10 by 50 micrometers. The laths form cubic masses. Marcasite laths are disseminated throughout black hornfels and form discontinuous horizontal layers. Pyrite cubes average 7.5 by 7.5 micrometers. The cubes are present between pre-ore quartz grain boundaries and occur in black hornfels.

Polished Thin Sections from a Drill Hole TR 94-172

Sample #: TR 64-172 1637.5

Brown hornfels that contains pre-ore quartz, plagioclase, calcite, biotite, pyrrhotite, and pyrite. Pre-ore stage quartz occurs as masses or individual grains throughout brown hornfels. These fractured anhedral quartz crystals range from 25 to 50 micrometers and average 250 micrometers in diameter. Pre-ore quartz forms over pyrite. Sparse pyrrhotite is anhedral and strained. Pyrite crystals vary from euhedral to anhedral, and range from 2.5 to 800 micrometers and average 15 micrometers in diameter. They contain less than 5 % void spaces. Pyrite crystals are encompassed by calcite in veins. Jasperoid quartz crystals are anhedral to subhedral. The crystals range from 10 to 100 micrometers, average 25 micrometers in diameter, and exhibit equigranular texture. Calcite precipitated on jasperoid quartz, and occurs as masses and veins. Individual calcite crystals in masses range from 2.5 to 250 micrometers and average 25 micrometers in diameter. Calcite crystals are distinctive in this sample, and compose approximately 30 % of this sample. The veins range from 100 micrometers to 3.6 millimeters in width, and calcite crystals range from 75 to 175 micrometers and average 100 micrometers in diameter. Calcite veins crosscutting each other indicate presence of multiple generations of calcite. Approximately 30 % of hornfels is covered with clay minerals.

Sample #: TR 94-172 1645.5

Marcasite, pre-ore quartz, and jasperoid quartz are the main constituents. Pre-ore quartz crystals are anhedral and average 100 micrometers and up to 600 micrometers. Subhedral to anhedral marcasite masses range from 2.5 to 30 micrometers and average 25 micrometers in diameter. The marcasite crystals take a good polish. Individual marcasite crystals form strained masses and also are disseminated throughout the brown hornfels. However, most marcasite crystals are aggregated into masses. These are similar in appearance to porous pyrite crystals. Jasperoid quartz contains marcasite crystals. Jasperoid quartz comprises approximately 25 % of this sample. Anhedral jasperoid quartz crystals range from 5 to 50 micrometers and average 15 micrometers in diameter. Jasperoid quartz crosscut pre-ore quartz. The brown hornfels exhibits a mylonitic texture in this sample.

Sample #: TR 94 – 172 1645.5

Brown hornfels is covered with clay minerals and crosscut by quartz and calcite veins. Clay minerals comprise approximately 50 % of this section. The crystals are perhaps sericite or pyrophyllite as indicated by feathery texture and high interference color. Clay Crystals that are smaller than 2 micrometers fill fractures in quartz veins. Anhedral pyrrhotite precipitated on quartz in vein. Anhedral quartz crystals in the veins range from 10 to 50 micrometers and average 15 micrometers in diameter. Calcite veins cut quartz veins. The veins reach 200 micrometers in width, and calcite crystals average 80 micrometers in size. This brown hornfels exhibits mylonitic texture.

Sample #: TR 94-172 1688.6

This section consists of quartz, potassium feldspar, plagioclase, and biotite that are perhaps relicts of brown hornfels. Approximately 70 % of original rock are pervasively altered to clay-sized minerals. Marcasite crystals occur as aggregates, which form strained masses. Marcasite masses reach 40 micrometers in length. Individual marcasite crystals are disseminated throughout the brown hornfels.

Sample #: TR 94-172 1699.2

Pyrrhotite, potassium feldspar, quartz, and plagioclase make up this sample. Clay minerals cover 10 % of brown hornfels. Pyrrhotite crystals form strained masses, which reach 8 millimeters in width. Quartz, plagioclase, and potassium feldspar also forms strained masses, which are cut by calcite veins. This sample exhibits mylonitic texture.

Sample #: TR 94-172 1788.6

Brown hornfels is crosscut by calcite, pyrite, jasperoid quartz, and realgar. Pyrite is strained and fractured. Fractures in pyrite grains are filled with realgar. Jasperoid quartz occurs as masses and exhibits equigranular texture. Calcite occurs as a vein that is 300 micrometers and cuts the bedding plane nearly perpendicularly. Realgar precipitated on jasperoid quartz and cuts calcite veins.

Sample #: TR 94-172 1811.5

Major constituents of this sample are calcite, plagioclase, potassium feldspar, jasperoid quartz, and pyrrhotite that are perhaps co-genetic with brown hornfels. Pre-ore quartz occurs in a vein that is 700 micrometers in width. Fractured subhedral to anhedral crystals range from 400 micrometers to 3.6 millimeters and average 25 micrometers in diameter. Jasperoid quartz exhibits equigranular texture and fills fractures in brown hornfels that are perpendicular to bedding planes. Jasperoid quartz crystals range from 10 to 25 micrometers in size. Calcite and pyrrhotite precipitated on jasperoid quartz crystals. Calcite comprises nearly 30 % of this sample. Subhedral to anhedral calcite crystals range from 25 to 500 micrometers and average 10 by 150 micrometers in size. Pyrrhotite crystals are locally fractured, but not porous. The grain size ranges from 2.5 micrometers to 1.6 millimeters and average 50 micrometers in diameter. Pyrrhotite crystals occur perpendicular to bedding and also are disseminated throughout the brown hornfels. Clay-minerals are also present and may be sericite as indicated by feathery texture and high interference color.

Sample #: TR 94-172 1977

Brown hornfels that contains pre-ore jasperoid quartz, pyrrhotite, calcite, and sericite. Jasperoid quartz makes up 10 % of this sample and occurs in brown hornfels and veins. Subhedral to anhedral jasperoid quartz crystals range from 5 by 5 to 75 by 75 micrometers and average 50 by 50 micrometers. They exhibit jigsaw puzzle and, locally, reticulated texture. Pyrrhotite precipitated on jasperoid quartz. This textural relationship and assay suggest that this jasperoid precipitated pre-ore stage. Pyrrhotite occurs as individual crystals and masses. Subhedral to anhedral pyrrhotite crystals range from 10 to 200 micrometers and average 50 micrometers in diameter. Masses of pyrrhotite crystals range from 50 micrometers to 3.6 millimeters and average 250 micrometers in diameter. A calcite vein, 200 micrometers in width, cuts jasperoid quartz and pyrrhotite masses and perpendicular to bedding. Subhedral to anhedral calcite crystals range from 25 to 100 micrometers, but average 50 micrometers in diameter and exhibit equigranular texture. Sericite composes 10 % of this sample. The paragenetic position of sericite is undetermined because of lack of cross-cutting relationship. Mylonitic texture is distinctive in this sample.

Doubly Polished Thick Sections

Sample #: TR 95-039 1809.5

Veins that cut black hornfels characterize this sample. Pre-ore pyrite, pre-ore quartz, and realgar are the main constituents of the vein. Pre-ore pyrite is disseminated throughout black hornfels and is also present in pre-ore quartz veins. Pyrite crystals in black hornfels take a good polish and contain few or no solid inclusions. The crystal size ranges from 1.5 to 30 micrometers and average 3.5 micrometers in diameter. Pyrite makes up 60 % of veins. Pyrite crystals in the veins vary from euhedral to anhedral, are fractured, and take a poor polish. They range from 65 micrometers to 1.8 millimeters, and average 1.2 millimeters in diameter. Pre-ore quartz contains subhedral pyrite crystals. This quartz occurs in veins and makes up 30 to 35 % of veins. Subhedral to anhedral quartz crystals range from 10 to 600 micrometers and average 180 micrometers in diameter. Realgar precipitated on quartz and also contains subhedral pyrite. Subhedral to anhedral realgar is fractured. Realgar crystals range from 10 to 75 and average 40 micrometers in diameter.

Sample #: TR 95-039 1958

A pre-ore quartz vein cuts black hornfels. The vein is 400 micrometers in width and consists of pre-ore quartz, pre-ore pyrite, and jasperoid quartz. Subhedral to anhedral pre-ore quartz crystals range from 25 to 1 millimeter and average 50 micrometers in diameter. Euhedral to subhedral pyrite crystals in the vein range from 2.2 to 200 micrometers and average 25 micrometers in diameter. They are fractured but take a good polish. Jasperoid quartz comprises 30 % of this sample and precipitated on pyrite. Anhedral jasperoid quartz ranges from 10 to 125 micrometers and averages 25 micrometers in diameter. The crystals are equigranular and locally have reticulated texture.

Sample #: TR 95-046 1634

A pre-ore quartz vein that comprises approximately 25 % of the area of this section cuts black hornfels. Pre-ore quartz and pyrite are major components of this sample. Pyrite crystals are preferentially present in

the pre-ore quartz vein and also disseminated throughout black hornfels. Euhedral to subhedral pyrite crystals range from 15 to 300 micrometers and average 25 micrometers in diameter. Pre-ore quartz precipitated on pyrite and occurs as vein and masses. The subhedral to anhedral crystals are fractured. Pre-ore quartz crystal size varies from 25 to 3.6 millimeters in diameter.

Sample #: TR 95-072 1892.7

This sample consists of marcasite, pyrite, pre-ore quartz, jasperoid quartz, and realgar. Anhedral pyrite crystal size ranges from 10 by 10 to 200 by 600 micrometers and averages 50 by 50 micrometers. Pyrite crystals are encompassed by pre-ore quartz and jasperoid quartz. Pre-ore quartz crystals range from 10 by 10 to 600 by 600 micrometers and average 25 by 25 micrometers in size. Subhedral to anhedral pre-ore quartz crystals are fractured and occur as masses. Jasperoid quartz is present in a vein that is 200 micrometers in width. Anhedral jasperoid quartz crystals range from 10 by 10 to 50 by 50 micrometers and range 25 by 25 micrometers in size. Jasperoid quartz contains marcasite. Subhedral marcasite crystals exhibit porous textures and form aggregates in jasperoid quartz masses. Marcasite crystals range from 2.5 by 2.5 to 5 by 25 micrometers and average 2.5 by 20 micrometers in size. Realgar forms over jasperoid quartz. Realgar does not exhibit distinctive crystal shape but fills open spaces. Open space is as large as 3 by 3.6 square millimeters. 10 % of this sample is realgar.

Sample #: TR 95-076 1483.5

Pyrite, marcasite, jasperoid quartz, pre-ore quartz, and realgar are present in black hornfels. Pyrite crystals range from 2.5 by 2.5 to 7.5 by 12.5 micrometers and average 5 by 5 micrometers in size. Cores of pyrite take a good polish, but rims are porous. Marcasite crystals form aggregates. The size of individual marcasite crystals ranges from 2.5 by 10 to 10 by 50 and averages 10 by 25 micrometers. Aggregates average 10 by 10 micrometers but can reach 360 by 600 micrometers in size. Jasperoid quartz forms over marcasite crystals. Jasperoid quartz exhibits reticulated texture. Subhedral to anhedral quartz crystals range from 10 by 10 to 25 by 150 micrometers and average 25 by 25 micrometers in size. Jasperoid quartz most commonly occurs in a vein that is 200 micrometers in width. Pre-ore quartz is also present in this sample. Subhedral to anhedral pre-ore quartz crystals are fractured. Crystal size ranges from 10 by 10 to 300 by 300 micrometers and average 200 by 200 micrometers. Realgar forms over jasperoid quartz and pre-ore quartz. Subhedral to euhedral realgar crystals range from 0.2 by 0.4 to 0.8 by 5 micrometers. Realgar fills in veins and fractures.

Sample #: TR 95-095 1760.5

Marcasite and pre-ore quartz are the most distinctive minerals in this black hornfels. Pre-ore quartz forms a vein that is 7 millimeters in width. Pre-ore quartz varies in shape from euhedral to anhedral. Quartz crystal size ranges from 10 by 10 to 800 by 800 micrometers and average 50 by 50 micrometers. Euhedral to subhedral marcasite crystals range from 2.5 by 2.5 to 125 by 125 micrometers and average 10 by 10 micrometers in size.

Sample #: TR 95-095 1786.7

Pyrite, pre-ore quartz, jasperoid quartz, and realgar are present in black hornfels. At least two types of pyrite are present in this sample. The first type of pyrite is fractured but takes a good polish. These anhedral to subhedral pyrite crystals range from 2.5 to 50 micrometers and average 2.5 micrometers in diameter. The pyrite crystals are encompassed by pre-ore quartz. Pre-ore quartz occurs as masses and a vein that is 400 micrometers in width. Subhedral to anhedral quartz crystals are fractured. Their size ranges from 15 to 400 micrometers and averages 100 micrometers in diameter. The second type of pyrite exhibits a porous texture. The core of the pyrite takes a good polish, but the rims are porous and contain solid inclusions, which are too small to be identified. The subhedral to anhedral grains range from 2.5 to 12.5 micrometers and average 5 micrometers in diameter. Jasperoid quartz forms over pyrite. Jasperoid occurs as a vein and also is randomly present throughout black hornfels. Jasperoid quartz exhibits an equigranular texture, and subhedral to anhedral quartz crystals range from 5 to 50 micrometers and average 15 in diameter. Realgar precipitated on pre-ore quartz and comprises 20 % of this sample. It does not exhibit a distinctive crystal but filled open spaces.

Sample #: TR 95-122 1617.5-1

Pre-ore quartz, jasperoid quartz, pyrite, and realgar compose this sample. Pre-ore quartz comprises approximately 50 %, and jasperoid quartz comprises 10 % of the section. 25 % of this section contains realgar. Pre-ore quartz occurs as masses that reach 15 millimeters in diameter. Individual crystals range from 40 to 3.6 millimeters in diameter. Subhedral to anhedral pyrite crystals range from 2.5 to 100 micrometers and average 10 micrometers in diameter. Cores of pyrite crystals take a good polish, but rims are porous. Pyrite crystals that do not have distinctive cores are also present. These crystals are present within jasperoid quartz crystals and also along jasperoid quartz and pre-ore quartz crystal boundaries. Jasperoid quartz crystals vary from euhedral to subhedral, and range from 5 to 100 micrometers and average 50 micrometers in diameter. They exhibit jigsaw puzzle and locally reticulated textures. Realgar precipitated on pre-ore quartz and ore-stage jasperoid quartz. Realgar does not form distinctive crystals but filled open spaces as large as 7.5 millimeters in diameter.

Sample #: TR 95-122 1617.5-2

Refer to sample # TR 95-122 1617.5-1. Thin section of TR 95-122 1617.5-1 and -2 were made from the same billet.

Sample #: TR 95-122 1617.5-3

This sample consists dominantly of realgar, pre-ore quartz, jasperoid quartz, and pyrite. Realgar makes up 30 % of this section, while pre-ore quartz composes 20 to 25 %. Pre-ore quartz occurs as masses. Individual quartz crystals are fractured and range from 20 to 800 micrometers in diameter. Subhedral to anhedral pyrite crystals range from 2.5 to 10 micrometers and average 5 micrometers in diameter. Some pyrite crystals contain cores that take a good polish, but the rims are porous. These pyrite crystals are dominantly disseminated within jasperoid quartz crystals and along fractures in jasperoid quartz. Pyrite grains are also present along jasperoid quartz and pre-ore quartz crystal boundaries. Jasperoid quartz crystals vary from euhedral to subhedral, and range from 5 to 50 micrometers and average 12.5 micrometers in diameter. The crystals exhibit jigsaw puzzle and, locally, reticulated textures. Realgar precipitated on pre-ore quartz and jasperoid quartz. Realgar does not exhibit a distinctive crystal shape, but filled open spaces as large as 5 millimeters in diameter.

Sample #: TR 95-122 1619.5-1

Realgar, pre-ore quartz, jasperoid quartz, and pyrite compose this sample. Pre-ore quartz occurs as masses that are as large as 10 by 15 millimeters in size. Individual crystals are fractured and range from 10 to 600 micrometers and average 50 micrometers in diameter. Pyrite crystals are spherical and locally fractured. Pyrite cores take a good polish, but rims are porous and contain abundant solid inclusions, which are too small to be identified. Crystals range from 2.5 to 50 micrometers and average 10 micrometers in diameter. Pyrite Crystals are most commonly present between jasperoid quartz Crystal boundaries, but a few are present between pre-ore quartz boundaries. Subhedral to anhedral jasperoid quartz Crystals range from 10 to 450 micrometers and average 50 micrometers in diameter. Jasperoid quartz Crystals exhibit reticulated texture. Pre-ore quartz and jasperoid quartz are encompassed by realgar that does not form distinctive crystals but fills open spaces as large as 7 millimeters. Realgar composes approximately 25 % of this sample. Clay minerals exhibit a radial feathery texture and contain ore-stage pyrite crystals. Crystal size ranges from 5 to 200 micrometers and averages 75 micrometers in diameter.

Sample #: TR 95-122 1619.5-2

This sample consists of adularia, jasperoid quartz, realgar, and pyrite. Subhedral to anhedral pyrite crystals range from 1 to 25 micrometers in diameter and have a porous, spherical appearance. Cores of pyrite crystals are smooth, but rims are porous and contain solid inclusions. These pyrite crystals are present in rims of jasperoid quartz and adularia. Jasperoid quartz exhibits jigsaw puzzle and, locally, reticulated textures. The size of jasperoid quartz crystals ranges from 10 to 100 micrometers and averages 50 micrometers in diameter. Adularia ranges from 10 to 320 micrometers and averages 50 micrometers in diameter. Realgar precipitated on jasperoid quartz crystals, which range from 50 micrometers to 3.6 millimeters and averages 1.2 millimeters in diameter.

APPENDIX V

SUMMARY OF FLUID INCLUSION PETROGRAPHY

APPENDIX V

Sample #: TR 94-172 1655

Fluid inclusions are present in realgar. Realgar contains very rare fluid inclusions. Because most inclusions in realgar are less than 2.5 micrometers in diameter, phase cannot be distinguished. Several inclusions are 5 to 10 micrometers in diameter. Liquid dominant dark inclusion contains vapor and liquid phase. Two-phase and vacant-looking Inclusions with are present on the same plane indicating their secondary origins.

Sample #: TR 94-172 1660.5

Jasperoid quartz, fluorite, and realgar are almost fluid inclusion-free, or inclusions are too small to be identified. Orpiment contains very small inclusions, which are generally smaller than 2 micrometers. Fluid inclusions in orpiment are present along planes indicating their secondary origins. Calcite contains sparse that are generally less than 2 micrometers in diameter. They are dominantly either unknown or secondary in their origins. Empty looking inclusions and vapor and inclusions containing liquid phase on a plane are identified as secondary in their origins. A few inclusions that are larger than 5 micrometers in diameter are present. They contain approximately 10 vol. % vapor.

Sample #: TR 94-172 1661.5

Jasperoid quartz is free of inclusions or contains dominantly inclusions that are less than 2.5 micrometers in diameter. Rare inclusions are larger than 3 micrometers containing liquid phase with approximately 5 vol. % vapor bubble. Empty looking inclusions are also present. Calcite and realgar contain sparse inclusions, which are less than 2.5 micrometers in diameter. They are vacant or too small to distinguish phase. Barite contains inclusions that are average 2.5 micrometers in diameter. They are liquid dominant, and their origins are unknown. However, fluid inclusions exhibiting inconsistent phase ratios are present on a same plane indicating secondary origin.

Rare inclusions are larger than 3 micrometers. Inclusion that is larger than 7.5 micrometers is present. It contains liquid phase with an approximately 5 vol. % of vapor bubble. Inclusions in pre-ore quartz are abundant. They are generally larger than 5 micrometers in diameter containing vapor and liquid phase. A few three-phase inclusions that contain solid, vapor, and liquid are present.

Sample #: TR 94-172 1676

Quartz that has an appearance of pre-ore quartz contains small inclusions. They are usually less than 2.5 micrometers in diameter. Crystalline quartz is almost free of fluid inclusion. Fluid inclusions in calcite are abundant and generally less than 2.5 micrometers in diameter. A few inclusions are larger than 10 micrometers, which contains liquid phase with 5 vol. % of vapor bubble. Primary inclusions along growth zones are identified as primary in their origins. Secondary inclusions are present along a plane. Fluid inclusions in realgar are sparse or too small to be identified as fluid inclusions.

Sample #: TR 94-172 1686

Pre-ore quartz contains abundant inclusions that are 2.5 to 5 micrometers in diameter. Origins of inclusions are mostly unknown or secondary. Inclusions are dominantly two-phase that contains liquid phase with 5 vol. % of vapor bubble. Jasperoid quartz and realgar contain rare inclusions. They are generally less than 2.5 micrometers in diameter, and either liquid dominant or empty looking.

Sample #: TR 94-172 1730.3

Jasperoid quartz is almost fluid inclusion free or too small to be identified as fluid inclusions. Fluid inclusions in pre-ore quartz are abundant, and they are generally less than 2.5 micrometers in diameter. Liquid-rich and empty looking inclusions are also present on a same plane indicating their secondary origin.

Sample #: TR 94-172 1760.3

Fluid inclusions in pre-ore quartz are abundant. They are generally 2.5 micrometers in diameter. Inclusions that are larger than 5 micrometers in diameter with unknown origin are present. They consist of liquid phase with 10 vol. % vapor bubble. Fluid inclusions in jasperoid quartz and calcite are rare. They are generally less than 2.5 micrometers in diameter. Realgar contains inclusions that are less than 2.5

micrometers in diameter. They are too dark or too small to identify phases, and their origins cannot be identified.

Sample #: TR 94-172 1855.4

Pre-ore quartz contains sparse inclusions. They are less than 2.5 micrometers in diameter. Calcite is almost fluid inclusion free.

Sample #: TR 94-172 1865.5

Pre-ore quartz contains abundant inclusions. Secondary inclusions are present along planes. They range from 2.5 to 10 micrometers and average 5 micrometers in diameter, and are liquid dominant or liquid phase with 5 to 15 vol. % vapor bubble. Fluid inclusions that are less than 2.5 micrometers in diameter are randomly present in pre-ore quartz. Their origins are unknown. Crystalline quartz is almost free of fluid inclusion. Jasperoid quartz contains inclusions, which are less than 2.5 micrometers in diameter. Realgar contains sparse inclusions, which are less than 2.5 micrometers. They are too dark or too small to identify phases, and their origins cannot be identified.

Sample #: TR 94-172 1912.4

Pre-ore quartz contains abundant inclusions. Primary inclusions along growth zone in pre-ore quartz are present. They are average 5 micrometers and up to 10 micrometers in diameter. Secondary inclusions are present along planes. They are 2.5 to 10 micrometers and average 5 micrometers in diameter. Secondary inclusions in pre-ore quartz are empty looking or liquid dominant with 5 vol. % vapor bubble. Fluid inclusions that are less than 2.5 micrometers are also randomly present in pre-ore quartz. Realgar contains sparse inclusions. Because of their size that are less than 2.5 micrometers, phase cannot be identified.

Sample #: TR 94-172 1913

Pre-ore quartz contains abundant inclusions that average 2.5 micrometers in diameter. Most inclusions are present along planes that are identified as secondary in their origins. They contain liquid or liquid with 5 vol. % vapor bubble. Jasperoid quartz is free of inclusions, or they are too small to be identified. Realgar contains sparse inclusions. Empty-looking inclusions are most dominant and average 2.5 micrometers in diameter. However, inclusions that are larger than 10 micrometers in diameter are also identified. Their origins are either secondary or unknown.

Sample #: TR 94-172 1999.8

Pre-ore quartz contains abundant inclusions that average 5 micrometers in diameter. They contain liquid phase with approximately 10 vol. % vapor bubble. Empty looking inclusions are also present. Secondary inclusions are identified by their presence along planes and inconsistent phase ratios. Some inclusions reach 20 micrometers in diameter.

Sample #: TR 94-172 2016.8

Pre-ore quartz contains abundant inclusions. They average 5 micrometers in diameter. Some inclusions reach 7.5 to 10 micrometers in diameter. Most inclusions contain liquid phase with 5 vol. % vapor bubble. However, empty looking inclusions are also present. Secondary inclusions are identified as their presence along planes. Jasperoid quartz contains sparse inclusions. They are generally less than 2.5 micrometers in diameter. Crystalline quartz grains are free of fluid inclusion.

APPENDIX VI

MICROTHERMOMETRIC DATA OF FLUID INCLUSIONS

IN PRE-ORE STAGE QUARTZ AND

ORE-STAGE JASPEROID

QUARTZ

APPENDIX VI Microthermometric Data of Fluid Inclusions in Pre-Ore Stage Quartz								
Chip #	F.I. #	F.I. Origin	Tm	CO ₂ Th	CO ₂ Tmc	Salinity	Th	Pyrite
			(°C)	(°C)	(°C)	(wt. % NaCl)	(°C)	
95-95 1760.5 IQ-1a	1	p	-4.3			6.881027399	170	no
	2	p	-3.9			6.302758683	153	
	3	p	-3.9			6.302758683	156	
95-95 1760.5 IQ-1b	1	s	-3.8			6.156315704	158	no
	2	s	-4.3			6.881027399	166	
	3	s	-3.5			5.712431375	185	
	4	s	-3.6			5.861155392	190	
	5	s						
	6	s	-3.4			5.562940328	152	
	7	s					160	
	8	s						
	9	s						
95-95 1760.5 IQ-1c	1	p	-3			4.957239	157	no
	2	p	-2.8			4.649699264	126	
	3	p	-2.8			4.649699264	171	
	4	p	-5.3			8.275346489		
	5	p	-2.9			4.803862673		
94-172 1912.4 IQ-1	1	u (P?)					0	no
	2	u	-0.7			1.224533051		
	3	u					255	
	4	u (P?)	-3.7			6.009115721		
	5	u (P?)	-5.9			9.077794103		
	6	u (P?)	-4.8			7.587231744	259	
	7	u (P?)						
	8	u (P?)	-5.7			8.813094501		
	9	u (P?)	-1.5			2.572429875		
	10	u (P?)	-6.4			9.727582208	325	
	11	u (P?)	-5.1			8.002244607		
	12	u (P?)	-4.6			7.306944152		
	13	u (P?)	-5.1			8.002244607		
	14	u (P?)	-5.2			8.139150656		
	15	u (P?)	-5.2			8.139150656		
	16	u (P?)	-5.9			9.077794103		
	17	u (P?)	-7.8			11.45919746		
	18	u						
	19	u	-9.8			13.72327594		
	20	u	-3.8			6.156315704		
	21	u (P?)						
	22	u	-5.8			8.945789384	208	
	23	u	-15.8			19.28689378		
94-172 1912.4 IQ-2	1	u						no
	2	u	-5.3			8.275346489		
	3	u (P?)	-14.8			18.46811014		

Chip #	F.I. #	F.I. Origin	Tm (°C)	CO2 Th (°C)	CO2 Tmc (°C)	Salinity (wt. % NaCl)	Th (°C)	Pyrite
94-172 1912.4 IQ-2	4	u (P?)	-8.4			12.16338413		
	5	u	-4.3			6.881027399		
	6	u (P?)	-7.3			10.85526447	247	
	7	u (P?)	-4.6			7.306944152		
	8	u	-7.4			10.97731777		
	9	u	-4.4			7.023735488	224	
	10	u	-2.6			4.338997832		
	11	u	-5.9			9.077794103		
	12	u	-5.7			8.813094501		
	13	u	-7.2			10.73257114	292	
	14	u	-5.4			8.410835448		
	15	u	-4.8			7.587231744	294	
	16	u	-5.4			8.410835448	289	
	17	u	-4.8			7.587231744	264	
	18	u						
	19	u	-6.9			10.36061751		
	20	u	-4.2			6.737579016	272	
	21	u	-6.2			9.469700696		
	22	u	-4.8			7.587231744		
	23	u	-5.3			8.275346489		
	24	u	-3.7			6.009115721		
94-172 1912.4 IQ-3	1	s	-4.8			7.587231744	241	no
	2	s	-4.2			6.737579016	207	
	3	s	-4			6.448448	212	
	4	s	-3.8			6.156315704	243	
	5	s	-4.9			7.726288493	236	
	6	s	-4.6			7.306944152	208	
94-172 1912.4 IQ-3	7	s	-4.2			6.737579016	224	no
	8	s	-4.4			7.023735488		
	9	s	-4.8			7.587231744	226	
	10	s	-4			6.448448	205	
	11	s	-6.1			9.339746417	180	
	12	s	-4.2			6.737579016	188	
	13	s	-3.8			6.156315704	181	
	14	s	-6.3			9.598978179	185	
	15	s	-4.5			7.165706625		
94-172 1865.5 IQ1a	1	s					135	no
	2	s						
	3	s	-18.5			21.32926513	213	
	4	s						
	5	s	-9.7			13.61558086	211	
	6	s						
	7	s					208	
	8	s					172	

Chip #	F.I. #	F.I. Origin	Tm (°C)	CO2 Th (°C)	CO2 Tmc (°C)	Salinity (wt. % NaCl)	Th (°C)	Pyrite
94-172 1865.5 IQ1a	9 s		-18.1			21.04050374	194	
	10 s							
	11 s						182	
	12 s						179.4	
	13 s							
	14 s		-19.4			21.96375889		
	15 s		-15.9			19.3667592	154	
	16 s		-18.1			21.04050374		
	17 s		-15.9			19.3667592	151	
	18 s		-15.6			19.12609171	147	
	19 s						154	
94-172 1865.5 IQ1b	1 p?		-19.4			21.96375889		no
	2 p?							
	3 p?							
	4 p?		-20.5			22.71357463		
	5 u (p?)							
	6 u (p?)							
	7 u (p?)							
	8 u (p?)		-16.7			19.99326889		
	9 u							
	10 u		-8			11.696384		
	11 u		-11.1			15.07388847		
	12 u							
	13 u							
	14 u (p?)		-14.3			18.0443253		
	15 u		-0.5			0.879019625		
	16 u		-0.7			1.224533051		no
	17 u							
	18 u		-23			24.335219		
	19 u							
	20 u							
94-172 1865.5 IQ2a	1 u (p?)		-18			20.967624	141	no
	2 u (p?)		-10.6			14.56508391	159	
	3 u (p?)		-19.4			21.96375889	159.3	
	4 u (p?)		-19.2			21.82449562	211	
	5 u (p?)		-18.4			21.25748173	191	
	6 u (p?)		-19.9			22.30785164	208	
	7 u		-19.9			22.30785164	222	
	8 u		-17.4			20.52429737	194	
	9 u		-19.7			22.17089476	147	
	10 u (p?)							
94-172 1865.5 IQ2b	1 u					3		no
	2 u (p?)		-15.1			18.71768171		
	3 u (p?)		-15.3			18.88216039		

Chip #	F.I. #	F.I. Origin	Tm (°C)	CO2 Th (°C)	CO2 Tmc (°C)	Salinity (wt. % NaCl)	Th (°C)	Pyrite
94-172 1865.5 IQ2b	4	u (p?)	-9.9			13.83041454		
	5	u	-7			10.485251		
	6	u	-13.2			17.07567418		
	7	u	-12.9			16.80238377		
	8	u	-6.1			9.339746417		
	9	u (p?)	-14.7			18.38414531		
	10	u (p?)	-8			11.696384		
94-172 1913 IQ-2'	1							no
	2	s	-11.2			15.1740969	280	
	3							
	4							
	5							
	6	s					285	
	7	s	-9.5			13.39850788		
	8							
	9	s	-9			12.845853	288	
	10							
	11							
	12	s	-9			12.845853	239	
	13	s						
	14							
	15							
	16	s	-11.6			15.56986707	264	
	17	s	-11.6			15.56986707	262	
	18							
	19							
	20							
	21							
	22	s	-4.3			6.881027399	261	
	23	s					280	
95-122 1619.5 IQ-1	1	s	-1.5			2.572429875	264	boudary
	2	s	-0.7			1.224533051	234	
	3	s	-7			10.485251		
	4	s	-8.3			12.04754736		
	5	s	-8.3			12.04754736		
	6	s	-8.2			11.93110398		
	7	s	-8.4			12.16338413		
	8	s	-8.5			12.27861763	142	
	9	s	-8.6			12.39325119		
	10	s						
	11	s	-4.8			7.587231744	176	
	12	s	-7.8			11.45919746	193	
	13	s	-7.6			11.21951763		
	14	u					>290	
	15	u	-2.3			3.866959019	>290	

Chip #	F.I. #	F.I. Origin	Tm (°C)	CO2 Th (°C)	CO2 Tmc (°C)	Salinity (wt. % NaCl)	Th (°C)	Pyrite
95-122 1619.5 IQ-1	16	u					>290	
	17	u					>290	
	18	s	-6.5			9.855516125		
	19	u	-7.3			10.85526447		
	20	u	-13.3			17.16588081	284	
	21	s						
	22	s					>290	
	23	s	-13.9			17.69800778	264	
	24	s	-6.4			9.727582208		
	25	s	-13.7			17.52234562	204	
95-122 1619.5 IQ-1	26	s	-13.6			17.43387699	217	
	27	s	-0.8			1.395997184	240	
	28	u	-6.5			9.855516125	262	
	29	u	-7.3			10.85526447	206.8	
	30	s?	-9.2			13.06864122	>290	
	31	s?	-7.2			10.73257114	>290	
95-122 1619.5 IQ-2	1	u	-0.5			0.879019625	147	qtz rim
	2	u	-24			24.960768	210	
	3	u	-17.6			20.67324723	208	

APPENDIX VI Microthermometric Data of Fluid Inclusions in Ore-Stage Jasperoid Quartz									
Chip #	F.I. #	F.I. Origin	Tm (°C)	CO ₂ Th (°C)	CO ₂ Tmc (°C)	Salinity (wt. % NaCl)	Th (°C)	Pyrite	
95-122 1619.5 JQ3a	1	u	-2			3.387656	>220	qtz rim	
	2	u	-3.3			5.412678909	>220		
95-122 1619.5 JQ3b	1	s						no	
	2	s	-3.8			6.156315704	165		
	3	s							
	4	s	-5.2			8.139150656	182		
	5	s	-5.3			8.275346489	187		
	6	s	-4.5			7.165706625	185		
95-122 1619.5 JQ4	1	s	-3.2			5.261643776	270	boundary	
	2	s	-3.8			6.156315704	200		
	3	s					239		
	4	s	-5.2			8.139150656			
	5	s	-4.7			7.447451411	133		
	6	s					180		
	7	s	-6.3			9.598978179	196		
	8	u	-5.1			8.002244607	185		
	9	u	-2.7			4.494745431			
	10	s	-3.2			5.261643776	174		
	11	s	-5.6			8.679706112	163		
	12	s	-5.7			8.813094501			
	13	s	-6			9.209112	200		
	14	u	-6.3			9.598978179	201		
	15	u	-4.6			7.306944152	210		
	16	u	-5.4			8.410835448	200		
	17	u	-5.1			8.002244607	190		
	18	s	-5.3			8.275346489			
	19	u	-1.6			2.737129472	120		
	20	u	-5.8			8.945789384	205		
	21	s	-5.9			9.077794103	205		
95-122 1617.5-2 JQ1	1	s					0	142 within xtal	
	2	s	-12.7			16.61793133			
	3	s	-11.2			15.1740969			
	4	s	-14.3			18.0443253			
	5	s	-6.6			9.982783272	281		
	6	s	-18.7			21.47203807	183		
	7	s					276		
	8	s					270		
	9	s	-6.6			9.982783272			
	10	s					>286		
	11	s							
	12	s	-8.2			11.93110398	>286		
	13	s	-6.6			9.982783272	230		
	14	s	-4.3			6.881027399	255		
	15	s	-7.2			10.73257114	198		
	16	s	-5.9			9.077794103	238		
	17	s					260		

Chip #	F.I. #	F.I. Origin	Tm (°C)	CO ₂ Th (°C)	CO ₂ Tmc (°C)	Salinity (wt. % NaCl)	Th (°C)	Pyrite
	18	s	-6.7			10.10938699		
	19	s	-11.9			15.86147156	201	
	20	s						
	21	s	-6.8			10.23533062		
	22	s	-5.4			8.410835448		
	23	s	-11.4			15.37298801		
	24	s	-5.1			8.002244607		
95-122 1617.5-2 JQ2	1	u (p?)	-6.1			9.339746417	170	rim
	2	u (p?)						
	3	u (p?)	-5			7.864625		
	4	u (p?)					230	
	5	u (p?)	-3.9			6.302758683	205	
	6	s	-6.4			9.727582208	98	
	7	u (p?)	-10.7				198	
	8	u (p?)			7.8		>233	
	9	u (p?)						
	10	s					199	
	11	u (p?)	-6.4				197	
	12	u (p?)	-6.5			9.855516125		
	13	u (p?)			2.4			
	14	u (p?)	-11.8			15.76476082		
	15	u (p?)					192	
	16	u (p?)	-11.8			15.76476082		
	17	s					<50?	
	18	u (p?)					202	
	19	u (p?)					198	
	20	u (p?)	-5.6					
	21	u (p?)	-5.4			8.410835448	<50?	
	22	u (p?)	-11.4			15.37298801	48	
	23	u (p?)					112	
	24	u (p?)					173	
95-122 1617.5-2 JQ4	1	s	-6.2			9.469700696	156	
	2	s						
	3	s	-5.9			9.077794103	111	
	4	s	-7.3			10.85526447	122	
	5	u					108	
	6	u	-5.9			9.077794103	165	
	7	u					166	
95-122 1617.5 JQ-1	1	p	-10.7			14.66789095	155	within
	2	p	-13			16.893929	143	
	3	p	-9.5			13.39850788	84	
	4	p	-13.5			17.34497888	162	
	5	p	-13.5			17.34497888	157	
	6	p	-12.7			16.61793133	160	
	7	p	-11.9			15.86147156	131	
	8	u	-11.9			15.86147156	187	
	9	p	-16			19.446272	221	

Chip #	F.I. #	F.I. Origin	Tm (°C)	CO ₂ Th (°C)	CO ₂ Tmc (°C)	Salinity (wt. % NaCl)	Th (°C)	Pyrite
	10	p	-12.7			16.61793133		
	11	p	-9.9			13.83041454	176	
	12	p	-8.8			12.6207319	193	
95-122 1617.5 JQ-3	1	u	-12.3			16.24348492	152	no
	2	u	-15.8			19.28689378	226	
	3	u	-14.8			18.46811014	192	
	4	u	-7.6			11.21951763	140	
	5	u	-15.8			19.28689378	248	
95-122 1617.5 JQ-6	1	u	-23.5			24.64922638	304	no
	2	u	-9.6			13.50732595	298	
	3	u	-24.7				255	
	4	u	-23.2			24.46114458	282	
	5	u	-23.4			24.58663553	135	
	6	u	-9.3				330	
	7	u	-14.6			18.29978775	80	
	8	u	-9.6			13.50732595	306	
	9	u	-25.1			25.63953881	277	
	10	u	-24.3			25.1466832	129	
	11	u	-24.1			25.0228172	179	
	12	u	-23.4			24.58663553	197	
	13	u	-19.9			22.30785164	266	
	14	u	-5.4			8.410835448		
	15	u	-14.8			18.46811014	123	
	16	u	-23.6			24.71171859	226	
	17	u	-9.1			12.95753705	229	
94-172 1913 JQ-1	1	s						no
	2	s	-5.1			8.002244607	186	
	3	s						
	4	s	-6.3			9.598978179	182	
	5	s						
	6	s						
	7	s						
	8	s	-6.5			9.855516125	210	
	9	s					240	
	10	s	-3.4			5.562940328		
	11	s	-3.2			5.261643776		
	12	s	-9.4			13.28912329	118	
	13	s					164	
	14	s					182	
	15	s						
	16	s						
	17	s	-3.8			6.156315704		
	18	s					128	
	19	s						
	20	s	-1.8			3.064040424	233	
	21	s					167	
	22	s						

Chip #	F.I. #	F.I. Origin	Tm (°C)	CO ₂ Th (°C)	CO ₂ Tmc (°C)	Salinity (wt. % NaCl)	Th (°C)	Pyrite
	23	s					128	
	24	s						
	25	s						
	26	s	-3			4.957239		
	27	s					219	
94-172 1913 JQ-2	1	s					173	no
	2	s	-17.5			20.59892188	131	
	3	s	-16.7			19.99326889	186	
	4	s	-19.4			21.96375889		
	5	s						
	6	s						
	7	s	-15.6			19.12609171		
	8	s	-26.1			26.25174462		
	9	s					170	
94-172 1913 JQ-4	1	s	-3.2			5.261643776	192	no
	2	s	-2.9			4.803862673	145	
	3	s	-13.9			17.69800778		
	4	s	-1.5			2.572429875	217	
	5	s	-18.8			21.5430343		
	6	s	-21.7			23.50426234		
	7	s	-11.3			15.27379563	214	
94-172 1913 JQ-6	1	p	-4.3			6.881027399		no
	2	p	-4.4			7.023735488		
	3	p	-5			7.864625		
	4	u	-5.3			8.275346489		
	5	p	-6.1			9.339746417	149	
	6	s	-6.8			10.23533062	168	
	7	s	-6.4			9.727582208	189	
	8	s					163	
	9	s	-5			7.864625	168	
	10	s	-4.9			7.726288493	172	
	11	s	-5.6			8.679706112	179	
	12	s					160	
	13	s	-5.1			8.002244607		
	14	s	-5			7.864625		
	15	s	-5.5			8.545620875	137	
	16	s					188	
	17	s						
	18	s						
	19	s						
	20	s						
	21	s					166	
	22	s	-5			7.864625		
	23	s	-5.8			8.945789384	84	
	24	s	-4.8			7.587231744	139	

Chip #	F.I. #	F.I. Origin	Tm (°C)	CO ₂ Th (°C)	CO ₂ Tmc (°C)	Salinity (wt. % NaCl)	Th (°C)	Pyrite
94-172 1913 JQ-6	1	u	-18.4			21.25748173	208	no
	2	u	-9.2			13.06864122	259	
	3	u	-9			12.845853		
	4	u	-17.4			20.52429737	175	
	5	u	-8.5			12.27861763	239	
	6	u	-21.9			23.63366466	200	
	7	u	-17.4			20.52429737	173	
	8	u	-22.2				235	
	9	u	-18.9			21.61377483	207	
	10	u	-19.8			22.23948434	172	
	11	u	-16.3			19.68272808	168	
	12	u	-17.2				139	

REFERENCES CITED

- Archart, G. B., 1996, Characteristics and origins of sediment-hosted disseminated gold deposits: a review: *Ore Geology Reviews*, v. 11, p. 383-403.
- Atkin S., 1989, The geology of the north pit, Chimney Creek mine, *in* Buffa, R., Klessig, P., and Schafer, R. eds., *Geology and Gold Deposits of the Osgood Mountains, Nevada*, Geological Society of Nevada, 1989 Fall Field Trip Guidebook, Special Publication no. 10, 13 p.
- Berentsen E. J., Nanna, R. F., Baumann, M. C., and Gingrich, M. K., 1999, The geology and ore control at the Getchell and Turquoise Ridge mines, Humboldt County, Nevada: Geological Society of Nevada, January Letter, 2 p.
- Berentsen, E. J., Nanna, R. F., Hazlitt, J. S., and Estes, L. D., 1996, Discovery and geology of the Turquoise Ridge gold deposit: *Mining Engineering*, v. 48, no. 10, p. 31-35.
- Bloomstein, E. I., Massingill, G. L., Paratt, R. L., and Peltonen, D. R., 1991, Discovery, geology, and mineralization of the Rabbit Creek gold deposit, Humboldt County, Nevada, *in* Raines, G. L., Lisle, R. E., Schafer, R. W., and Wilkinson, W. H. eds. *Geology and Ore Deposits in the Great Basin*: Geological Society of Nevada and U. S. Geological Survey, Reno, v. 2, p. 821-843.
- Bodnar R. J., and Vityk, M. O., 1994, Interpretation of microthermometric data for H₂O-NaCl fluid inclusions *in* De Vivo, B., and Frezzotti, M.L., eds., *Fluid Inclusions in Minerals: Methods and Applications*, Short Course of the Working Group Inclusions in Minerals, Pontignano-Siena, Italy, p. 117-130.
- Burchfiel, B. C., Cowan, D. S., and Davis, G. A., 1992, Tectonic overview of the Cordilleran orogen in the western United States *in* Burchfiel, B.C., Lipman, P. W., and Zoback, M. L. ed., *the Cordilleran Orogen: Conterminous U.S.: the Geological Society of America*, v. G-3, p. 407-479.
- Cline, J.S., 1999, Gold mineralization at the Getchell, Carlin-type gold deposit, north-central Nevada: Part I: Mineral paragenesis and fluid evolution: *Economic Geology* (in review), 36 p.
- Cline, J. S., Hofstra, A. A., Landis, G., and Rye, R., 1997, Ore Fluids at the Getchell, Carlin-type Gold deposit, north-central Nevada *in* Vikre, P., Thompson, T. B., Bettles, K., Christensen, O., and Parratt, R. eds., *Carlin-type Gold Deposits Field Conference Guidebook prepared for the Society of Economic Geologists Field Conference*, v. 28, p. 155-166.
- Culver, J. C., 1997, Turquoise Ridge section interpretations, memo to the Getchell Gold Corp., 6 p.
- Dickinson, W. R., 1992, Cordilleran sedimentary assemblages *in* Burchfiel, B.C., Lipman, P. W., and Zoback, M. L. ed., *The Cordilleran Orogen: Conterminous U.S.: Geological Society of America*, v. G-3, p. 539-551.
- Friedman, I., and O'Neil, J. R., 1977, Compilation of stable isotope fractionation factors of geochemical interest *in* Fleischer, M. ed., *Data of Geochemistry, Sixth Edition*: U.S. Geological Survey, Professional Paper 440-KK, p. KK1-KK12.

- Getchell Gold Corp., 1996, Turquoise Ridge and Powder Hill area drill hole plan map showing minable and global geologic resource, *in* DeLong, R., ed., *Geology and Ore Deposits of Northwestern Nevada*: Geological Society of Nevada, 1996 Fall Field Trip Guidebook, Special Publication n. 24, p. 69-73.
- Getchell Mine staff, 1998, Geologic map showing the location of the Turquoise Ridge deposit.
- Goldstein, R. H., and Reynolds, T. J., 1994, Systematics of Fluid Inclusions in Diagenetic Minerals: Society for Sedimentary Geology Short Course 31, 199 p.
- Groff, J., 1996, $^{40}\text{Ar}/^{39}\text{Ar}$ geochronology of gold mineralization and origin of auriferous fluids for the Getchell and Twin Creeks mines, Humboldt County, Nevada [Ph.D. thesis]: Socorro, New Mexico Institute of Mining and Technology, 291 p.
- Groff, J. A., Heizler, M. T., McIntosh, W. C., and Norman, D. I., 1997, $^{40}\text{Ar}/^{39}\text{Ar}$ Dating and mineral paragenesis for Carlin-type gold deposits along the Getchell trend, Nevada: *Economic Geology*, v. 92, p. 601-622.
- Guilbert, J. M., and Park, C. F. Jr., 1986, *The Geology of Ore Deposits*: New York, W. H. Freeman and Company, 985p.
- Hofstra, A. H., and Rye, R. O., 1998, Contribution to the gold metallogeny of northern Nevada, U.S. Geological Survey open file report 98-338, CD-ROM, p. 202-210.
- Hofstra, A. H., Leventhal, J. S., Northrop, H. R., Landis, G. P., Rye, R. O., Birak, D. J., and Dahl, A. R., 1991, Genesis of sediment hosted disseminated gold deposits by fluid mixing and sulfidation: Chemical-reaction-path modeling of ore-depositional processes documented in the Jerrett Canyon district, Nevada: *Geology*, v. 19, p. 30-40.
- Hotz, P. E., and Willden, R., 1964, *Geology and mineral deposits of the Osgood Mountains quadrangle Humboldt County, Nevada*: U. S. Geological Survey Professional Paper 431, 128 p.
- Hsu, L. C., Bonham, H. F. Jr., Price, J. G., Garside, L. J., Desilets, M. O., and Lechler, P. J., 1995, Geochemical characteristics of the Paleozoic sedimentary rocks in the Winnemucca Quadrangle, Nevada, U.S.A; background value for gold exploration *in* *Exploration and Mining Geology*: Geological Society of the Canadian Institute of Mining, Metallurgy and Petroleum, 4, p. 227-242.
- Kreschmer, E. L., 1984, Geology of the Pinson and Preble gold deposits, Humboldt County, Nevada *in* Buffa, R., Klessig, P., and Schafer, R. eds., *Geology and Gold Deposits of the Osgood Mountains, Nevada*, Geological Society of Nevada, 1989 Fall Field Trip Guidebook, Special Publication no. 10, 8 p.
- Kuehn, C. A., and Rose, A. W., 1992, Geology and geochemistry of wall-rock alteration at the Carlin gold deposit, Nevada: *Economic Geology*, v. 87, no. 7, p. 1697-1721.
- Madden-McGuire, D. J., 1991, Stratigraphy of the limestone-bearing part of the Lower Cambrian to lower Ordovician Preble Formation near its type locality, Humboldt County, North-Central Nevada Nevada Bureau of mines and Geology, 1997, Nevada Geology, Newsletter of the NBMG, Reno, Nevada, n, 32, 4 p.
- Madden-McGuire, D. J., and Marsh, S. P., 1991, Lower Paleozoic host rocks in the Getchell gold belt: Several distinct allochthons or a sequence of continuous sedimentation?, *Geology*, v. 19, p. 489-492.
- Matsuhisa, Y., Goldsmith, J. R., and Clayton, R. N., 1979, Oxygen isotopic fractionation in the system quartz-albite,-anorthite-water: *Geochimica et Cosmochimica Acta*, v. 43, p. 1131- 1140.

- Miller, E. L., Miller, M. M., Stevens, C. H., Wright, J. E., and Madrid, R., 1992, Late Paleozoic paleogeographic and tectonic evolution of the western U.S. Cordillera, *in* Burchfiel, B.C., Lipman, P. W., and Zoback, M. L. ed., the Cordilleran Orogen: Conterminous U.S.: the Geological Society of America, v. G-3, p. 57-106.
- Nevada Bureau of Mines and Geology, 1997, Economic impacts of Mining in Nevada—1997: Quarterly Newsletter of the Nevada Bureau of Mines and Geology Available: <http://www.nmg.unr.edu/mm97/text7.htm>. June 29, 1999.
- Poole, F. G., Stewart, J. H., Palmer, A. R., Sandberg, C. A., Madrid, R. J., Ross, R. J. Jr., Hintze, L. F., Miller, M. M., Wruck, C. T., 1992, Latest Precambrian to latest Devonian time; development of a continental margin Burchfiel, B.C., Lipman, P. W., and Zoback, M. L. ed., the Cordilleran Orogen: Conterminous U.S.: the Geological Society of America, v. G-3, p. 9-56.
- Richardson, C. K., Rye, R. O., and Wasserman, M. D., 1988, The chemical and thermal evolution of the fluids in the Cave-in-Rock Fluorspar district, Illinois: Stable isotope systematics at the Dear Dorff mine; *Economic Geology*, 83, p. 765–783.
- Rees, M. N., and Rowell, A. J., 1980, Preble Formation, a Cambrian outer continental shelf deposit in Nevada: *Brigham Young University Geology Studies*, v. 27, p. 1-8.
- Reid, R. R., 1995, Getchell-Turquoise Ridge structure: summary report to First Miss Gold, 19 p.
- Roberts, R. J., 1964, Stratigraphy and structure of the Antler Peak Quadrangle Humboldt and Lander Counties Nevada; U. S. Geological Survey Professional Paper 459, 90 p.
- Roedder, E., 1984, Fluid Inclusions: Mineralogical Society of America, *Reviews in Mineralogy*, v.12, 646 p.
- Smith, J. F., and Ketner, K. B., 1975, Stratigraphy of Paleozoic Rocks in the Carlin-Pinon range area, Nevada; U. S. Geological Survey Professional Paper 867-A, 83 p.
- State of Nevada Commission on Mineral Resources Division of Minerals, 1999, Nevada minerals industry fact sheet available: <http://www/state.nv.us/minerals/>. June 29, 1999.
- Thompson, A. J. B., Thompson, J. F. H., and Dunne, K. P. E., editors, 1996, Atlas of alteration: Vancouver, British Columbia, Mineral Deposits Division, Geological Association of Canada, 119 p.
- Thorman, C. CH., Ketner, K.B., Snee, W. E., and Zimmermann, R. A., 1991, Late Mesozoic-Cenozoic Tectonics in Northeastern Nevada *in* Raines, G. L., Lisle, R. E., Schafer, R. W., and Wilkinson, W. H. ed., *Geology and Ore Deposits of the Great Basin, Symposium Proceedings: Geological Society of Nevada and U.S. Geological Survey*, v. 2, p. 25-45.

VITA

Graduate College
University of Nevada, Las Vegas

Michiko Shigehiro

Local Address:

5292 S. Maryland Parkway Apartment 188
Las Vegas, Nevada 89119
USA

Home Address:

1-5-19 Mochimune
Shizuoka-shi, Shizuoka-ken 421-01
Japan

Degrees:

Associate of Arts, 1994
Temple University, Japan, Tokyo

Bachelor of Science, Geology, 1996
Temple University, Philadelphia, Pennsylvania

Special Honors and Awards:

Bernada French Geoscience Scholarship, 1997-1999
Nevada EPSCoR Women in Science and Engineering Assistantship, 1997-1998
The Society of Economic Geologists Foundation Student Research Grant, 1997

Publications:

Shigehiro, M., and Cline, J.S., 1999, Mineral paragenesis and P-T constraints during Au deposition at the Turquoise Ridge Carlin-type gold deposit, Geological Society of America Cordilleran Section Abstracts, v. 31, n. 6, p A-94.

Taylor, W. J., Williams, N. W., and Shigehiro, M., 1999, Tectonic setting and paleogeography of K-Eocene basins, Nevada and Utah, Geological Society of America Cordilleran Section Abstracts, v. 31, n. 6, p A-101.

Shigehiro, M., 1999, Mineral paragenesis and pressure and temperature constraints during gold mineralization at the Turquoise Ridge Carlin-type gold deposit, Nevada, Geological Society of Nevada Southern Nevada Chapter April News letter.

Shigehiro, M., and Cline, J.S., 1998, Mineral paragenesis and pressure and temperature constraints during gold mineralization at the Turquoise Ridge Carlin-type gold deposit, Nevada, the Pan American Conference on Research on Fluid Inclusions, Program and Abstracts, p. 60.

Thesis Title:

Mineral Paragenesis and Ore Fluids at the Turquoise Ridge Gold Deposit, Nevada

Thesis Examination Committee:

Chair Person, Dr. Jean S. Cline, Ph. D.
Committee Member, Dr. Margaret Rees, Ph. D.
Committee Member, Dr. Wanda J. Taylor, Ph. D.
Graduate Faculty Representative, Dr. Stephen Lepp, Ph. D.